



Photocatalytic Studies of Cr(III) and Fe(III) Doped Amorphous TiO₂ Powders

Supat Buddee

A Thesis Submitted in Partial Fulfillment of the Requirements for the Degree of

Master of Science in Inorganic Chemistry

Prince of Songkla University

2009

Copyright of Prince of Songkla University

Thesis Title Photocatalytic Studies of Cr(III) and Fe(III) Doped Amorphous
TiO₂ Powders
Author Mr. Supat Buddee
Major Program Inorganic Chemistry

Major Advisor :

.....
(Assoc. Prof. Dr. Sumpun Wongnawa)

Co-advisor :

.....
(Dr. Walailak Puetpaiboon)

Examining Committee :

.....Chairperson
(Asst. Prof. Dr. Chaveng Pakawatchai)

.....
(Assoc. Prof. Dr. Sumpun Wongnawa)

.....
(Dr. Walailak Puetpaiboon)

.....
(Assoc. Prof. Dr. Supasarote Muensit)

.....
(Dr. Chuleeporn Puttnual)

The Graduate School, Prince of Songkla University, has approved
this thesis as partial fulfillment of the requirement for the Master of Science Degree in
Inorganic Chemistry

.....
(Assoc. Prof. Dr. Krerchai Thongnoo)

Dean of Graduate School

ชื่อวิทยานิพนธ์	การศึกษาปฏิกิริยาโฟโตคะตะไลติกของผงไทเทเนียมไดออกไซด์ที่เจือด้วยโครเมียม(III) และเหล็ก(III)
ผู้เขียน	นายสุวัฒน์ บุตรดี
สาขาวิชา	เคมีอนินทรีย์
ปีการศึกษา	2551

บทคัดย่อ

ไทเทเนียมไดออกไซด์อัญฐาน (TiO_2) ที่เจือด้วยเหล็กและโครเมียม (Fe-TiO_2 และ Cr-TiO_2) เตรียมได้จากวิธี อิมเพรอกเนชันแบบเปียก ศึกษาคุณสมบัติทางกายภาพและทางเคมีของสารที่เตรียมได้โดยใช้เทคนิค XRD, ESR, FT-IR, SEM, TEM, BET, DRS และ UV-vis พบว่าไอออนของโลหะที่เจือในช่วงความเข้มข้นที่ศึกษาตั้งแต่ 0.05 - 0.2 mol% ไม่มีผลต่อการเปลี่ยนแปลงเฟสของ TiO_2 ค่าพลังงานของแถบช่องว่างเปลี่ยนแปลงจาก 3.2 eV เป็น 2.5 eV และ 2.8 eV สำหรับ Fe-TiO_2 และ Cr-TiO_2 ตามลำดับ อาศัยการสลายสีย้อมเมทิลีนบลูภายใต้แสงยูวีและแสงวิสิเบิลในการศึกษาความสามารถในการเป็นโฟโตคะตะลิสต์ของสารตัวอย่าง พบว่าทั้ง Fe-TiO_2 และ Cr-TiO_2 ที่ความเข้มข้น 0.1 mol% สามารถสลายสีย้อมเมทิลีนบลูได้ทั้งภายใต้แสงยูวีและแสงวิสิเบิล ในกรณีภายใต้แสงยูวี ภายใน 5 ชั่วโมง Fe-TiO_2 และ Cr-TiO_2 สามารถสลายสีย้อมได้ดีเทียบเท่ากับไทเทเนียมไดออกไซด์เชิงการค้า (anatase และ Degussa P25) และในกรณีภายใต้แสงวิสิเบิล ซึ่ง anatase และ Degussa P25 ไม่สามารถสลายสีย้อมได้เลย แต่ทั้ง Fe-TiO_2 และ Cr-TiO_2 สามารถสลายสีย้อมได้หมด โดยอาศัยเวลา 12 ชั่วโมง งานวิจัยนี้สามารถเปลี่ยนไทเทเนียมไดออกไซด์อัญฐานให้สามารถเป็นโฟโตคะตะลิสต์ได้ด้วยการเจือไอออนของโลหะลงไปโดยอาศัยวิธีที่ง่ายและมีราคาถูก จึงเป็นอีกวิธีหนึ่งในการใช้กำจัดน้ำเสียจากอุตสาหกรรม

Thesis Title	Photocatalytic Studies of Cr(III) and Fe(III) Doped Amorphous TiO ₂ Powders
Author	Mr. Supat Buddee
Major Program	Inorganic Chemistry
Academic Year	2008

Abstract

Amorphous TiO₂ doped with Fe(III) and Cr(III), designated as Fe-TiO₂ and Cr-TiO₂, were prepared via an incipient wetness impregnation. The resulting products were characterized by X-ray diffraction, electron spin resonance spectroscopy, Fourier-transformed infrared spectroscopy, scanning electron microscopy, transmission electron microscopy, specific surface area by the Brunauer, Emmett and Teller method, diffuse reflectance spectroscopy and UV-vis absorption. Experimental results revealed that the dopants had no effect, at these concentrations: from 0.05 to 0.2 mol%, on the phase of products. The band gap energies shifted from 3.2 to 2.5 eV and 2.8 eV for Fe-TiO₂ and Cr-TiO₂, respectively. The effect of dopant concentration on the photocatalytic activity of amorphous TiO₂ was investigated by degradation of aqueous methylene blue under UV and visible light irradiation. The doped amorphous TiO₂ showed photocatalytic activities under both UV and visible light with optimal results at 0.1 mol% dopants. Under UV irradiation, the 0.1 mol% doped samples decolorized dye solutions to the same extent as the commercial TiO₂ samples (anatase and Degussa P25) in 5 h. Under visible light while the commercial ones did not show photocatalytic activity, the doped samples decolorized dye solutions in 12 h compared with 5 h under UV light. The results from this work showed that doping with transition metal ions could turn the inert amorphous TiO₂ to become photocatalytically active. Considering the simplicity in preparation and low cost due to exclusion of calcination process, this should be an attractive choice to wastewater treatment industries.

Contents

Subject	Page
Abstract (Thai)	iii
Abstract (English)	iv
Acknowledgments	v
The relevancy of the research work to Thailand	vi
Contents	vii
List of Figures	viii
Lists of Tables	xii
Abbreviation and Symbols	xiii
Chapter 1: Introduction	1
Introduction	1
Literature reviews	3
Objectives	45
Chapter 2: Methodology	46
Materials	46
Instruments	46
Methods	47
Chapter 3: Results	58
Syntheses and characterizations of TiO ₂ powders	58
Photocatalytic activities of methylene blue	96
Chapter 4: Discussions	107
Syntheses and characterizations of TiO ₂ powders	107
Photocatalytic activities of methylene blue	122
Kinetics of photocatalytic reactions	126
Effect of pH on the photocatalytic activity	128
Chapter 5: Conclusions	131
References	133
Vitae	147

List of Figures

Figure	Page
1. Crystal structures of TiO ₂ , (a) Anatase, (b) Rutile, and (c) Brookite	5
2. TiO ₂ pigment manufactured by the sulfate process	7
3. TiO ₂ pigment manufactured by the chloride process	9
4. An overview of products prepared by sol-gel methods	11
5. The structure of MB	18
6. UV-vis absorption spectrum of MB aqueous solution	21
7. The heterogeneous photocatalytic oxidation processes of TiO ₂ photocatalyst	23
8. Flow chart of the preparation of undoped TiO ₂ powder by sol-gel method	50
9. Flow chart of the preparation of Cr-TiO ₂ powder by impregnation method	51
10. Flow chart of the preparation of Fe-TiO ₂ powder by impregnation method	52
11. The photograph of undoped TiO ₂ powder	58
12. The photographs of doped TiO ₂ powders; (a) Fe-TiO ₂ , and (b) Cr-TiO ₂	59
13. X-ray diffraction patterns for (a) undoped TiO ₂ , (b) 0.05Fe-TiO ₂ , (c) 0.1Fe-TiO ₂ , (d) 0.2 Fe-TiO ₂ , (e) 0.05Cr-TiO ₂ , (f) 0.1Cr-TiO ₂ , (g) 0.2 Cr-TiO ₂ , (h) Degussa P25, and (i) anatase TiO ₂	60
14. DRS spectrum of undoped TiO ₂	62
15. DRS spectra of doped TiO ₂ ; (a) Fe-TiO ₂ , (b) Cr-TiO ₂	63
16. DRS spectrum of commercial TiO ₂ ; (a) anatase, and (b) Degussa P25	64
17. Plot of $(\alpha E_{phot})^2$ versus E_{phot} for a direct transition of TiO ₂ samples; (a) undoped TiO ₂ , (b) Fe-TiO ₂ , (c) Cr-TiO ₂ , and (d) commercial TiO ₂	66
18. Plot of $(\alpha E_{phot})^{1/2}$ versus E_{phot} for an indirect transition of TiO ₂ samples; (a) undoped TiO ₂ , (b) Fe-TiO ₂ , (c) Cr-TiO ₂ , and (d) commercial TiO ₂	66
19. PL spectrum of undoped TiO ₂	68
20. PL spectrum of commercial TiO ₂ powders, (a) anatase, and (b) Degussa P25	69
21. PL spectra of doped TiO ₂ ; (a) Fe-TiO ₂ , and (b) Cr-TiO ₂	70
22. FT-IR spectrum of undoped TiO ₂	71

List of Figures (Continued)

Figure	Page
23. FT-IR spectrum of Fe(III) doped TiO ₂ powders; (a) 0.05Fe-TiO ₂ , (b) 0.1Fe-TiO ₂ , and (c) 0.2Fe-TiO ₂	72
24. FT-IR spectrum of Cr(III) doped TiO ₂ powders; (a) 0.05Cr-TiO ₂ , (b) 0.1Cr-TiO ₂ , and (c) 0.2Cr-TiO ₂	73
25. FT-IR spectrum of commercial TiO ₂ powder, anatase	74
26. FT-IR spectrum of commercial TiO ₂ powder, Degussa P25	74
27. SEM images of undoped TiO ₂	78
28. SEM images of Fe(III) doped TiO ₂	79
29. SEM images of Cr(III) doped TiO ₂	80
30. SEM images of commercial TiO ₂ (anatase)	80
31. SEM images of commercial TiO ₂ (Degussa P25)	80
32. TEM micrograph of undoped TiO ₂ at x 80,000	81
33. TEM micrographs at x 80,000 of doped TiO ₂ ; (a) Fe-TiO ₂ , and (b) Cr-TiO ₂	81
34. TEM micrographs at x 80,000 of commercial TiO ₂ ; (a) anatase, and (b) Degussa P25	82
35. N ₂ adsorption isotherm of undoped TiO ₂	86
36. N ₂ adsorption isotherm of doped TiO ₂ ; (a) Fe-TiO ₂ , and (b) Cr-TiO ₂	86
37. T-plot of N ₂ adsorption isotherm of undoped TiO ₂	87
38. T-plot of N ₂ adsorption isotherm of doped TiO ₂ ; (a) Fe-TiO ₂ , and (b) Cr-TiO ₂	87
39. Pore size distribution curve of undoped TiO ₂	88
40. Pore size distribution curve of doped TiO ₂ ; (a) Fe-TiO ₂ , and (b) Cr-TiO ₂	88
41. ESR spectrum of undoped TiO ₂	89
42. ESR spectra of doped TiO ₂ ; (a) Fe-TiO ₂ , and (b) Cr-TiO ₂	90
43. Effect of dopant concentrations in the preparation of doped TiO ₂ ; (a) Fe-TiO ₂ , and (b) Cr-TiO ₂	93
44. Effect of doping duration in the preparation of doped TiO ₂ ; (a) Fe-TiO ₂ , and (b) Cr-TiO ₂	94

List of Figures (Continued)

Figure	Page
45. Effect of stirring speed in the preparation of doped TiO ₂ ; (a) Fe-TiO ₂ , and (b) Cr-TiO ₂	95
46. The standard calibration graph of MB solution in the range of 1.0 x 10 ⁻⁶ M to 1.0 x 10 ⁻⁵ M	96
47. The standard calibration graph of MB solution in the range of 1.0 x 10 ⁻⁵ M to 1.0 x 10 ⁻⁴ M	97
48. The standard calibration graph of MB solution in the range of 1.0 x 10 ⁻⁴ M to 1.0 x 10 ⁻³ M	97
49. Decolorization of MB by undoped TiO ₂ at various concentrations	99
50. Photocatalytic activity of undoped TiO ₂ under UV irradiation at high MB concentrations	100
51. Photocatalytic activity of undoped TiO ₂ under visible light irradiation at high MB concentrations	101
52. Decolorization efficiency of MB by Fe-TiO ₂ (adsorption)	102
53. Decolorization efficiency of MB by Cr-TiO ₂ (adsorption)	102
54. Degradation efficiency of MB by Fe-TiO ₂ under UV irradiation	103
55. Degradation efficiency of MB by Cr-TiO ₂ under UV irradiation	104
56. Degradation efficiency of MB by Fe-TiO ₂ under visible light irradiation	104
57. Degradation efficiency of MB by Cr-TiO ₂ under visible light irradiation	105
58. Comparative degradation efficiencies of MB by 0.1Fe-TiO ₂ , Cr-TiO ₂ and commercial TiO ₂ under UV irradiation	106
59. Comparative degradation efficiencies of MB by 0.1Fe-TiO ₂ , Cr-TiO ₂ and commercial TiO ₂ under visible light irradiation	106
60. DRS spectra of undoped, doped, and commercial TiO ₂ ., Inset: λ_{onset} of absorption of TiO ₂ samples	111
61. SEM images of TiO ₂ from the study of Zhang et al., (2007)	117
62. IUPAC classification of adsorption isotherms	118
63. Comparison the degradation of MB by TiO ₂ samples under UV irradiation	123

List of Figures (Continued)

Figure	Page
64. Energy levels of impurity ions in TiO ₂	126
65. Kinetics plots of TiO ₂ under (a) under UV light irradiation, and (b) visible light irradiation	127
66. Effect of pH on photodegradation under UV light irradiation for (a) Fe-TiO ₂ , and (b) Cr-TiO ₂	129
67. Effect of pH on photodegradation under visible light irradiation for (a) Fe-TiO ₂ , and (b) Cr-TiO ₂	130

Lists of Tables

Table	Page
1. Properties of the three modifications of TiO ₂	4
2. X-ray data on TiO ₂ modifications	6
3. Structures and UV-vis absorption characteristics of MB and its common reduced and oxidised forms	19
4. Photophysical properties of MB	20
5. The crystalline phase of synthesized TiO ₂ and commercial	61
6. The wavelength at onset of absorption and the band gap energy of all TiO ₂	67
7. Assignment of the FT-IR bands of synthetic TiO ₂	75
8. Assignment of the FT-IR bands of commercial TiO ₂	77
9. Surface area of all TiO ₂ samples	84
10. Porosity of all TiO ₂ samples	85
11. ESR signal of synthesized TiO ₂ samples	90
12. Percentage of Fe(III) and Cr(III) amount in doped TiO ₂	91
13. Drying temperature, drying duration and phase of undoped TiO ₂	92
14. The percentage of MB decolorization by undoped TiO ₂ at various concentrations	99
15. Band gap energies of some TiO ₂ samples obtained from PL	115
16. IUPAC classification of the pore	119
17. The kinetics rate constants of TiO ₂ samples under difference photocatalytic conditions	128

Abbreviation and Symbols

<i>et al.</i>	=	And other people
Å	=	Angstrom
~	=	Approximately
<i>ca.</i>	=	Approximately
°C	=	Degree Celsius
ϵ	=	Dielectric constant
eV	=	Electron volt
<i>S</i>	=	Entropy
h	=	Hour
i.e.	=	In other words
λ_{\max}	=	Maximum wavelength
MB	=	Methylene blue
mL	=	Milliliter
min	=	Minute
M	=	Molar
mol/L	=	Mole per liter
nm	=	Nanometer
pzc	=	Point of zero charge
η	=	Refractive index
rpm	=	Round per minute
SPE	=	Solid-phase extraction
TiO ₂	=	Titanium dioxide
UV	=	Ultraviolet

Chapter 1

Introduction

1.1 Introduction

Environmental pollution and destruction on a global scale are issues of increasing concern in today's society. The presence of several organic pollutants results in a serious environmental problem. Dye pollutants from the textile industry are an important source of environmental contamination. Large quantities of dyes are extensively used in the fundamental processing steps of textile industries. It is estimated that *ca.* 1-15 % of the dye is lost during the dyeing processes and is released as wastewater (Zainal, *et al.*, 2005). The color is usually the first contaminant to be recognized in wastewater, which generated by using synthetic dyes in the industrials. Considering both volumes discharged and effluent compositions, the wastewater generated by the textile industry is rated as one of the most polluting among all industry sectors. Given the great variety of fibers, dyes, process aids and finishing products in use, the textile industry generated wastewater of great chemical complexity, diversity and volume (Bizani, *et al.*, 2006). Synthetic dyes are extensively used in the textile industries because of their simple dyeing procedure and good stability during washing process. Synthetic dyes, classified by their chromophores, have different and stable chemical structures to meet various coloring requirements (Toor, *et al.*, 2006). The release of the wastewater into the ecosystem, for instance, as much as many million gallons discharged per year to waste water treatment systems, is a dramatic source of aesthetic pollution, eutrophication, and perturbation in aquatic life. Therefore, the removal of colored wastewater is a necessary before being released to the environmental (Sauer, *et al.*, 2002).

The traditional techniques used for color removal are filtration, activated carbon (charcoal), and coagulation. Each method has few advantages and disadvantages. For example, the use of charcoal is technically easy but has high waste disposal cost. Coagulation using alums, ferric salts or limes is a low cost process, but all these methods have a major disadvantage of simply transferring the pollutants

form one phase to another phase rather than destroying them and sometime the by-products may be more toxic than the dye itself. Biological treatment is a proven method and cost effective. However, it has been reported that majority of dyes are adsorbed on the sludge and very long degraded times, due to the biorecalcitrant nature of these dyes molecules. This leads to search for highly effective method to degrade the dye into environmentally compatible products (Toor, *et al.*, 2006).

In recent years, there has been an extensive interest in heterogeneous photocatalysis using semiconductors for the treatment of recalcitrant chemical present in the wastewater. The main advantage of the method is that the pollutants are destroyed with no requirement for secondary disposal of concentrated wastes, providing a more environmentally sustainable solution. Among the semiconductors being studied, such as TiO_2 , ZnO , Fe_2O_3 , CdS , and ZnS , TiO_2 has been successfully used to decolorize and mineralize many organic pollutants including several dyes and their intermediates present in aqueous systems using both artificial light and under sunlight using solar technology (Muruganandham, *et al.*, 2005). TiO_2 is the most widely used photocatalyst because of its good activity, chemical stability, commercial availability and inexpensiveness. It is generally used as a photocatalyst for environmental applications such as air purification, water disinfection, hazardous waste remediation and water purification (Nagaveni, *et al.*, 2004).

However, TiO_2 is active only under ultraviolet light (UV) because of its wide band gap, ~ 3.2 eV for anatase and ~ 3.0 eV for rutile, corresponding to 388 and 410 nm, respectively, and high rate of recombination of photogenerated electron - hole pairs resulting in low photo quantum efficiency. Several approaches have been applied to optimize the photocatalyst itself in order to improve the photocatalytic activity.

Nowadays, doping with transition metal elements have been attempted to improve TiO_2 catalyst with visible-light response because transition elements have many valences and trace transition metal ions doped in the TiO_2 matrix can be superficial potential trap of photogenerated electron - hole pairs, then lengthen the lifetime of electrons and holes and increase photocatalytic activity (Yang, *et al.*, 2004). Unfortunately, nearly all photocatalytic studies on TiO_2 have focused their

studies on the crystalline forms, as it is commonly accepted that amorphous TiO₂ contains high concentration of defects that will invariably function as rapid electron - hole pairs recombination centers to render them inactive (Ohtani, *et al.*, 1997). However, amorphous TiO₂ has one interesting property: the high surface area which can lead to high adsorptivity. Up to date, there have been only a few reports that studied or showed interest in amorphous TiO₂.

We have had experience involving the synthesis of amorphous TiO₂ and studied its adsorptivity with metal ions (Mn(II), Fe(III), Cu(II), Pb(II)) with aimed application in solid-phase extraction (SPE). We found that amorphous form, previously thought rather inactive, with small amount of crystalline anatase form also showed photocatalytic properties. Furthermore, these synthesized, amorphous, TiO₂ showed good adsorption property towards metal ions (Randorn, *et al.*, 2004; Kanna, *et al.*, 2005).

In this work, we focus on the improvement of amorphous TiO₂ powder by doping with trivalent Cr and Fe ions using incipient wetness impregnation method. Hopefully, the trivalent (Cr, Fe) doped TiO₂ can act as photocatalysts under both UV and visible light irradiation, for directly improvement and application in the water purification of amorphous TiO₂ powder.

1.2 Review of Literatures

1.2.1 Titanium dioxide

(1) Background

Titanium dioxide (TiO₂) also known as titanium(IV) oxide or titania, is the naturally occurring oxide of titanium. It exists in three polymorphous structures, namely, anatase, brookite and rutile. The most common structures are anatase and rutile, since brookite is rather unstable. Both anatase and rutile are tetragonal, whereas brookite is orthorhombic. In all three oxide modifications, each titanium atom is coordinated to six almost equidistant oxygen atoms, and each oxygen atom to three titanium atoms (Clark, *et al.*, 1968). These polymorphic forms of TiO₂ are shown in Figure 1. The structure of anatase, brookite and rutile can be discussed in term of

(TiO_6^{2-}) octahedral. The three crystal structures differ by the distortion of each octahedral and by the assembly patterns of the octahedral chains. In the case of anatase, the TiO_6^{2-} octahedron is slightly distorted, with two Ti-O bonds slightly greater than the other four, and with some of the O-Ti-O bond angles deviating from 90° . The distortion is greater in anatase than rutile. The third form of TiO_2 , brookite, the interatomic distances and the O-Ti-O bond angles are similar to those of rutile and anatase. The essential difference is that there are six different Ti-O bonds ranging from 1.87 to 2.04 Å. Accordingly, there are 12 different O-Ti-O bond angles ranging from 77° to 105° . Brookite is formed by joining together the distorted TiO_6^{2-} octahedral sharing three edges. All three oxide modifications are birefringent; anatase is uniaxial negative, brookite is biaxial positive and rutile is uniaxial positive. Further data are given in Table 1. Crystallographic data on the three oxide modifications are summarized in Table 2.

Table 1 Properties of the three modifications of TiO_2 (Clark, *et al.*, 1968 : 270).

	<i>Anatase</i>	<i>Brookite</i>	<i>Rutile</i>
Density (g/cm^3)	3.90	4.13	4.27
Hardness (Mohs' scale)	5.5-6.0	5.5-6.0	6.0-6.5
Melting Point ($^\circ\text{C}$)	change to rutile	change to rutile	1840 ± 10
Entropy $S_{298.16}^\circ$ (cal/deg/m)	11.93	-	12.01
Refractive Index (25°C) ($\lambda = 5893 \text{ \AA}$)	n_o 2.5612 n_e 2.4880	n_α 2.5831 n_β 2.5843 n_γ 2.7004	n_o 2.6124 n_e 2.8993
Dielectric Constant	$\epsilon = 48$ (powder)	$\epsilon = 78$	$\epsilon_{av} \approx 110$ $\epsilon_{II} = 180$ $\epsilon_{\perp} = 89,$ at $3 \times 10^5 \text{ c/s}$ 25 $^\circ\text{C}$

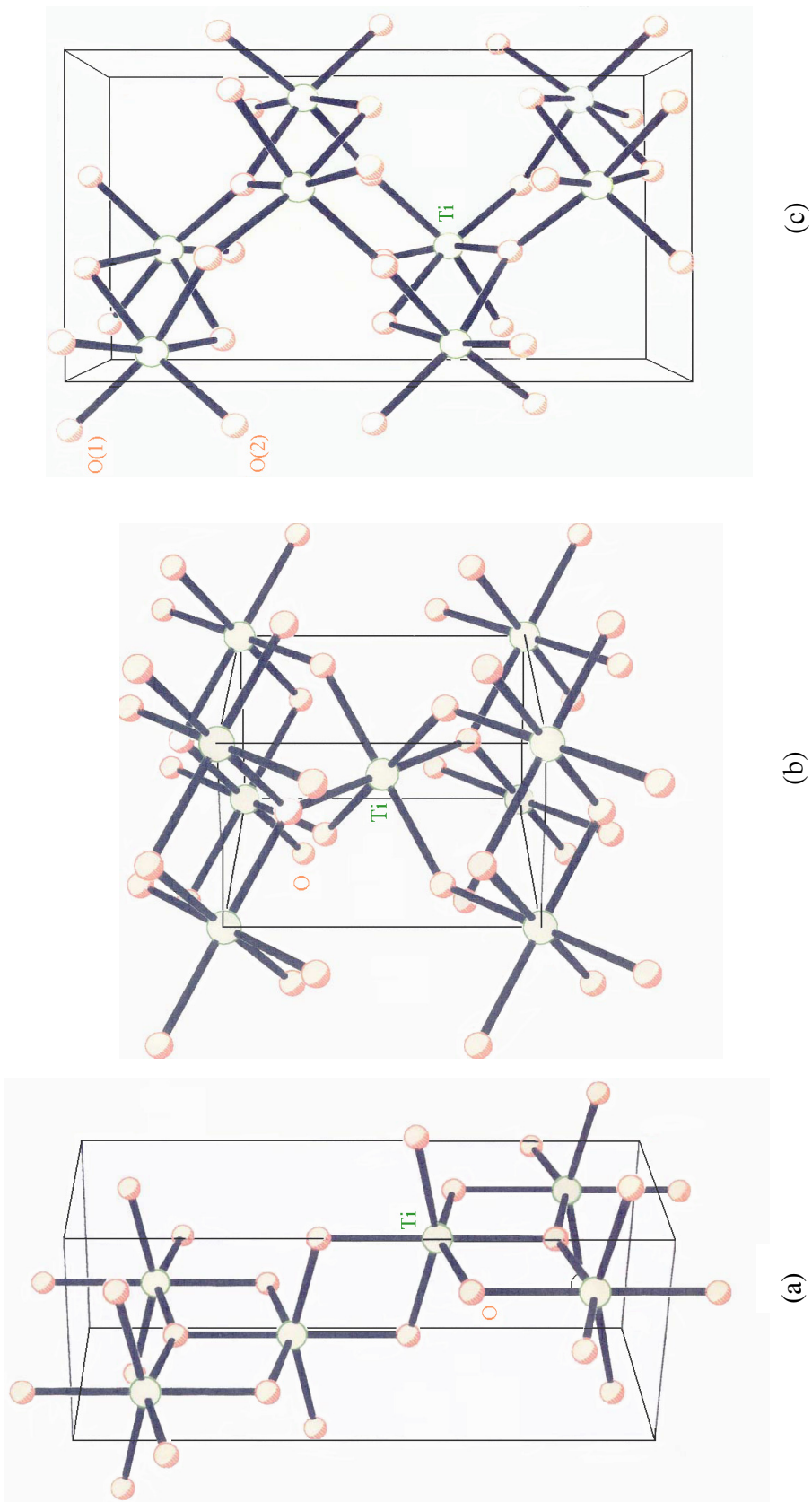


Figure 1 Crystal structures of TiO_2 , (a) Anatase, (b) Rutile, and (c) Brookite.

Table 2 X-ray data on TiO₂ modifications (Clark, *et al.*, 1968 : 268).

	Space group	Z	Cell parameters (Å)			Ti-O (Å) ^a
			A	B	C	
Anatase	$C_{4h}^{19} = C4/amc$	8	5.36		9.53	1.91(2) 1.95(4)
Brookite	$D_{2h}^{15} = Pbca$	8	9.15	5.44	5.14	1.84-2.03
Rutile	$D_{4h}^{14} = P4_2/mnm$	2	4.954		2.959	1.944(4) 1.988(2)
α - PbO ₂ form	$D_{2h}^{14} = Pbcn$	4	4.515	5.497	4.939	1.91(4) 2.05(2)

^aThe numbers in parentheses refer to the number of equivalent oxygen atoms at the stated distance from a titanium atom

Of the three forms, the most common structures are anatase and rutile since brookite is rather unstable. The brookite type cannot be used in industries because of its instability at room temperature. The anatase type has the problems of poor light, heat resistance, and gradually decreasing in whiteness due to weather. It also has drawbacks for applications involving adsorption technology owing to its low surface energy. The rutile type has outdoor applicability because of its good light resistance and can be applied to surfaces by the use of adsorption technology without advanced skills or sophisticated equipment.

TiO₂ is extensively used as a white permanent pigment with good covering power in paint, paper, printing ink, plastic, polymer and cosmetic products. Paints made with TiO₂ are excellent reflectors of infrared radiation and are used in exterior paints. It is also used as strengthening filler in paper and cement. Recently, there has been increasing interest in application of nanocrystalline materials for catalyst, supports, ceramics, inorganic membranes, gas sensing, water purification, and solar energy conversion (Yanqing, *et al.*, 2001). Furthermore, photocatalysis of nanocrystalline TiO₂ has a great many advantages on waste water treatment such as high catalysis efficiency, energy saving, no pollution, etc. and can degrade all kinds of

organic pollutants from water effectively. All of those merits make photocatalysis of water treatment and it is supposed to be used widely in the future (Baolong, *et al.*, 2003).

(2) Synthesis of TiO₂

TiO₂ can be prepared in the form of powder, crystal, or thin film. Generally, TiO₂ may be manufactured by either older sulfate or newer chloride processes. The economics of the two processes are very much dependent upon the raw material available. The starting materials for TiO₂ production are ilmenite and titaniferous slag in the case of the sulfate process and leucoxene, rutile, synthetic rutile, and in the future possibly also anatase, for the chloride process (Büchner, *et al.*, 1989). TiO₂ pigment manufactured by the sulfate process is shown in Figure 2.

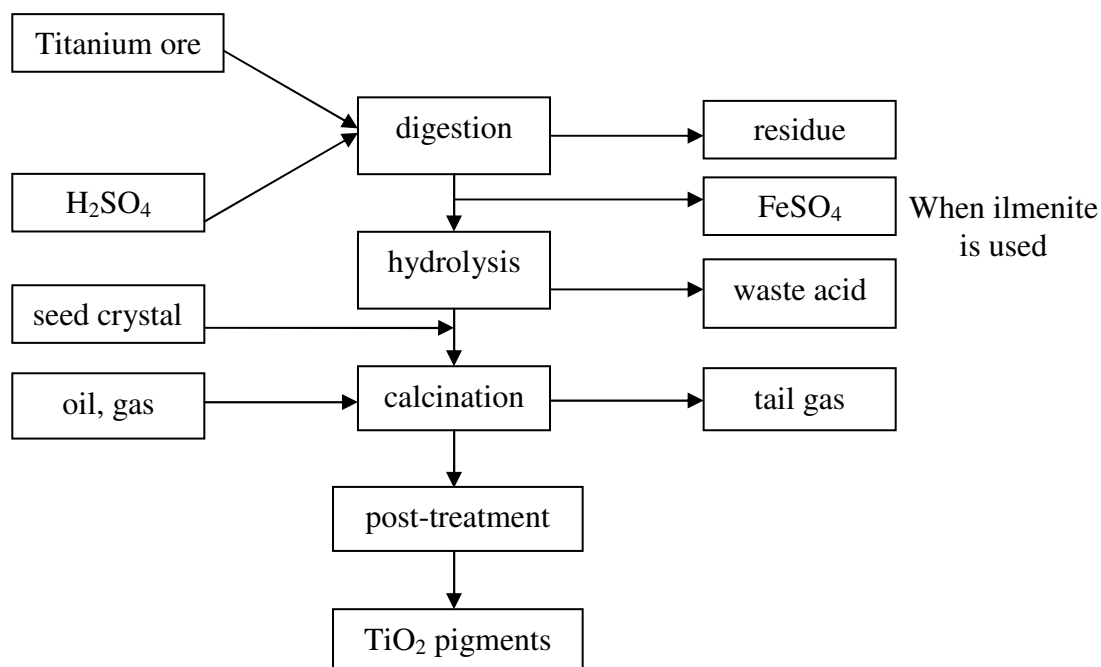


Figure 2 TiO₂ pigment manufactured by the sulfate process

(Büchner, *et al.*, 1989 : 526).

The sulfate process was the first commercial scale technology used to convert ilmenite to TiO_2 . The process started from digestion the finely ground raw materials in an exothermic reaction with concentrated sulfuric acid, the digested cake dissolved in cold water and the residue separated off. To prevent their precipitation during the subsequent hydrolysis the Fe(III) ions are reduced to Fe(II) by adding a Ti(III) solution or scrap-ions. Upon evaporation of the solution, the large quantities of iron(II) sulfate heptahydrate are produced, when ilmenite is used, and crystallizes out. The titanium oxysulfate is then hydrolyzed to titanium oxyhydrate by heating the clear solution with steam at 95-110 °C. TiO_2 seed crystals are added or formed before hydrolysis to ensure yields of 93-96 % TiO_2 and to obtain a hydrolysis product which yields the optimum particle size of *ca.* 0.2 μm upon firing. Diluted sulfuric acid remains as “waste acid”. The hydrolysis product is washed, treated with a Ti(III) solution to remove adsorbed heavy metal ions (Fe, Cr, Mn, V) and calcined at temperature between 800-1,000 °C. Anatase or rutile pigments can be produced in the calcination process depending upon the choice of additives, which determine the characteristics of the product. TiO_2 obtained in this way usually has the structure of anatase since the sulfate ions stabilize this modification which could not be removed during the process of washing, and it would benefit to the formation of anatase and the transformation temperature must take place at high temperature to obtain rutile TiO_2 (Yang, *et al.*, 2002).

The newer chloride process offers tighter product control, less labor intensive, avoids the iron sulfate waste problem and, at larger scales, is cheaper to operate. Currently about 60 % of 4 million tons of pigment produced world-wide is produced by this process. This process required the ilmenite to be processed to the rutile form (i.e. removal of the iron component to yield crude TiO_2 (synthetic rutile)).

The chloride process started from the reaction of chlorine with synthetic rutile to form raw titanium tetrachloride which is then mixed with reducing agent to convert impurities such as vanadium oxychloride, iron chloride to lower oxidation state compounds. It is then distilled yielding titanium tetrachloride in almost any required purity. Finally, it is combusted with pure oxygen to TiO_2 and chlorine, which is reused in the chlorination. Usually, TiO_2 prepared from this process has the

mixture structure of anatase and rutile with the average diameter about 20 nm. For instance, the typical commercial formed TiO_2 (anatase) made by Degussa contain about 25 % rutile. TiO_2 pigment manufactured by the chloride process is shown in Figure 3.

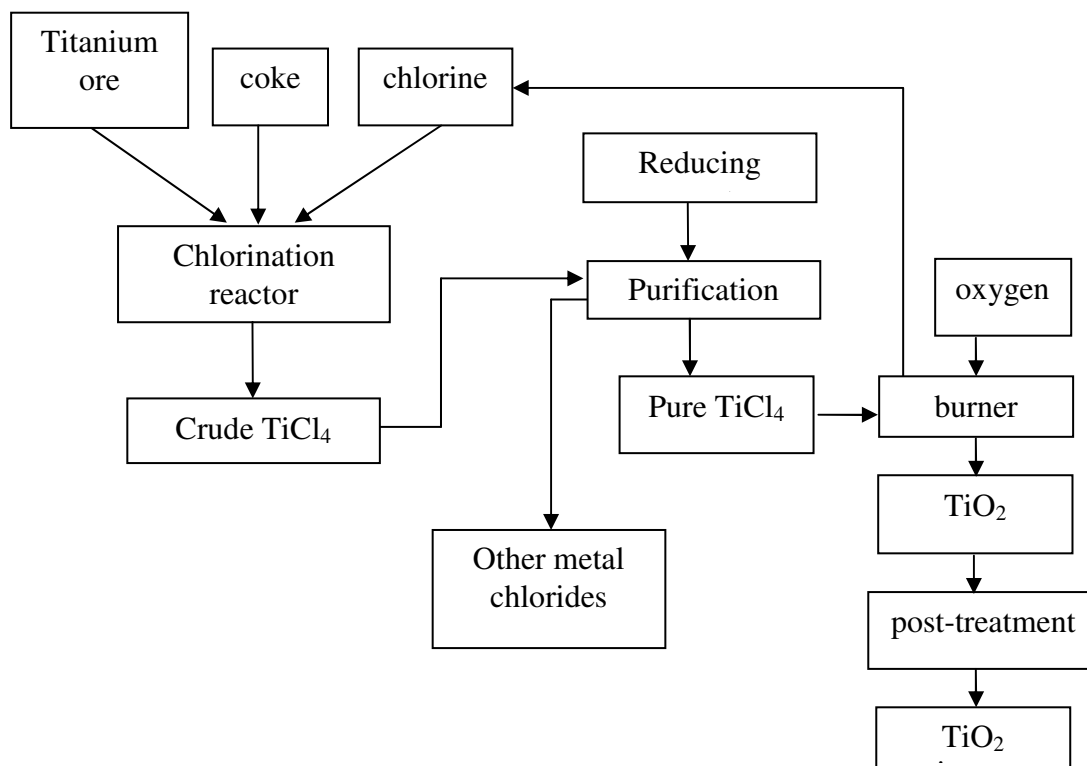


Figure 3 TiO_2 pigment manufactured by the chloride process
(Büchner, *et al.*, 1989 : 528).

On a laboratory scale, TiO_2 has been prepared by various methods, such as sol-gel method, hydrothermal method, combustion synthesis, inert-gas conversion, impregnation, and so on. The different preparation route and the experiment conditions of TiO_2 result in products with different structures, morphology, particle size and contaminants. The metal alkoxide is usually used as a precursor on a laboratory scale to prepare TiO_2 powders. However, strick control of

the reaction conditions is required because of the intense hydrolysis of alkoxide in the air and the prices of the alkoxide limit the commercialization. So, the commercial inorganic compounds such as titanium tetrachloride (TiCl_4) and titanium disulfate ($\text{Ti}(\text{SO}_4)_2$) are more extensively used in the preparation of TiO_2 than the metal alkoxide.

In this work the sol-gel based on base-catalysis through precipitation processes and incipient wetness impregnation methods for prepared amorphous TiO_2 and trivalent (Cr, Fe) doped TiO_2 powder, respectively

(a) Sol-Gel method

It is known that TiO_2 prepared by sol-gel method has been used in many applications in science and technology such as membranes, porous substrate, photocatalytic oxides, ceramics, glass materials and also in electronic devices (Kumar, *et al.*, 1999). In general, the sol-gel method involves the transition of system from a liquid “sol” into solid “gel” phase. An overview of the sol-gel product is presented in Figure 4. The starting materials in the preparation of the “sol” are usually inorganic metal salts or metal organic compounds. In a typical sol-gel method, the precursor is subjected to a series of hydrolysis and polymerization (condensation) reactions to form a colloidal suspension or a “sol”. Further processing of the “sol” enables one to make ceramic materials in different forms. Thin films can be prepared on a piece of substrate by spin coating or dip-coating. When the “sol” is cast into a mold, a wet “gel” will form. With further drying and heat-treatment, the “gel” is converted into dense ceramic or glass articles. If the liquid in a wet “gel” is removed under a supercritical condition, a highly porous and extremely low density material called “aerogel” is obtained. As the viscosity of a “sol” is adjusted into a proper viscosity range, ceramic fibers can be drawn from the “sol”. Ultra-fine and uniform ceramic powders are formed by precipitation, spray pyrolysis, or emulsion techniques (Chemat Technology, Inc., 1998).

In comparison to the other methods, the sol-gel method offers many advantages in easily control and strongly influenced by the synthesis conditions.

Strick control on synthesis parameters is necessary to obtain reproducibility in sample with the desired characteristics and high level of chemical purity (Suresh, *et al.*, 1998). Moreover, in these method precursor materials are metallic halide or alkoxide that favor the building of a solid network in a gel which eventually become a stable solid (Sanchez, *et al.*, 1996). When this method is used for developing catalytic materials, it provides very interesting results. For instance, in metal supported catalysis, the active metal and the support can be prepared in one step. This allows an economy in the catalyst preparation, and also allows one to develop catalyst with new properties (Bokhimi, *et al.*, 1995). Furthermore, the sol-gel method can be used for preparing the support alone, this supports determine the dispersion and stabilization of the active metal and has a specific surface area that can be regulated by controlling its particle size and porosity (Tauter, *et al.*, 1978).

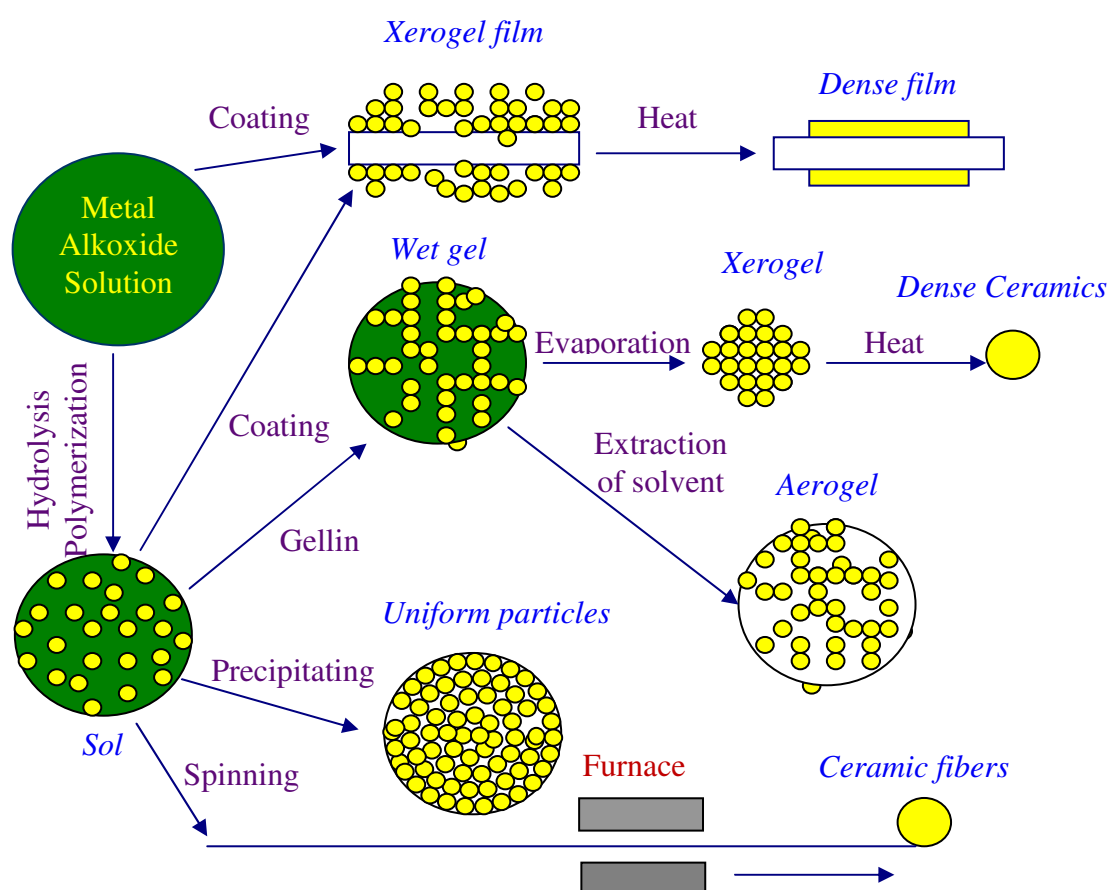


Figure 4 An overview of products prepared by sol-gel methods
(Chemat Technology, Inc., 1998).

(b) Impregnation method

Preparative chemistry has for many years been critical to heterogeneous catalysis, defining as it does the number and type of active sites produced. One frequently used route to real heterogeneous catalysts involves impregnation of a porous solid support, using a solution of a precursor to the active phase. Impregnation is technically and superficially simple, but is in fact rather complex and multistep, involving:

- (i) support wetting,
- (ii) drying, and
- (iii) calcination or reduction.

Within the first of these, (i) ion-exchange/adsorption, (ii) ligands exchange reactions, and (iii) support modification and dissolution may occur to an equilibrium extent or may be kinetically defined by (i) the previous state of the support and its surface chemistry, (ii) the concentration, pH, temperature and viscosity of the impregnating solution, (iii) the chemistry of the solution species present, and (iv) the presence of any competing ions (Alexiou and Sermon, 1993).

Usually, the active catalyst constituent is coated by filling the granulated carrier with the theoretical volume of a solution of given chemical composition and later holding in static conditions while mixing. The volume ratio of solvent and pores is most often 1 to 1.5. The term "impregnation" implies several physical and chemical processes: wetting of carrier, capillary solution suction, diffusion of dissolved substances in the external solution and in the pore body, phase conversion of dissolved substances caused by chemical changes during impregnation with changes of temperature, solution concentration and composition, and also medium pH, and adsorption by reaction between dissolved substances and surface groups of carrier.

Two types of impregnation technology, for heterogeneous catalysts, are recognized: dry and diffusion. In the former, the baking carrier is mixed with the impregnating solution containing all the required constituents. In diffusion technology, most widely adopted industrially, the impregnating solution contacts with the carrier whose pores are already filled with the solvent. The process commences

with the diffusion of substances dissolved in the external solution and in the pore body.

Catalyst production consists of some stages: carrier preparation, coating the active phase constituents, drying, and baking the catalyst. The first two stages proceed in one apparatus (impregnator) at 20-100 °C. Carrier preparation involves air removal from the pores under vacuum to prevent disintegration of granules and treating it with competing substances to create adsorption centers of chemical type. This stage extends for 30-60 min. The second stage involves the adsorption of one or more constituents of the active phase on the prepared carrier in the circulation regime of the impregnating solution. When producing low-percentage catalysts, the process is carried out in gradient-free conditions with gradual dosing of concentrated solutions of active constituents into the circulation system at a rate that ensures uniform chemical composition all through the stationary carrier bed. This process extends for 30-90 min at 20-40 °C. At the end of sorption, the catalyst obtained is charged into the drying and baking system by conventional methods (Duplyakin, *et al.*, 1991).

The main drawback of these methods is the absence of consideration of physical and chemical principles and the optimum conditions of stages comprising the process, especially the fixing of the precursor of the active constituent on the carrier surface.

1.2.2 Dye and treatment method for dye pollutant

(1) Dyes

A dye can generally be described as a colored substance that has an affinity to the substrate to which it is being applied. The dye is generally applied in an aqueous solution, and may require a mordant to improve the fastness of the dye on the fiber. Both dyes and pigments appear to be colored because they absorb some wavelengths of light preferentially. In contrast with a dye, a pigment generally is insoluble, and has no affinity for the substrate. Some dyes can be precipitated with an

inert salt to produce a lake pigment, and based on the salt used they could be aluminum lake, calcium lake or barium lake pigments.

Coloration is a key factor in the commercial success of textile products, particularly those with high fashion content, especially garments, furnishings and upholstery. The business generated by the dye industry over the last two years was approximately US\$ 22 billion, and constituted a total employment of about 1.45 million people. Excluding fluorescent brighteners, the dye consumption per capita is approximately 150 g per year, serving an average consumption of textile fiber of about 14.0 kg per year per inhabitant. Despite, the high economic importance of the textile industry in the world, this industry is responsible for over 7×10^5 metric tons of about 10,000 different types of dyes on pigments produced each year. During dye use among the several industries responsible for pollution of the aquatic ecosystems, the textile dyeing and printing industries are major players, around a half of a ton of these dyestuffs are lost per day to the environment. Approximately 200 liters of water are required, for every kilogram of finished cotton fabric. The reactions necessary to fix these dyes to the fibers are not very efficient. Therefore, residual dyes, several types of chemicals and salts are dumped into the water and are discharged in the wastewater system. At least 15% of those not used dyes might enter the environment through effluents from wastewater treatment plants (Carneiro, *et al.*, 2004).

The first human-made (synthetic) organic dye, mauveine, was discovered by William Henry Perkin in 1856. Many thousands of synthetic dyes have since been prepared. Synthetic dyes quickly replaced the traditional natural dyes. They cost less, they offered a vast range of new colors, and they imparted better properties upon the dyed materials. Dyes are now classified according to how they are used in the dyeing process (Garfield, 2000).

(a) Acid dyes

Acid dyes are water-soluble anionic dyes that are applied to fibers such as silk, wool, nylon and modified acrylic fibers using neutral to acid dye baths. Attachment to the fiber is attributed, at least partly, to salt formation between anionic

groups in the dyes and cationic groups in the fiber. Acid dyes are not substantive to cellulosic fibers. Most synthetic food colors fall in this category.

(b) Basic dyes

Basic dyes are water-soluble cationic dyes that are mainly applied to acrylic fibers, but find some use for wool and silk. Usually acetic acid is added to the dye bath to help the uptake of the dye onto the fiber. Basic dyes are also used in the coloration of paper.

(c) Direct dyeing

Direct or substantive dyeing is normally carried out in a neutral or slightly alkaline dye bath, at or near boiling point, with the addition of either sodium chloride (NaCl) or sodium sulfate (Na₂SO₄). Direct dyes are used on cotton, paper, leather, wool, silk and nylon. They are also used as pH indicators and as biological stains.

(d) Mordant dyes

Mordant dyes require a mordant, which improves the fastness of the dye against water, light and perspiration. The choice of mordant is very important as different mordants can change the final color significantly. Most natural dyes are mordant dyes and there is, therefore, a large literature base describing dyeing techniques. The most important mordant dyes are the synthetic mordant dyes, or chrome dyes, used for wool; these comprise some 30% of dyes used for wool, and are especially useful for black and navy shades. The mordant, potassium dichromate, is applied as an after-treatment. It is important to note that many mordants, particularly those in the heavy metal category, can be hazardous to health and extreme care must be taken in using them.

(e) Vat dyes

Vat dyes are essentially insoluble in water and incapable of dyeing fibres directly. However, reduction in alkaline liquor produces the water soluble alkali metal salt of the dye, which, in this leuco form, has an affinity for the textile fibre. Subsequent oxidation reforms the original insoluble dye. The color of denim is due to indigo, the original vat dye.

(f) Reactive dyes

Reactive dyes utilize a chromophore attached to a substituent that is capable of directly reacting with the fibre substrate. The covalent bonds that attach reactive dye to natural fibers make them among the most permanent of dyes. "Cold" reactive dyes, such as Procion MX, Cibacron F, and Drimarene K, are very easy to use because the dye can be applied at room temperature. Reactive dyes are by far the best choice for dyeing cotton and other cellulose fibers at home or in the art studio.

(g) Disperse dyes

Disperse dyes were originally developed for the dyeing of cellulose acetate, and are substantially water insoluble. The dyes are finely ground in the presence of a dispersing agent and then sold as a paste, or spray-dried and sold as a powder. Their main use is to dye polyester but they can also be used to dye nylon, cellulose triacetate, and acrylic fibres. In some cases, a dyeing temperature of 130 °C is required, and a pressurised dyebath is used. The very fine particle size gives a large surface area that aids dissolution to allow uptake by the fibre. The dyeing rate can be significantly influenced by the choice of dispersing agent used during the grinding.

(h) Azo dyeing

Azo dyeing is a technique in which an insoluble azoic dye is produced directly onto or within the fibre. This is achieved by treating a fibre with both diazoic and coupling components. With suitable adjustment of dyebath conditions the two components react to produce the required insoluble azo dye. This

technique of dyeing is unique, in that the final color is controlled by the choice of the diazoic and coupling components.

(i) Sulfur dyes

Sulfur dyes are the most commonly used dyes manufactured for cotton in terms of volume. They are cheap, generally have good wash-fastness and are easy to apply. The dyes are absorbed by cotton from a bath containing sodium sulfide or sodium hydrosulfite and are made insoluble within the fiber by oxidation.

In the present work, methylene blue was selected as a model of dye pollutant with which the degradation efficiencies of the as-prepared catalysts are to be investigated.

Methylene blue (MB), (3,7-bis(dimethylamino)phenothiazin-5ium chloride), $C_{16}H_{18}ClN_3S$, is a brightly colored blue cationic thiazine dye, with λ_{max} values at 665, 614 and 292 nm. It has many uses in a range of different fields such as biology and chemistry. The uses of MB include being an antidote for cyanide poisoning in humans, antiseptic in veterinary medicine and, most commonly, in vitro diagnostic in biology, cytology, hematology and histology, it used as redox indicators in analytical chemistry. At room temperature it appears as a solid, odorless, dark green powder, that yields a blue solution when dissolved in water (Mills and Wang, 1999). The structure of MB is shown in Figure 5.

MB is used in endoscopic polypectomy as an adjunct to saline or epinephrine, and is used for injection into the submucosa around the polyp to be removed. This allows the submucosal tissue plane to be identified after the polyp is removed, which is useful in determining if more tissue needs to be removed, or if there has been a high risk for perforation. MB is also used as a dye in chromoendoscopy, and is sprayed onto the mucosa of the gastrointestinal tract in order to identify dysplasia, or pre-cancerous lesions. Intravenously injected methylene blue is readily released into the urine and thus can be used to test the urinary tract for leaks or fistulas. In surgeries such as sentinel lymph node dissections, MB can be used to visually trace the lymphatic drainage of pertinent tissues. Similarly, MB is added to bone cement in orthopedic operations to provide easy discrimination between native

bone and cement. Additionally, MB accelerates the hardening of bone cement, increasing the speed at which bone cement can be effectively applied (Steven, 2008).

The doubly reduced form of MB, leuco-methylene blue, i.e., LMB, is colourless (typically, $\lambda_{\max} = 256 \text{ nm}$) and stable in de-aerated aqueous solutions. The singly reduced form of MB, the semi-reduced radical, MB^{\bullet} , is pale yellow ($\lambda_{\max} = 420 \text{ nm}$) and readily disproportionates ($k = 3 \times 10^9 \text{ dm}^3 \text{ mol}^{-1} \text{ s}^{-1}$) to form MB and LMB, i.e.,



Less research has been conducted into the oxidised form of MB, i.e., $\text{MB}^{\bullet+}$, $\lambda_{\max} = 520 \text{ nm}$, which appears to be quite stable and it easily reduced back to MB in acidic solution, but decomposes irreversibly in slightly alkaline ($\text{pH} = 9.1$) solution. MB readily forms dimers in aqueous solution, i.e.,



A typical value for K_D , the equilibrium constant associated with the dimerisation process, is $3,970 \text{ dm}^3 \text{ mol}^{-1}$. The structures of most of the methylene blue-type compounds highlighted above are illustrated in Table 3 along with the associated pK_a and redox potential data (Mills and Wang, 1999).

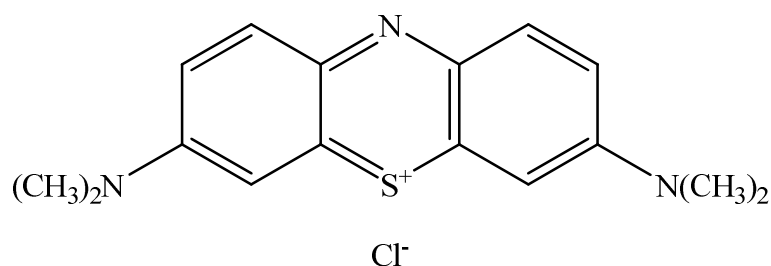
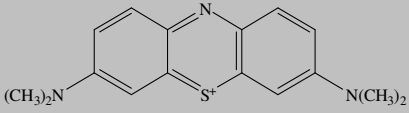
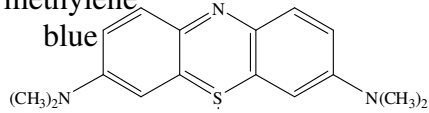
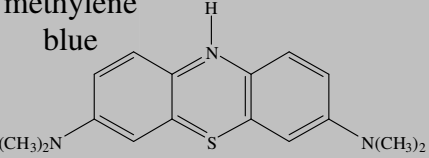
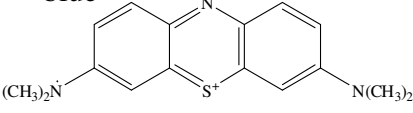


Figure 5 The structure of MB.

Table 3 Structures and UV-vis absorption characteristics of MB and its common reduced and oxidised forms (Mills and Wang, 1999).

Species	Structure	Abbreviation	pK _a	E ⁰ _{vs.NHE(V)}	λ _{max}	Other properties
Methylene Blue		MB	0		660, 614, 292	K _D = 3970 dm ³ mol ⁻¹
Semi-reduced methylene blue		MB ^{•-}	-3.29	(MB/MB ^{•-}) = -0.23	420	Readily disproportionates to form MB and LMB
Leuco methylene blue		LMB	4.5,5.8	(MB/LMB) = 0.011(pH7) and 0.532 (pH0)	562	
Oxidised methylene blue		MB ^{•+}		(MB ^{•+} /MB) = 1.08	52012	Stable in acid(pH1) and unstable at pH9

The photochemistry of MB has been widely studied. MB remains a popular dye sensitizer in photochemistry especially in the areas of singlet oxygen production and reductive electron transfer. The wide and varied use of MB in photochemistry is attributable to its relatively long-lived, triplet state, $\tau_T = 450 \mu\text{s}$, with its high probability of formation, $\phi_T = 0.52$, large energy (1.44 eV above the ground state) and high triplet oxidation potential E^0 (MBT / MB^{•+}) = 1.21 V versus NHE. The major photophysical and redox characteristics of MB are summarized in Table 4 (Mills and Wang, 1999).

Table 4 Photophysical properties of MB (Mills and Wang, 1999).

	Singlet: MB ¹	Triplet: MB ³
ϕ_T	-	0.52
E (excited state) (kJ mol ⁻¹)	180	138
τ	30-390 ps	450 μ s
ϕ (fluorescence)	0.04	-
E ⁰ (excited state/ MB ^{•-}) vs. NHE (V)	1.60	1.21

Given the well-established photochemical activity of MB, initially it might appear surprising to note that MB has often been used as a reactant in semiconductor photocatalysis. This surprise may well increase when it is realized that the semiconductor most often employed in such studied is TiO₂, a UV absorber. However, a brief inspection of the UV-vis absorption spectra of MB, illustrated in Figure 6 (solid line), reveal that MB absorbs a little light between 300 and 400 nm. The latter wavelength region is usually the region of illumination in TiO₂-sensitised semiconductor photocatalysis, since most UV irradiation sources used in such work are designed to emit light of $\lambda < 400$ nm, and most of the glassware used is Pyrex, which cuts off at 300-310 nm. To emphasize the latter point a little further, the relative emission intensity versus λ profile for one of the most common light sources in use in semiconductor photocatalysis, the blacklight bulb ($\lambda_{\max}(\text{emit}) = 355$ nm), is also illustrated in Figure 6 (dotted line). A brief inspection of the two spectra in Figure 6 reveals a marked lack of overlap. As a result, it is not surprising that most workers find that aqueous solutions of MB in the absence of TiO₂ and in the absence or presence of oxygen (Mills and Wang, 1999).

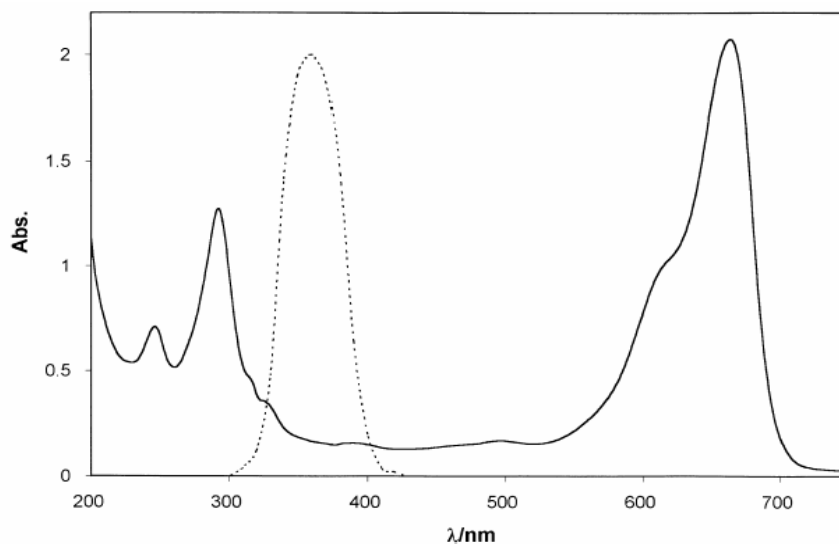


Figure 6 UV-vis absorption spectrum of MB aqueous solution (solid line) and the relative emitted light intensity (dotted line) for 8W blacklight bulb (Mills and Wang, 1999).

(2) Treatment of dye pollutant

Removal of color in wastewater generated by the textile industries is a color issue of discussion and regulation all over the world. Among the relative dyes, the textile azo dyes with synthetic intermediates as contaminant and its degradation products have undoubtedly attracted the most attention with regard to high environmental impact, because of their widespread use, their potentiality to form toxic aromatic products (carcinogenicity and mutagenicity properties) and their low removal rate during primary and secondary treatment. They represent about 50% of the worldwide production and correspond to an important source of contamination considering that a significant part of the synthetic textile dyes are lost in waste streams during manufacturing or processing operations. Therefore it is important to develop effective wastewater remediation technologies for these compounds (Senthikumaar, *et al.*, 2005).

Various chemical and physical treatment processes are currently proposed for these dyes. These largely fall into the categories of direct precipitation or elimination by adsorption, flocculation, membrane separation, coagulation and chlorination (Da browski, 2001; Fu and Viraraghavan, 2001). These methods have been largely incomplete and ineffective because the problem is not completely resolved, being required further treatment. A number of biological processes, such as sequenced anaerobic/aerobic digestion, have been proposed in the treatment of textile wastewater, but they are limited due to the fact that many of the dyes are xenobiotic and non-biodegradable. Alternative methods based on advanced oxidation processes combining ultraviolet irradiation and oxidative agents for dye treatment have been also investigated, but the presence of intermediates arising from the photodegradation reaction could be more harmful than the pollutant itself (Robinson, *et al.*, 2001).

In recent years attention has been focused on heterogeneous photocatalysis for the treatment of recalcitrant chemical present in the wastewater. Among these heterogeneous photocatalysis in the presence of irradiated semiconductors (TiO_2 , WO_3 , SnO_2 , ZnO , CdS and others), TiO_2 has been successfully used to decolorize and mineralize many organic pollutants including several dyes and their intermediates present in aqueous systems using both artificial light and under sunlight using solar technology (Muruganandham, *et al.*, 2005). TiO_2 is the most widely used photocatalyst because of its good activity, chemical stability, commercial availability and inexpensiveness. It is generally used as a photocatalyst for environmental applications such as air purification, water disinfection, hazardous waste remediation and water purification (Nagaveni, *et al.*, 2004).

The efficiency of advanced oxidation processes for degradation of recalcitrant compounds has been extensively documented. Photochemical processes are used to degrade toxic organic compounds to CO_2 and H_2O without the use of additional chemical oxidants, because the degradation is assisted by high concentrations of hydroxyl radicals (OH^\bullet) generated in the process. In this case, the photoexcitation of TiO_2 particles promotes an electron from the valence band to the conduction band, generating an electron/hole pair. Both reductive and oxidative processes can occur at or near the surface of the photoexcited TiO_2 particle. In

general, oxygen is used to scavenge the conduction band electron, producing a superoxide anion radical ($O_2^{\bullet -}$), effectively preventing electron/hole recombination, and prolonging the lifetime of the hole. The photogenerated hole has the potential to oxidize several substrates by electron transfer. In aqueous solutions, oxidation of water to hydroxyl radical by the photogenerated hole appears to be the predominant pathway. Hydroxyl radicals and, to a lesser extent, superoxide anion can act as oxidants, ultimately leading to the mineralization of organic compounds (Gomes de Moraes, *et al.*, 2000).

The mineralization of most of the organic pollutants could be degraded following the usually proposed mechanism (equations (3)-(11)), for the heterogeneous photocatalytic oxidation processes as shown in Figure 7.

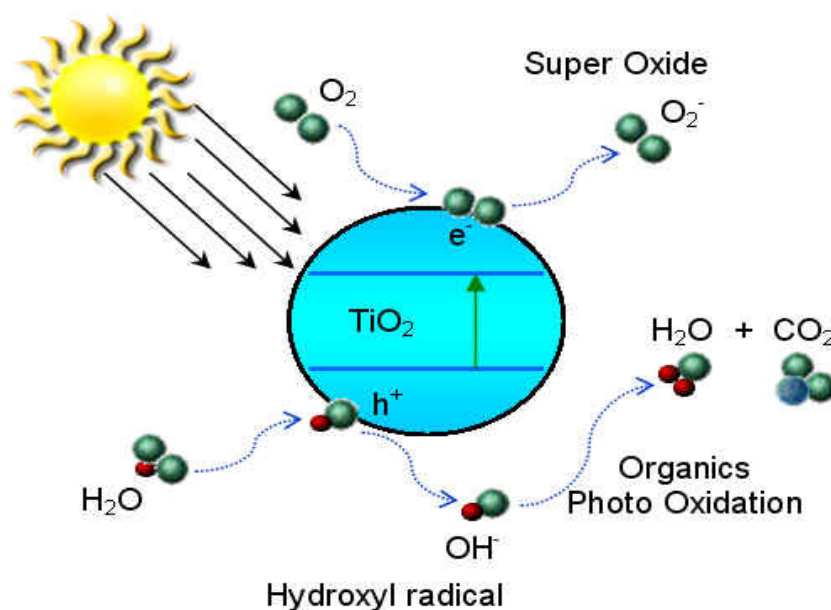


Figure 7 The heterogeneous photocatalytic oxidation processes of TiO_2 photocatalyst. (<http://puregreencoatings.com>)

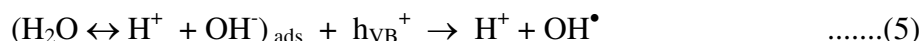
1. Absorption of efficient photons ($h\nu > E_g = 3.2 \text{ eV}$) by titania



2. Oxygen ionosorption (first step of oxygen reduction; oxidation state of oxygen changes from 0 to -1/2)



3. Neutralization of OH^- groups by photoholes which produces OH^\bullet radicals



4. Neutralization of $\text{O}_2^{\bullet-}$ by protons



5. Transient hydrogen peroxide formation and dismutation of oxygen



6. Decomposition of H_2O_2 and second reduction of oxygen



7. Oxidation of the organic reactant via successive attacks by OH^\bullet radicals



8. Direct oxidation by reaction with holes



As an example of the last process, holes can react directly with carboxylic acid generating CO_2



In most cases, the degradation is conducted for dissolved compounds in water with UV-illuminated titania. The possible extents of the technique concern the irradiation source and the physical state of the pollutant. Recently, many works have been reported on the degradation of organic dyes induced by visible light by photosensitization. The interest is to use solar visible light which is free and inexhaustible (Houas, *et al.*, 2001).

In the last 2 decades, many studies for TiO_2 , synthesis, doping TiO_2 , and photocatalytic degradation of MB, others textile dyes and pollutants by TiO_2 powder in aqueous suspension are as follows.

Anderson, *et al.*, (1995) synthesized mixed oxide of $\text{SiO}_2/\text{TiO}_2$ powders by sol-gel method. They also investigated the photodecomposition of

rhodamine-6G (R-6G). The powders prepared from the reaction of tetraisopropyl orthotitanate (TIOT) and tetraethoxysilane (TEOS). A mixture TIOT/TEOS with the desired Ti/Si ratio was prepared in a dry box, sealed, and then removed from the drybox. This solution was added dropwise to a solution of 250 mL anhydrous 2-propanol and 1 mL of concentrated HCl at 0 °C with vigorous stirring. The mixture was allowed to age at room temperature in a covered beaker for 1 week after gelling. Solvent was then removed under vacuum, and while still under vacuum, the catalysts were heated to 200 °C for 12 h. The resulting glassy material was ground in a mixture mill for 1 h. The products determined by XRD, BET surface area and UV-vis techniques. Their studies indicated that SiO₂/TiO₂ powders with weight ratio of 30/70 show more efficient photocatalyst about 3 times for the destruction of R-6G than Degussa P25 TiO₂. The presence of an adsorbent (SiO₂) promoted efficiency by increasing the quantity of R-6G near the TiO₂ sites relative to the solution concentration of R-6G. Photogenerated oxidants from TiO₂ had been shown to be mobile either in solution or on the surface of SiO₂.

Marci, *et al.*, (1996) prepared tungsten oxide/TiO₂ polycrystalline sample (W/Ti) by the sol-gel method. The mixed propan-2-ol solution of tungsten and titanium alkoxides were stirred and suddenly from a yellow suspension for 1 h. Then it was heated to reflux for 5 h giving a transparent pale-green solution. Different volumes of tungsten precursor solution (1.3, 2.6, 12.8, 25.7, and 51.4 mL) were added to the titanium alkoxide solution to obtain the desired W/Ti molecular ratios. All these solutions, together with a solution of titanium alkoxide without tungsten, used for obtaining the precursor of pure TiO₂, were hydrolyzed by adding diluted HCl solution in 10 mL of propan-2-ol. The resulting almost colorless solutions were stirred at room temperature for 24 h and aged in open vessels. Gelatin occurred after 2-3 days yielding pale-yellow gels. The gels were dried under reduced pressure for 7 days and then were ground and sieved, collecting a powder fraction with particle size < 200 μm. The powders obtained in this way were crystallized by heat treatment at 823 K for 15 h. After crystallization, the samples appeared to be different colors. The powder change from pale yellow to pale blue as the W/Ti ratio decreased, whereas the pure TiO₂ sample was white. These products have been characterized using several

techniques, namely TGA, GC, MS, GC-MS, XRD, XPS, SEM, and FT-IR. Moreover, W-TiO₂ samples have been employed as catalysts for 4-nitrophenol photodegradation in aqueous suspensions used as a probe reaction. The results indicate that the surface of the W/Ti particle is enriched with homogeneously dispersed tungsten as well as microcrystalline or amorphous species. A tentative explanation for the photocatalytic behavior of the samples has been provided, taking into account both the formation of surface layers of W species. The maximum photoactivity for 4-nitrophenol photodegradation was achieved for a sample containing 1.7 mol of W per 100 mol of Ti.

Ding, *et al.*, (1997) synthesized nanocrystalline TiO₂ by sol-gel method, and studied the influence of several factors during processing, such as hydrolysis catalyst used, hydrolysis degree, room temperature aging process, and some oxide dopants, on the microstructural evolution of these powders. The samples were investigated by TGA, XRD techniques. The product prepared by using tetrabutyl titanate (Ti(O-Bu)₄) as precursor and anhydrous ethanol was used as the solvent. Either hydrochloric acid or acetylacetone (C₅H₈O₂) was added to monitor the hydrolysis reaction of Ti(O-Bu)₄ in water. The molar ratio of these reactants was: Ti(O-Bu)₄ : H₂O : EtOH : catalyst (HCl or C₅H₈O₂) = 1 : r : 15 : 0.3 (r = 1 or 4 represents the hydrolysis water amount). In order to avoid strong hydrolysis reactions, Ti(O-Bu)₄ was diluted with half the prescribed amount of ethanol at first, then water and catalyst dissolved in the remaining ethanol were added dropwise to the ethanolic solution of alkoxide with continuous stirring. Through a sequence of hydrolysis and condensation reactions, the sol-gel transition took place gradually. The drying process of the wet-gel was performed in a vacuum tube (10⁻¹ Pa) furnace at 333 K for 5 h. After mechanically grinding for 10 min, the dry-gel powders were heat-treated at various temperatures for 2 h under oxygen atmosphere to obtain the nanostructure TiO₂ powders. During sample processing, most of the dry-gel powders were heat-treated soon after the preparation. In order to examine the effect of the room temperature aging process on the structural evolution of the as-prepared dry-gel powder, the dry-gel powder was sealed in a small glass bottle and heat-treated after 1 year. In preparation the doped TiO₂ powders, aluminum isopropoxide, tin

tetrachloride and ferric nitride were used as the precursors of alumina, tin oxide, and ferric oxide, respectively. At first, one of these doping precursors was added into the mixed solution of $\text{Ti}(\text{O-Bu})_4\text{-EtOH}$ and this mixture was stirred by a magnetic mixer and ultrasonic wave successively. The next steps were the same as those in the preparation of pure TiO_2 powders. The amount of dopants in the prepared powders was calculated to be 4 mol% according to the molar ratio between the precursors of TiO_2 and doping oxides. The characterization of the product was determined by XRD, TGA analysis. The results showed that the structural evolution of the powders could be significantly influenced by preparation conditions. In comparison with $\text{C}_5\text{H}_8\text{O}_2$ -catalyzed titanium dioxide gel, the HCl -catalyzed one crystallized into anatase at a much lower temperature, and the crystalline size is smaller after the same heat treatments. On the other hand, pure rutile phase could be more easily obtained in the $\text{C}_5\text{H}_8\text{O}_2$ -catalyzed gel. In the lower hydrolysis water content samples, the grain size was smaller, and the starting temperature of the anatase to rutile transformation was a little lower, in comparison with those higher water content samples. A long period of aging at room temperature evidently enhances the anatase to rutile transformation in the dry-gel powders. Some oxides additives, such as alumina, tin oxide and ferric oxide could effectively prevent the grain growth and quite different in anatase to rutile transformation in these nanocrystalline. Both tin oxide and ferric oxide dopants can enhance the anatase to rutile transformation, while alumina doping can significantly prevent this transformation.

Suresh, *et al.*, (1998) prepared TiO_2 powders by sol-gel method with acetic acid as a modifier at different pH conditions. The phase transformation during heat treatment was investigated by impedance spectroscopic measurements and the data were compared with those obtained from thermal analysis and XRD techniques. The sample was prepared by hydrolysis of 25 mL titanium isopropoxide dissolved in 48 mL acetic acid and was stirred for 0.5 h. To this solution 150 mL double distilled water was added dropwise under continuous stirring for 1 h. The pH was adjusted to 3 by adding 10 % ammonium hydroxide. The mixture was heat to 70 °C in an air oven to get a gel. Similar procedures were followed to prepare TiO_2 samples at pH values 4, 5 and 6. The studies showed that the anatase to rutile phase transformation was

delayed in the case of acetic acid modified gel precursor at pH 3 and 4, showing the presence of anatase phase even at 1,000 °C. On the other hand, in the sample precursor prepared at pH 6, anatase to rutile transformation was complete at 800 °C, under identical conditions of heat-treatment.

Xu, *et al.*, (1999) synthesized ultrafine TiO₂ particles by sol-gel method and studied the influence of particle size of TiO₂ on the photocatalytic degradation of MB in aqueous solution. The results suggested that the adsorption rate and adsorbability of MB on suspended TiO₂ particles increased as the particle sizes of TiO₂ decreased. Photocatalytic activity of TiO₂ also increased as the particle sizes of TiO₂ became smaller, especially when the particle size is less than 30 nm. The half-life of the photocatalytic degradation of MB also decreased as the particle sizes of TiO₂ decreased. The first order reaction rate constant for photocatalytic degradation of MB increased as particle size of TiO₂ decreased. The initial degradation rate of MB in a suspended model was higher than that of a fixed-bed model. This will overcome the difficulty of preparation of ultrafine TiO₂ particles. The industrialization of the TiO₂ suspended-type photoreactor will be easier once the problem of separation of fine TiO₂ particles is solved. The application of the ceramic membrane for this problem is now in progress and will be published.

Aruna, *et al.*, (2000) synthesized nanosized rutile TiO₂ particles by hydrothermal method. The synthesis involved was by adding an aliquot 5 mL of titanium isopropoxide and 5 mL of dry isopropanol dropwise to a well-stirred 40 mL solution of 0.5 M. HNO₃. The solution was stirred for 8 h whereupon the isopropanol was evaporated by heating the solution to 82 °C. The resulting solution was transferred into a Teflon container and placed in a titanium autoclave. The solution was stirred throughout the autoclaving period using a homemade magnet-based system. The autoclaving process was carried out at 250 °C for 26 h with a heating rate of 15 °C min⁻¹. Each synthesis was carried out twice, with and without stirring. The long aging experiments during the titanium dioxide synthesis involved the steps similar to above preparation but the pH of the solution was 0.5 in one case and 2.0 in the other and then the solutions were aged at room temperature for 6 months. As-prepared powders determined by XRD, TEM and BET surface area. The results

indicated that nanosize rutile TiO₂ particles had a diameter of 20 nm and large surface area about 45 m²/g with almost spherical shape and also relatively stable at high temperature. The significant effect of the stirring and long aging control experiments suggested that, at this composition, most of the condensation to TiO₂ occurred during the autoclaving step. The large colloid size distribution and the formation of anatase structure in the absence of stirring were attributed to the homogeneity developed in the solution under the extreme conditions of the hydrothermal process.

Ding, *et al.*, (2000) prepared a series of TiO₂ samples with different anatase-to-rutile ratios, and studied the roles of the two crystallite phase of TiO₂ on the photocatalytic activity in oxidation of phenol in aqueous solution. High dispersion of nanometer-size anatase in the silica matrix and the possible bonding of Si-O-Ti in SiO₂/TiO₂ interface were found to stabilize the crystallite transformation from anatase to rutile. The temperature for this transformation was 1,200 °C for the SiO₂/TiO₂ sample, much higher than 700 °C for Degussa P25 TiO₂. It is shown that samples with higher anatase-to-rutile ratios have higher activities for phenol degradation. However, the activity did not totally disappear after a complete crystallite transformation for P25, TiO₂ samples, indicating some activity of the rutile phase. Furthermore, the activity for the SiO₂/TiO₂ samples after calcinations decreased significantly even though the amount of anatase did not change much. The activity of the same samples with different anatase-to-rutile ratios is more related to the amount of the surface-adsorbed water and hydroxyl groups and surface area, leading to the decrease in activity.

Escobar, *et al.*, (2000) prepared Al₂O₃-TiO₂ materials by the sol-gel method using aluminium tri-*sec*-butoxide and titanium(IV) isopropoxide as precursors with different synthesis additives: HNO₃, NH₄OH, and CH₃COOH. The materials at two compositions: Al/Ti atomic ratio = 2 and 25 were synthesized at 278 K and calcined at temperature from 573 to 1,173 K. These solids were characterized by TGA, DTA, XRD, BET and SEM. The complexing (CH₃COOH) and the basic (NH₄OH) additives led to solids with high pore volumes and broad pore size distributions. On the one hand, very high surface area: 525 m²/g for solids calcined at 773 K was found for samples prepared with CH₃COOH. On the other hand, high

temperature stability was obtained with NH_4OH addition ($200 \text{ m}^2/\text{g}$, for Al_2O_3 -rich samples at 1,173 K). HNO_3 catalyzed samples showed lower surface areas and pore volumes. Surface areas and sintering behavior were a function of TiO_2 content. TiO_2 -rich samples showed higher surface area (773 K) than Al_2O_3 -rich samples, but at more severe conditions they suffered a severe specific area loss. The Al_2O_3 -rich formulations showed good stability in the whole range of temperature studied.

Harizonov, *et al.*, (2001) studied the mixed oxide system TiO_2/MnO prepared by the sol-gel method using titanium ethoxide and manganese nitrate as precursors. The xerogels of the solutions dried at $80 \text{ }^\circ\text{C}$ and treated at $560 \text{ }^\circ\text{C}$ in air for 1 h and then characterized by XRD, FT-IR, DTA and UV-VIS techniques. The results showed that the sol-gel method could be used to prepare good quality nanocrystalline TiO_2 coatings. In addition, the presence of MnO in TiO_2 xerogels was effective in decreasing the anatase-rutile transformation temperature. These coatings offered prospective applications in passive solar control glazing due to the relatively high refractive index.

Pal, *et al.*, (2001) studied the degradation of *o*-cresol sensitized by iron–titania binary photocatalysts. Fe/TiO_2 photocatalysts was investigated in oxygenated aqueous suspension in a spiral glass flow reactor. Iron–titania (1–10 wt% Fe) mixed catalysts have been prepared by sol–gel impregnation method using metal alkoxide precursors. The surface structure of Fe/TiO_2 catalyst was studied by surface analysis with XPS and TEM techniques. Characterization of these catalysts, fired at different temperatures (in the range $500\text{--}900 \text{ }^\circ\text{C}$) using X-ray diffraction (XRD) showed that the sintering temperature and incorporation of iron ions mediate the phase transformation and growth of pseudobrookite (Fe_2TiO_5) phase at higher temperatures. The rate of degradation of *o*-cresol decreases with the increasing sintering temperature and iron content of the catalysts and the initial pH of the aqueous solution of *o*-cresol changes with the illumination time due to the formation of various acidic intermediate photoproducts.

Ranjit, *et al.*, (2001) investigated the photocatalytic degradation of salicylic acid and *t*-cinnamic acid in aqueous suspensions of lanthanide oxide (Eu^{3+} , Pr^{3+} , Yb^{3+}) doped TiO_2 photocatalysts. Complete mineralization has been achieved in

the case of lanthanide oxide doped TiO₂ photocatalysts. The equilibrium dark adsorption of salicylic acid and *t*-cinnamic acid is *ca.* three times and two times higher, respectively, on the lanthanide oxide modified TiO₂ photocatalysts as compared to the non-modified TiO₂ catalyst. The enhance degradation is attributed to the formation of the lewis acid-base complex between the lanthanide ion and the substrates at the photocatalyst surface.

Yamazaki, *et al.*, (2001) reported novel TiO₂ pellets which were obtained from the preparation process of sol-gel method in sulfuric acid and also investigated the efficiency of these products for the photocatalytic degradation of ethylene. The samples were prepared by the hydrolysis of 45 mL Ti(OC₃H₇)₄ in 540 mL water containing 3.9 mL HNO₃, and the precipitation occurred immediately. Precipitates were stirred continuously at room temperature for 3 days. This peptization process formed a highly dispersed gel. This sol then dialyzed in a cleaned molecularly porous dialysis tube until a value of approximately pH 4 was obtained. The sol was concentrated in an oven at 40-50 °C for 2 days. The resulting gel was fired at 100-500 °C. On the other hand, when 2.6 mL H₂SO₄ was used instead of 3.9 mL HNO₃ to adjust pH in the precipitation methods, precipitates on hydrolysis were not dispersed to a colloidal solution during the precipitation for 10 days. The obtained fine precipitates were washed by repeating decantation to obtain a final pH of 3.7 and were filtered by aspirator. Finally, the solid was fired at 100-700 °C. As-prepared products were characterized by XRD, XPS, BET surface area, ion chromatography, hardness testers and UV-vis techniques. The results indicated that the use of sulfuric acid in the peptization process of sol-gel method produced sulphate ion incorporated TiO₂ which was mechanically strong by firing at 200 °C. Such oxide had larger surface area and retarded the phase transition from anatase to rutile compared with that prepared from the peptization with nitric acid. The XPS measurements indicated that sulfur exists mainly as sulphate ions. The titanium dioxide fired at 400 °C showed the highest photocatalytic activity for ethylene degradation. Especially, emphasized was put on the titanium dioxide sintered at 200 °C because it was extremely hard in spite of such a low sintering temperature.

This photocatalyst may provide a great potential for extensive applications as self-membranes.

Zhang, *et al.*, (2001) prepared nanocrystalline iron doped TiO₂ as a single-phase product by sol-gel method. The product synthesized from the reaction of titanium isopropoxide and Fe(NO₃)₃•9H₂O by varying the iron dopant amounts: 0, 1, 2, 3, 4, 5, and 6 at%. The mixture was aged at ambient temperature for a few days. During this time liquid became progressively more viscous and eventually a dry gel formed. Crystallization was achieved by subsequent calcination of the dry gel in air at different temperatures. By transmission, scanning, and analytical electron microscopy as well as by complementary techniques it has been found that the as-prepared solids exhibit a narrow size distribution and that the iron is homogeneously distributed in the TiO₂ matrix. The influence of the iron concentration on the phase transformations of the doped TiO₂ was investigated by X-ray diffractometer. The formation of the iron titanium dioxide pseudobrookite, Fe₂Ti₂O₅, was observed above 670 °C, but only for an iron content of more than 3 at%. UV-spectroscopic measurement revealed that the absorption spectrum of the iron doped TiO₂ is sensitively related to both the iron concentration and the calcination temperature. Whereas pure nanocrystalline TiO₂ undergoes grain growth (sintering) when the calcination temperature is increased, iron doped TiO₂ proves to be inert to grain growth, N₂ adsorption-desorption analysis indicated that the products calcined between 390 and 600 °C for 1 h in air have mesoporous structure and the distribution of mesopores are very narrowly, centered at 3.7 nm.

Arana, *et al.*, (2002) interested in degradation of carboxylic acids by using Fe-doped TiO₂ and studied the role of Fe²⁺/Fe³⁺ in photocatalytic partway. Results indicate that Fe is extracted by means of the formation of a [Fe-carboxylic acid]ⁿ⁺ complex by which the organic molecule is degraded. Fe²⁺ ions that remain in solution after the degradation go back to the catalyst surface due to their reaction with the photogenerated holes in the TiO₂. This way the catalyst is reactivated becoming ready for a new degradation process. XPS studies have confirmed these results. Also, it has been observed that the catalyst preparation method affects the photoactivity of the formed complexes. The catalyst with lower Fe content and prepared from

$\text{Fe}(\text{NO}_3)_3$ by the incipient wetness impregnation method degrades the formic acid more readily than the undoped catalyst and the catalysts prepared by other methods. Complexes formed by means of the iron interaction with formic and maleic acids are more photoactive than those formed with acetic or acrylic acids. The slower degradation of these last acids could be related with the photo-Kolbe reaction or other reduction processes. FTIR studies have been conducted with the goal of identifying the intermediates generated from the interaction of the different acids with the catalysts surface.

Chiang, *et al.*, (2002) synthesized Copper(II) oxide loaded onto the surface of Degussa P25 TiO_2 particles by photodecomposition. The doped sample was subsequently utilized as the photocatalyst for cyanide oxidation. The copper content on the TiO_2 surface was varied from 0.05 to 10.0 wt% of Cu. It was found that nanosized CuO deposited were present on the surface of TiO_2 . Modifying TiO_2 with CuO changed the optical properties of TiO_2 and the onset of absorption was red shifted. The photocatalytic activity of the CuO loaded TiO_2 was measured to determine their ability to oxidize cyanide. It was found that the rate of photooxidation of cyanide assisted with the doped catalyst was improved slightly at 0.10 wt% of Cu. Any further increase of the copper dopant concentration decreased the oxidation rate remarkably. The decrease in the activity was explained in terms of the competition reaction of Cu(II) cyanide complex ions for surface hydroxyl radical. In all cases cyanide was being oxidized to cyanate, the end product of cyanide photooxidation.

Di Paola, *et al.*, (2002) reported the preparation of TiO_2 polycrystalline powders loaded with some transition metal ions (chromium, cobalt, copper, iron, molybdenum, tungsten, and vanadium) by using the incipient wet impregnation method. The samples have been characterized by X-ray diffractometry (XRD), specific surface area determinations, measurements of the point of zero charge (pzc), scanning electron microscopy (SEM) coupled with electron microprobe used in an energy dispersive mode (EDX), and femtosecond pump-probe diffuse reflectance spectroscopy (PP-DRS). The photoactivity of the samples was tested for 4-nitrophenol photodegradation in aqueous medium, chosen as a probe reaction. The results of 4-nitrophenol photodegradation have shown that loading TiO_2 with Co, Cr,

Cu, Fe, Mo, and V causes a decrease of the TiO₂ HP photocatalytic activity, and this effect was more significant as the amount of loaded metal increased. The samples containing tungsten revealed reaction rates higher than that of pure TiO₂, with a maximum between 1 and 2 at% and a slightly lower photoactivity for TiO₂/W/0.3. These results are in agreement with previous studies performed by using powders prepared by the sol-gel method or by wet impregnation of P-25 Degussa TiO₂. The photoactivity of the powders roughly decreases according to the following sequence: TiO₂/W > TiO₂/Mo > TiO₂/Cu > TiO₂/Fe ~ TiO₂/Co > TiO₂/V > TiO₂/Cr.

Matsuo, *et al.*, (2004) examined the defect of simply adsorbed Sm, Eu, and Yb ions on TiO₂ (Ln/TiO₂) and Fe ions adsorbed onto TiO₂ (Fe/TiO₂) from the photocatalytic decomposition of adenosine 5'-triphosphate (ATP) as an anionic substance, 2-propanol as a neutral substance, and MB as a cationic substance. The amount of ATP disappearing in 40 min of reaction in the presence of Ln/TiO₂ increase in the order: Ln- Sm < Eu < Yb. For 2-propanol, the photocatalytic activity of Ln/TiO₂ catalyst were similar to that of unmodified TiO₂ (u-TiO₂) catalyst. For MB, the photocatalytic activities of Ln/TiO₂ catalyst were less than that of u-TiO₂ catalyst. By contrast, Fe/TiO₂ catalyst was excellent in photocatalytic decomposition of ATP, 2-propanol and MB. The photocatalytic activity of Yb/TiO₂-C calcined at 500 °C for 1 h decreased for ATP, slightly decreased for 2-propanol, and increased for MB compared with Yb/TiO₂. Photocatalytic activities of Fe/TiO₂-C for ATP, 2-propanol and MB were all less than that of Fe/TiO₂. Since EXAFS revealed that the coordination structure around Yb(III) ions on the surface of TiO₂ in Yb/TiO₂ was like a hydrated structure including chloride ions, and that in Yb/TiO₂-C was like an oxide structure, the difference in photodegradation between Fe/TiO₂ and Fe/TiO₂-C is believed to be a result of the coordination structure around Fe(III) ions on the surface of TiO₂. These facts together suggest that the selectivity of photocatalytic decomposition for target substances can be controlled and is a combination of the properties of adsorbed metal ions (e.g. ionic radius, d-electron or f-electron, redox potential) and the coordination structure of their ions on the surface of TiO₂. In the present study, Sm/TiO₂, Eu/TiO₂, and Yb/TiO₂ are more selective toward anionic

substances than Fe/TiO₂, which is excellent for decomposition of ionic and neutral substances.

Nagaveni, *et al.*, (2004) investigated the solar photocatalytic degradation of various dyes such as MB, remazol brill blue R (RBBR) and orange G (OG) over combustion synthesized nano-TiO₂ and the activity was compared with that of commercial Degussa P25 TiO₂ under similar conditions. The effect of catalyst loading, initial concentration of the dye and the deactivation studies of the catalysts were also investigated. The catalyst was characterized by techniques like X-ray diffraction (XRD), gravimetric-differential thermal analysis (TG-DTA), BET, IR and UV absorption. The initial degradation rate with combustion synthesized nano-TiO₂ was 20 times higher for RBBR, 4 times higher for MB and 1.6 times higher for OG, compared to Degussa P25 TiO₂. The enhanced photocatalytic of combustion synthesized catalyst is attributed to the crystallinity, nano-size, large amount of surface hydroxyl species and reduced band-gap.

Stylidi, *et al.*, (2004) investigated the photocatalytic degradation of Acid Orange 7 (AO-7) in aqueous TiO₂ suspensions with the use of a solar light simulating source. The photoreaction was followed by monitoring the degradation of the dye and the formation of intermediates and final products, as a function of time of irradiation, both in solution and on the photocatalyst surface. It has been found that the process leads to decolorization and, eventually, to complete mineralization of the dye solution. Evolution of intermediates and final products on both the photocatalyst surface and the solution has been monitored with a variety of techniques, which enable the identification of the reaction pathway, from adsorption of the dye molecule on the photocatalyst surface, to the formation of final products. AO-7 adsorbs on the photocatalyst surface via the oxygen of its hydrazone form and the two oxygen atoms of the sulfonate group. Interaction with solar light results, initially, in cleavage of the dye molecule in the vicinity of the azo bond and the formation of molecules containing naphthalene- and benzene- type rings. This step, which takes place, to a significant extent, via the photosensitized mechanism, results in decolorization of the solution but is not accompanied by significant decrease of the COD.

Sung-Suh, *et al.*, (2004) examined the photocatalytic degradation of the rhodamine B (RB) dye in aqueous suspensions of TiO₂ and Ag-deposited TiO₂ nanoparticles under visible and UV light irradiation. The Ag deposits significantly enhanced the RB photodegradation under visible light irradiation whereas the RB photodegradation under UV irradiation was slightly enhanced. The significant enhancement in the Ag-TiO₂ photoactivity under visible light irradiation can be ascribed to simultaneous effect of Ag deposits by both acting as electron traps and enhancing the RB adsorption on the Ag-TiO₂ surface.

Wu, *et al.*, (2004) synthesized vanadium doped TiO₂ catalysts by sol-gel method. The results show that the increase of vanadium doping promoted the particle growth, and enhanced red-shift in the UV-Vis absorption spectra. The photocatalytic activity was evaluated by the degradation of crystal violet (CV) and MB under visible light irradiation. The degradation rate of CV and MB on V-doped TiO₂ were higher than those of pure TiO₂.

Faisal, *et al.*, (2005) investigated the photocatalytic degradation of two selected dyes, such as Acridine Orang (1) and Ethidium Bromide (2) in aqueous suspension of TiO₂ under a variety of conditions, which is essential from application point of view. The degradation was monitored by measuring the change in substrate concentration as a function of irradiation time employing UV spectroscopy analysis technique. The degradation was studied using different parameters such as type of TiO₂, reaction pH, catalyst concentration, substrate concentration and in the presence of different electron acceptors such as hydrogen peroxide (H₂O₂), potassium bromate (KBrO₃) and ammonium persulphate (NH₄)₂S₂O₈) beside air. The degradation rates were found to be strongly influenced by all the above parameters. The photocatalyst, Degussa P25, was found to be more efficient for the photocatalytic degradation of dye derivative (1) and (2). The dye derivative (1) was found to degrade faster as compared to the dye derivative (2).

Muruganandham, *et al.*, (2005) investigated the photocatalytic decolorization and degradation of an azo dye Reactive Yellow 14 (RY14) in aqueous solution with TiO₂-P25 (Degussa) as photocatalyst in slurry using solar light. The study on the effect of various photocatalysts on the decolorization and degradation

reveals the following order of reactivity: $\text{ZnO} > \text{TiO}_2\text{-P25} > \text{TiO}_2$ (anatase). CdS , Fe_2O_3 and SnO_2 have negligible activity on RY14 decolorization and degradation. The effects of various parameters such as catalyst loading and initial dye concentration play an important role affecting the reaction rate on the decolorization and degradation. A study on the effect of electron acceptors on photooxidant reveals that both decolorization and degradation increase in the presence H_2O_2 , $(\text{NH}_4)_2\text{S}_2\text{O}_8$ and KBrO_3 to certain dosage beyond which the enhancement effect is negligible. Addition of dye assisting chemical such as CO_3^{2-} and Cl^- inhibits the dye removal rate.

Qamar, *et al.*, (2005) investigated the photocatalytic degradation of two selected dye derivatives, chromotrope 2B (1) and amido black 10B (2) in aqueous suspension of TiO_2 under a variety of conditions which is essential from an application point of view. The degradation was monitored by measuring the change in substrate concentration as a function of irradiation time employing UV spectroscopic analysis. In these studies, a number of byproducts are formed during the photooxidation process which can potentially be harmful to the environment, therefore, we have studies the mineralization of the pollutants by measuring the total organic carbon (TOC) as a function of irradiation time. The degradation was studied using different parameters such as type of TiO_2 , reaction pH, catalyst concentration, substrate concentration and in the presence of different electron acceptors such as hydrogen peroxide (H_2O_2), potassium bromate (KBrO_3) and ammonium persulphate ($(\text{NH}_4)_2\text{S}_2\text{O}_8$) besides molecule oxygen. The degradation rates were found to be strongly influenced by all the above parameters. The photocatalyst Degussa P25 was found to be more efficient as compared with other catalysts. The dye derivative (1) was found degrade faster as compared to the dye derivative (2).

Senthilkumar, *et al.*, (2005) prepared nanocrystalline pure anatase titania by sol-gel process at room temperature followed by ultrasonication (Ti-US). The photocatalytic activity of Ti-US has been evaluated by the degradation of textile dye, Methylene Blue in presence and absence of common inorganic salts (NO_3^- , $\text{C}_2\text{O}_4^{2-}$, SO_4^{2-} , and citrate). It was observed that, in presence of anions, the degradation of the dye increase significantly. The photocatalytic rate of methylene blue increased

in presence of hydrogen peroxide (H_2O_2). The dependence of photodegradation of the dye rate on various parameters such as dye concentration, photocatalyst concentration and pH were also observed. The photodegradation rate follows first order kinetic. H_2O_2 and UV light have a negligible effect in absence of Ti-US catalyst.

Bizani, *et al.*, (2006) investigated the photocatalytic degradation of two commercial azo dyes in the presence TiO_2 suspensions as photocatalyst. The degradation of the dyes follows pseudo-first order kinetics according to Langmuir-Hinshelwood model. Under the certain experimental conditions, in the presence of TiO_2 P-25 decolorization is achieved within 100 min of illumination, while in the presence TiO_2 Hombikat UV-100 complete color disappearance is accomplished in less than 50 min of light exposure. Parameters, such as concentration of the catalyst or initial pH value play an important role affecting the reaction rate. The mineralization of the two dyes was determined by measuring the dissolved organic carbon of the dye solutions and by evaluating toxicity. Although DOC was almost 80 % removed after 5 h of illumination, the toxicity of the solution is slightly decreased in the presence of the catalyst and the oxidant, but the intermediate degradation products seem to be more toxic than the initial compound. The application of the TiO_2 photocatalytic method to real wastewater proved to be efficient in decolorizing the wastewater (complete decolorization within 6 h of illumination) and it achieved partial DOC and toxicity removal (29 % DOC and 35 % toxicity removal for a 6 h illumination period).

Silva, *et al.*, (2006) investigated the degradation of three commercially available textile azo dyes, Solophenyl Green BLE 155 % (SG), Erionyl Red B (ER) and Chromotrope 2R (C2R) by using photochemical and photocatalytic process under UV irradiation. The adequacy of each process depends on the concentration of dye. At low dye concentration, the neat photochemical degradation is very efficient. The photocatalytic process, using either slurry of Degussa P-25 TiO_2 or a biphasic mixture of TiO_2 and activated carbon (AC), more effectively bleaches heavier colored solutions. The heterogeneous photocatalytic regime was characterized in terms of catalyst load, TiO_2 to AC mass ratio, initial dye concentration and oxygen partial pressure. The efficiency of the different photo-induced degradation process was evaluated in terms of apparent rate constants, mineralization degrees and initial

quantum yields. Overall, the results revealed the superiority of photocatalytic process over neat photolysis and the advantage of using a suspension of TiO₂+AC mixture instead of TiO₂ alone.

Toor, *et al.*, (2006) investigated the adsorption and photocatalytic degradation of diazo Direct Yellow 12 (Chrysophenine G), commonly used as a cotton, paper and leather in aqueous suspension of semiconductor oxide TiO₂ as photocatalyst in a non-concentrating shallow pond slurry type reactor under UV light. The adsorption of dye on the semiconductor shows a strong dependence on the pH and follows a Langmuir adsorption model. The studies include dark adsorption experiments at different pH conditions and their effect on initial rate of photocatalytic degradation. The photodegradation of dye on the semiconductor shows dependence effects of initial concentration of dye, catalyst loading, pH and addition of oxidant. The disappearance of the organic molecule follows approximately a pseudo-first kinetic order according to the Langmuir-Hinshelwood model. COD analysis of the dye under optimum conditions showed 94 % reductions in COD after 2.5 h and complete decolorization as determined by UV-vis analysis was achieved in 1.5 h.

Baiju, *et al.*, (2007) studied photocatalytic activity of nanocrystalline TiO₂ by measuring decomposition of the MB dye under exposure to the ultraviolet (UV) radiation ($\lambda = 200-400$ nm) in an aqueous solution. The results showed nanocrystalline TiO₂ powders in an aggregated form, having different morphology, average nanocrystalline size, surface area, crystalline, and phase structure, have been successfully synthesized via the sol-gel technique using an alkoxide precursor and varying the *R* value within the range of 5-60 and calcining the powders at higher temperatures within the range of 400-800 °C. The sol-gel-derived nanocrystalline TiO₂ powder, processed under different conditions, is shown to be an effective photocatalyst at room temperature for the decomposition of the MB dye in an aqueous solution under the UV radiation exposure.

Mora, *et al.*, (2007) studied morphological, optical and photocatalytic properties of TiO₂-Fe₂O₃ multilayers, the layers were deposited on glass substrate by the sol-gel method. The catalytic activity of the samples was studied by the photodecomposition of MB under visible light illumination. According to the results

of the photodecomposition of MB by TiO_2 , Fe_2O_3 and the $\text{TiO}_2\text{-Fe}_2\text{O}_3$ samples we conclude that the $\text{TiO}_2\text{-Fe}_2\text{O}_3$ is more photoactive than the single TiO_2 and Fe_2O_3 catalysts. The photocatalytic activity of the samples is increased as the number of constituent coatings is increased. The Fe_2O_3 is more photoactive than the TiO_2 catalyst and the reaction mechanism could be explained by means of a Fenton reaction in which the Fe^{3+} and the FeOH^{2+} play an important role.

Suriye, *et al.*, (2007) studied the effect of surface sites of TiO_2 support on the formation of cobalt-support compound in Co/TiO_2 catalysts. The effect of surface species (as a Ti^{4+} and Ti^{3+} on TiO_2 support) on the cobalt-support compound formation (Co-SCF) was investigated on the Co/TiO_2 catalyst. It revealed that the Co-SCF preferred to form on Co/TiO_2 catalyst when the most proportion surface site of TiO_2 support became Ti^{4+} . Based on ESR spectra, it was demonstrated that the Co-SCF had a simple chemical form as a $\text{CoO}(\text{H}_x\text{TiO}_y)$. This compound reached to be a higher non-uniform structure when the number of Ti^{4+} on TiO_2 surface increased. These are the promising knowledge that should be used to develop the characteristics of Co/TiO_2 catalyst especially the formation of Co-SCF. The number of Ti^{4+} should be decreased as much as possible to prevent the formation of such the compound. It might be done by treating the TiO_2 surface prior to preparing the Co/TiO_2 catalyst

Yuan, *et al.*, (2007) studied the Effect of metal ion dopants on photochemical properties of anatase TiO_2 films synthesized by a modified sol-gel method. TiO_2 samples were derived from TiCl_4 /ethanol/water solution at room temperature. The as-prepared films were further surface-doped by photodeposited Fe_2O_3 and Cr_2O_3 to improve its physicochemical properties. The phase and structure of the films were investigated by X-ray diffraction, scanning electron microscopy and X-ray photoelectron spectroscopy. The results show that both hydrophilicity and photocatalytic activity of the films were remarkably improved by doping transition metal ion Fe^{3+} . In case of Cr^{3+} doped films, hydrophilicity was also significantly enhanced but photocatalytic activity for methyl orange under UV irradiation was still comparable with the undoped films.

Baran, *et al.*, (2008) studied the effect of UV radiation absorption of cationic and anionic dye solutions on their photocatalytic degradation in the presence

TiO₂. The aim of the study was to examine the correlation between the absorbance of various cationic and anionic dye solutions exposed to UV radiation and their photocatalytic degradation in solution. The dye solutions were illuminated with UV radiation in the presence of a TiO₂ aqueous suspension. Photodegradation rate constant and adsorption efficiency of dyes were determined using spectrophotometric methods. The results showed that only cationic dyes can be adsorbed on the surface of the photocatalyst; simultaneously, their photocatalytic degradation is faster than the degradation of anionic dyes. The change of the nature of the dye particle from inert to cationic causes intensification of its adsorption and acceleration of photodegradation. There is a linear correlation between the absorbance of the illuminated dye solution and the photodegradation rate constant.

Fan, *et al.*, (2008) reported in the structural, physical and photocatalytic properties of the mesoporous Cr-doped TiO₂. Cr-doped TiO₂ was synthesized using an evaporation-induced self assembly approach and characterized by X-ray powder diffraction, nitrogen adsorption–desorption, X-ray photoelectron spectroscopy, transmission electron microscope, and UV–vis diffuse reflectance techniques. The characterizations indicated that the photocatalysts possessed a homogeneous pore diameter of about 8 nm with high surface area of 117 m²/g and a crystalline anatase pore wall doped by Cr³⁺. Compared with pure mesoporous TiO₂, the Cr-doped TiO₂ extended the photo-absorption edge into the visible light region. The results of gaseous acetaldehyde photodecomposition showed that mesoporous Cr-doped TiO₂ exhibited higher photocatalytic activities than pure mesoporous TiO₂ and nonporous Cr-doped TiO₂ under visible light irradiation.

Suwanchawalit and Wongnawa, (2008) studied the influence of calcination temperature on microstructures and photocatalytic activity of potassium oxalate dope TiO₂ powder. The TiO₂ samples were prepared by the base-catalyzed sol-gel process and then characterized with XRD, SEM, TEM, BET, FT-IR, DRS, and UV-vis techniques. Moreover, investigation on the photocatalytic activity was determined based on degradation of MB aqueous solution under UV light irradiation. Results indicated that the optimum calcination temperature of 800 °C yielding samples with enhanced photocatalytic activity compared to Degussa P25. On the other

hand, the non calcined TiO_2 , existed in amorphous phase with small of anatase phase, produced a better decolorization efficiency than did commercial P25, due to its excellent adsorptivity with high concentration of MB solution. More significantly, the dyed adsorbed onto the surface of the non-calcined TiO_2 samples could be removed by treating with H_2O_2 solution under UV irradiation.

All of photocatalytic studies on TiO_2 have focused their studies on the crystalline forms, as it is commonly accepted that amorphous TiO_2 contains high concentration of defects that will invariably function as rapid electron - hole pairs recombination centers to render them inactive (Ohtani, *et al.*, 1997). However, amorphous TiO_2 has one interesting property: the high surface area which can lead to high adsorptivity.

Up to date, there have been only a few reports that studies or show interest in amorphous TiO_2 .

Randorn, *et al.*, (2004) prepared hydrated TiO_2 (h- TiO_2) powder by hydrolysis of TiCl_4 with concentrated NH_3 solution and studied the photocatalytic activity in aqueous of MB dye under UV light irradiation. Moreover, investigation was extended to the effect of H_2O_2 on photodecomposition of MB. The synthesized powder was studied using XRD, FT-IR, BET, and TGA techniques. The characterized results indicating that TiO_2 appeared in amorphous form with some hydrated molecules. Due to its considerably high surface area of h- TiO_2 , could be adsorbed a large amount of MB on its surface, about nine times as much of Degussa P25. It could photocatalyze the decomposition of MB, albeit slightly inferior to Degussa P25 if adsorption is excluded. In the presence of dilute H_2O_2 and with UV light, h- TiO_2 can bleach methylene blue as well as Degussa P25. However, under similar conditions, but without UV light, h- TiO_2 can bleach methylene blue much better than Degussa P25.

Kanna, *et al.*, (2005) studied the adsorptivity of some transition metal ions (Mn(II), Fe(III), Cu(II), and Pb(II)) on amorphous TiO_2 powder. TiO_2 was prepared from TiCl_4 and diluted ammonia solution at low temperature. The product obtained was characterized by XRD, EDXRF, TGA, DSC, and FT-IR techniques. It was found that the product was in the form of hydrated amorphous TiO_2 , $\text{TiO}_2 \cdot 1.6\text{H}_2\text{O}$

(ha-TiO₂). The ha-TiO₂ exhibits high BET surface area at 449 m²/g. Adsorptions of metal ions onto the ha-TiO₂ surface were investigated in the batch equilibrium experiments, using Mn(II), Fe(III), Cu(II), and Pb(II) solutions. The concentrations of metal ions were determined by atomic absorption spectrometer. The adsorption isotherms of all metal ions were studied at pH 7. The adsorption of Mn(II), Cu(II), and Pb(II) ions on ha-TiO₂ conformed to the Langmuir isotherm while that of Fe(III) fit equally well to both Langmuir and Freundlich isotherms.

Zhang and Maggard, (2007) investigated photocatalytic activity of amorphous TiO₂ powder by measuring the H₂ produced in methanol solutions under Xe arc lamp. TiO₂ have been obtained starting from Ti(*n*-butoxide)₄ in ethanol, acetone, hexane or tetrahydrofuran solutions by either slow evaporation (TiO₂-A1) or from rapid precipitation in an aqueous HCl solution using ammonia (TiO₂-A2). The samples were characterized by using PXRD, SEM, TGA, DRS, GC, and FT-IR techniques. The washed products lost/reabsorbed water up to a maximum of 19 wt% for samples of TiO₂-A1 and 9.9 % for TiO₂-A2, and exhibited an optical band gap of ~3.5 eV. Under full spectrum irradiation in aqueous of methanol solutions, the photocatalytic rates for H₂ production reached a maximum of 314 and 1,158 μmol h⁻¹ g⁻¹ for bare and platinized (0.5 wt%) samples of TiO₂-A1, respectively, and 210 and 170 μmol h⁻¹ g⁻¹ for TiO₂-A2. The photocatalytic rates measured at a slightly elevated temperature of 58 °C were up to 2 times greater than those measured nearer room temperature, while these rates were independent of the amount or type of solvent used in their preparation. The UV-vis diffuse reflectance, post irradiation, indicate a higher concentration of Ti³⁺ sites in TiO₂-A1 compared to TiO₂-A2, and thus a higher density of active sites and reduced electron-hole recombination.

Li, *et al.*, (2008) studied adsorption and degradation of the cationic dyes over Co doped amorphous mesoporous titania-silica catalyst under UV and visible light irradiation. Undoped and Co dope TiO₂ were prepared followed: 5.0 g of cetyltrimethyl-ammonium bromide (CTAB) was added to 66 ml solution containing 1.0 g sodium hydroxide. Then, 10 ml of tetraethylorthosilicate (TEOS) was added to it slowly and get a clear gel, finally, the cobalt precursor (Co(NO₃)₂•6H₂O) and titanium tetraisopropoxide (TTIP) were also alternatively and slowly added to the above gel

and stirred for 2 h. The resulting gel was transferred into a Teflon bottle and treated under autogenous pressure without stirring at 363 K for 7 days. The final solid product was filtrated, dried, and calcined at 723 K for 24 h. The final product was denoted as Co-TiO₂-SiO₂. The catalyst was characterized by a combination of various physicochemical techniques, such as N₂ physisorption, diffuse reflectance UV-vis, X-ray diffraction, and FT-IR. And studied the photodegradation of six cationic dyes (gentian violet, methyl violet, methylene blue, fuchsin basic, safranin T, and Rhodamine B) under UV and visible light illumination. Co-TiO₂-SiO₂ exhibited activity under UV light and had better activity under visible light when compared with that of Degussa P25. The activity of Co-TiO₂-SiO₂ was also compared with that of Co-MCM-41, Co doped mesoporous titania with a crystalline framework (Co-MTiO₂) and titania-loaded Co doped MCM-41 (TiO₂/Co-MCM-41) for the degradation of gentian violet under visible light irradiation. It was also found that the degradation rates of Co-TiO₂-SiO₂ for gentian violet, methyl violet, methylene blue, fuchsin basic and safranin T were greater in alkaline media than in acid and neutral media, while it did not exhibit any significant activity for the photodegradation of Rhodamine B in alkaline media or in acid media under visible light irradiation.

The metal oxide such as TiO₂ has received a lot of attention as a promising material for photocatalyst, liquid solar cell and degradation of pollutants. The photocatalytic efficiency of TiO₂ depends partially upon the relative degree of branching of the relative electron-hole pairs into interfacial charge-transfer reactions (Wu, *et al.*, 2004). However, the wide spread use of titania is limited due to the wide band gap (3.2 eV, anatase crystalline TiO₂), which requires ultraviolet (UV) irradiation for its photocatalytic activations. Moreover, the UV light accounts for only *ca.* 4 % compared to *ca.* 45 % visible in solar energy spectrum. So, any shift in optical response from UV to visible range will have profound positive effect on photocatalytic efficiencies of the TiO₂ materials. Two approaches have been applied to extend the shift of photoresponse towards visible range of the titania materials: one direction is doping of metal ions, anions and synthesis of reduced form of TiO_x photocatalysts; and the other is ion implantation. Unfortunately, the ion implantation

is quite expensive and possible only in the high crystalline TiO₂. In recent years, doping with transition metal elements have been attempted to improve TiO₂ catalyst with visible-light response because transition elements have many valences and trace transition metal ions doped in the TiO₂ matrix can be superficial potential trap of photogenerated electron - hole pairs, then lengthen the lifetime of electrons and holes and increase photocatalytic activity (Reddy, *et al.*, 2002)

Many transition metal ion dopants have been investigated previously for the TiO₂ system, all of these, two transition metals, Cr(III) and Fe(III), have been most widely chosen as dopants on crystalline TiO₂, both anatase and rutile, but never seen in amorphous form.

The addition of a low percentage of metal was often proposed to improve the photocatalytic activity of TiO₂. The metal may be introduced through different ways;

(a) Doping, i.e. molecular combination of metal oxide in the lattice of TiO₂. This process is expected to modify the band gap of the photocatalyst.

(b) Metallization, i.e. deposition of noble metal on TiO₂.

(c) Impregnation of TiO₂ with a salt of metal followed by evaporation, i.e. deposition of small amount of salt on TiO₂ surface.

(d) Addition of low concentration of transition metal to the solution of substrate to be treated (Rao, *et al.*, 2003)

In this work we focused on trying to turn inactive amorphous TiO₂ to an active form by doping with trivalent transition metal ions (Cr, Fe) via sol-gel incipient wetness impregnation processes. The surface morphology was studied by using scanning electron microscopy (SEM), and transmission electron microscopy (TEM). The X-ray diffraction (XRD) was used to study crystalline phase identification and confirms structures of TiO₂ samples. The effect of various parameters such as dopant concentrations, doping time, and drying time were studied to optimize the preparation of trivalent (Cr, Fe) doped TiO₂ for maximum photocatalytic degradation of MB dye in aqueous solutions under UV and visible light irradiation, and comparing with the commercial TiO₂ powders (anatase; Carlo Erba, Italy and Degussa P25; Degussa AG, Germany). We hoped that the inclusion of these

dopants might improve the photocatalytic properties of amorphous TiO_2 when activated with UV or visible light. Activation by the latter is more preferred as it would be useful in real life applications with lower cost of operations.

1.3 Objectives

- 1.3.1 To study the optimum conditions for preparing trivalent (Cr, Fe) doped on amorphous TiO_2 powder by incipient wetness impregnation method.
- 1.3.2 To study some physical properties and photocatalytic activities of the as-prepared doped TiO_2 powder, and compare with the commercial TiO_2 powder catalysts under the same conditions.
- 1.3.3 To study the effect of various factors, such as pH, initial concentration of MB solution and the intensity of UV light on the photocatalytic degradation of the as-prepared doped TiO_2 powder.

Chapter 2

Methodology

2.1 Materials

- 2.1.1 Ammonium hydroxide (Ammonia solution), 28.0-30.0%, NH_4OH , A.R., code no. 9721-03, J.T. Baker, U.S.A.
- 2.1.2 Chromium (III) chloride hexahydrate, $\text{CrCl}_3 \cdot 6\text{H}_2\text{O}$, A.R., code no. 27096, Fluka, Switzerland.
- 2.1.3 Hydrochloric acid, HCl , A.R., code no. 9535-03, J.T Baker, U.S.A.
- 2.1.4 Iron (III) chloride anhydrous, FeCl_3 , Laboratory Reagent, code no. 220-250G, UNILAB, Australia.
- 2.1.5 Methylene blue, $\text{C}_{16}\text{H}_{18}\text{N}_3\text{SCl} \cdot 2\text{H}_2\text{O}$, Laboratory Reagent, code no. 1137-25G, UNILAB, Australia.
- 2.1.6 Silver nitrate, AgNO_3 , A.R., code no. 102333J, BDH, England.
- 2.1.7 Sodium hydroxide, NaOH , A.R., code no. K2001, Lab-scan, Ireland.
- 2.1.8 Titanium tetrachloride, TiCl_4 , A.R., code no. 8.12382.1000, Merck, Germany.
- 2.1.9 Titanium dioxide (Anatase), A.R., code no. 488257, Carlo Erba, Italy.
- 2.1.10 Titanium dioxide (Degussa P25), code no. D-60287, Degussa AG, Frankfurt, Germany.

2.2 Instruments

- 2.2.1 Chemistry Department, PSU
 1. Blacklight tube, 20 watts, F20T12-BLB, G.E., U.S.A.
 2. Centrifuge, EBA 20, Hettich, Germany.
 3. Diffuse reflectance spectrophotometer, DRS, UV-2401, Shimadzu, Japan.
 4. Fluorescence tube, TL-D 18W/54-765, PHILIPS, the Netherlands.
 5. Fourier-transformed infrared spectrophotometer, FT-IR, Spectrum GX, Perkin Elmer, U.S.A.

6. Photoluminescence spectrofluorimeter, LS55, Perkin Elmer, U.S.A.
7. Ultraviolet-visible spectrophotometer, SPECORD S100, Analytik Jena GmbH, Germany.
8. Wooden compartment (0.75m x 0.75m x 0.75m).

2.2.2 Scientific Equipment Center, PSU

1. Scanning electron microscope, SEM, JEOL JSM-5800LV, Japan.
2. Scanning electron microscope, SEM, JEOL JSM-5200, Japan.
3. Transmission electron microscope, TEM, JEOL JEM-2010, Japan.
4. Wavelength dispersive x-ray fluorescence spectrometer, WDXRF, PW2400, Philips, the Netherlands.
5. X-ray diffractometer, XRD, PHILIPS X'Pert MPD, the Netherlands.

2.2.3 Chemical Engineering Department, PSU

1. Surface area / pore size study, SA 3100, Coulter, U.S.A.

2.2.4 Scientific and Technological Research Equipment Centre, CU

1. Electron spin resonance spectrophotometer, ESR, JEOL JES-RE2X, Japan.

2.3 Methods

This work is divided into 2 parts: part (1) syntheses and characterization of (a) undoped TiO₂ by sol-gel method, and (b) trivalent (Cr, Fe) doped TiO₂ via incipient wetness impregnation; and part (2) studies of the photocatalytic degradation of those from part (1) by decolorizing MB dye in aqueous solutions under UV and visible light irradiation. In the first part, the X-ray diffractometer was used to study crystalline phase of all TiO₂ samples and the band gap energies were obtained by using diffused reflectance spectrophotometer. The surface morphology of all TiO₂ powders were investigated by using scanning electron microscopy and transmission electron microscopy techniques. The electron spin

resonance and x-ray fluorescence spectrometer were used to confirm the presence of trivalent metal ions in samples. In the second part, UV-vis technique was used in studying photocatalytic activity of TiO₂ samples. The effects of various parameters such as the dopant concentrations, initial dye concentration, and doping time were studied to optimize the preparation of trivalent metals ion doped TiO₂ for maximum photocatalytic degradation of MB, and comparing with commercial TiO₂ powders. Furthermore, the effect of pH, and various factors affecting the preparation of samples were studied for directly improvement and application in the water purification of amorphous TiO₂.

2.3.1 Synthesis and characterization of TiO₂

2.3.1.1 Synthesis of undoped TiO₂

Titanium tetrachloride (TiCl₄) was used as a main starting material to prepare TiO₂ without further purification. A flow chart for the synthesis of TiO₂ is shown in Figure 8. Detailed procedure for the preparation is as follows: ammonia solution (NH₃, 2.93 M, 240 mL) was added slowly to TiCl₄ (0.267 mol, 30 mL) in a 2-necked round bottom flask which was placed in an ice-water bath with vigorous stirring to yield the white precipitate. The precipitate was filtered gravimetrically with Whatman no.42 filter paper followed by washing several times with distilled water until free of chloride ions (using 0.1 M AgNO₃ solution). The white powder obtained was dried at 105 °C for 24 h and ground to fine powder. This sample is designated as *undoped TiO₂*.

2.3.1.2 Synthesis of Cr(III)-doped TiO₂

Chromium(III) chloride hexahydrate (CrCl₃.6H₂O) was used as source of Cr(III) dopant without further purification. Detailed procedure for the preparation of three doping concentrations, 0.05, 0.1, 0.2 mol%, of trivalent Cr is as follows: the appropriate amount of CrCl₃.6H₂O was dissolved in distilled water and then was added into dry undoped TiO₂ powder with constant stirring for 1 h. The product was filtered gravimetrically and subsequently washed with distilled water until free of chloride ions. The greenish product was dried at 105 °C for 24 h and ground to fine

powder. This sample is designated as $x\text{Cr-TiO}_2$, where x is the chromium content in mol%. A flow chart for the preparation of Cr-TiO₂ is shown in Figure 9.

2.3.1.3 Synthesis of Fe(III)-doped TiO₂

Iron(III) chloride anhydrous (FeCl₃) was used as source of Fe(III) dopant without further purification. Detailed procedure for the preparation of three doping concentrations, 0.05, 0.1, 0.2 mol%, of trivalent Fe is as follows: the appropriate amount of FeCl₃ was dissolved in distilled water and then was added into dry undoped TiO₂ powder with stirring for 1 h. The product was filtered gravimetrically and subsequently washed with distilled water until free of chloride ions. The brownish product was dried at 105 °C for 24 h and ground to fine powder. This sample is designated as $x\text{Fe-TiO}_2$, where x is the ferric content in mol%. A flow chart for the preparation of Fe-TiO₂ is shown in Figure 10.

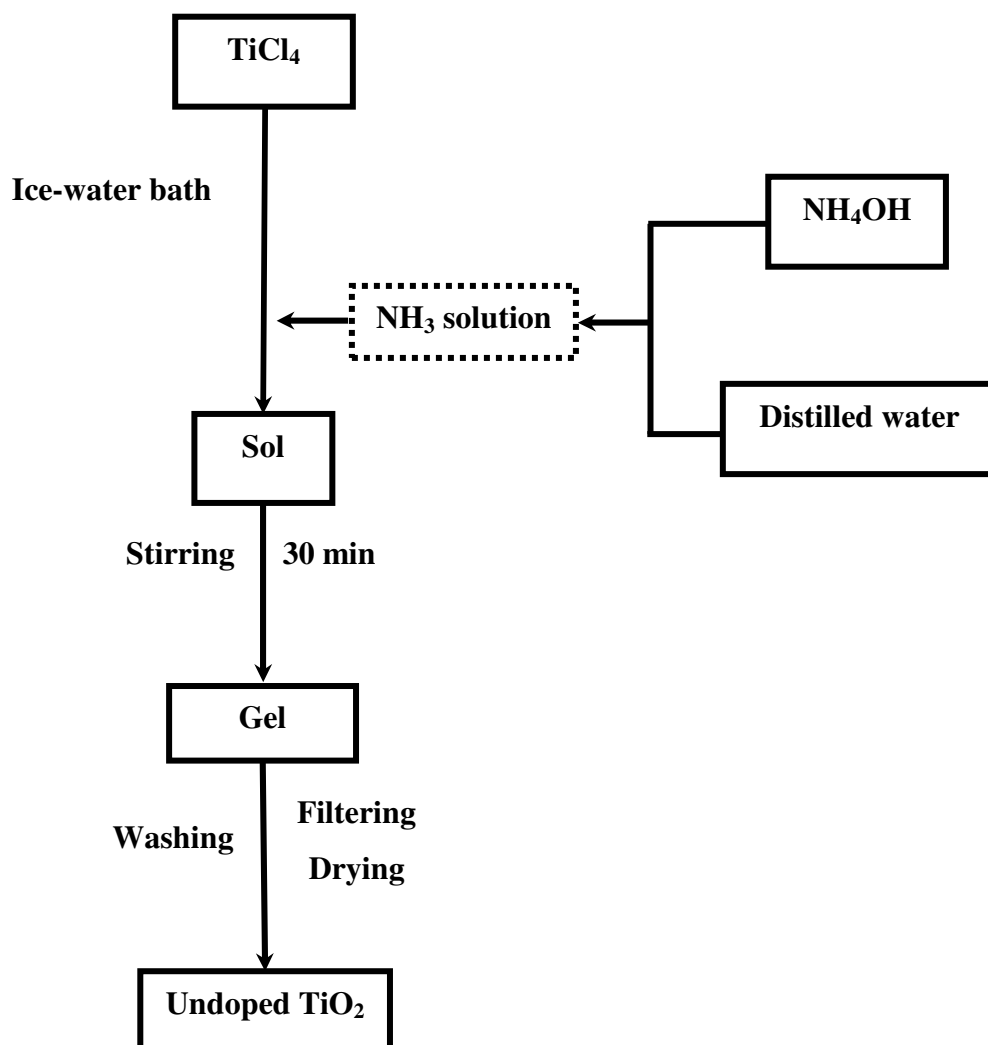


Figure 8 Flow chart of the preparation of undoped TiO₂ powder by sol-gel method.

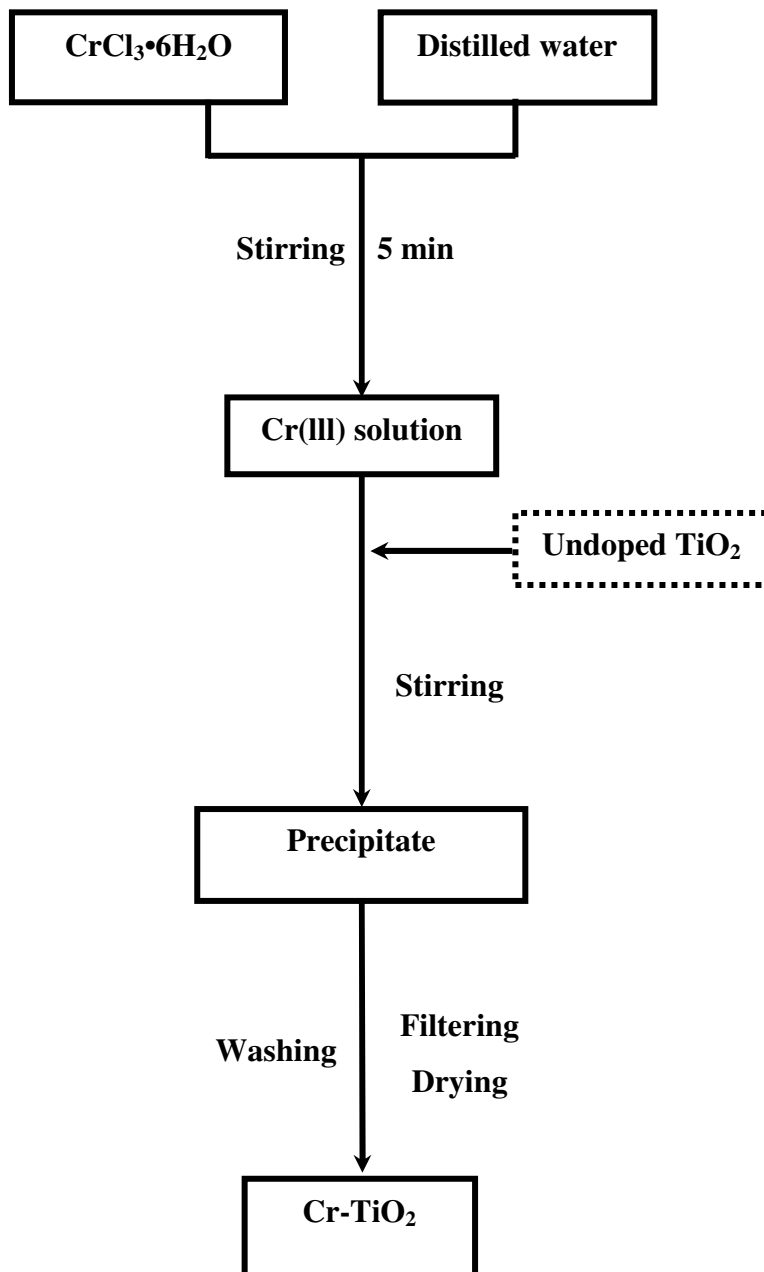


Figure 9 Flow chart of the preparation of Cr-TiO₂ powder by impregnation method.

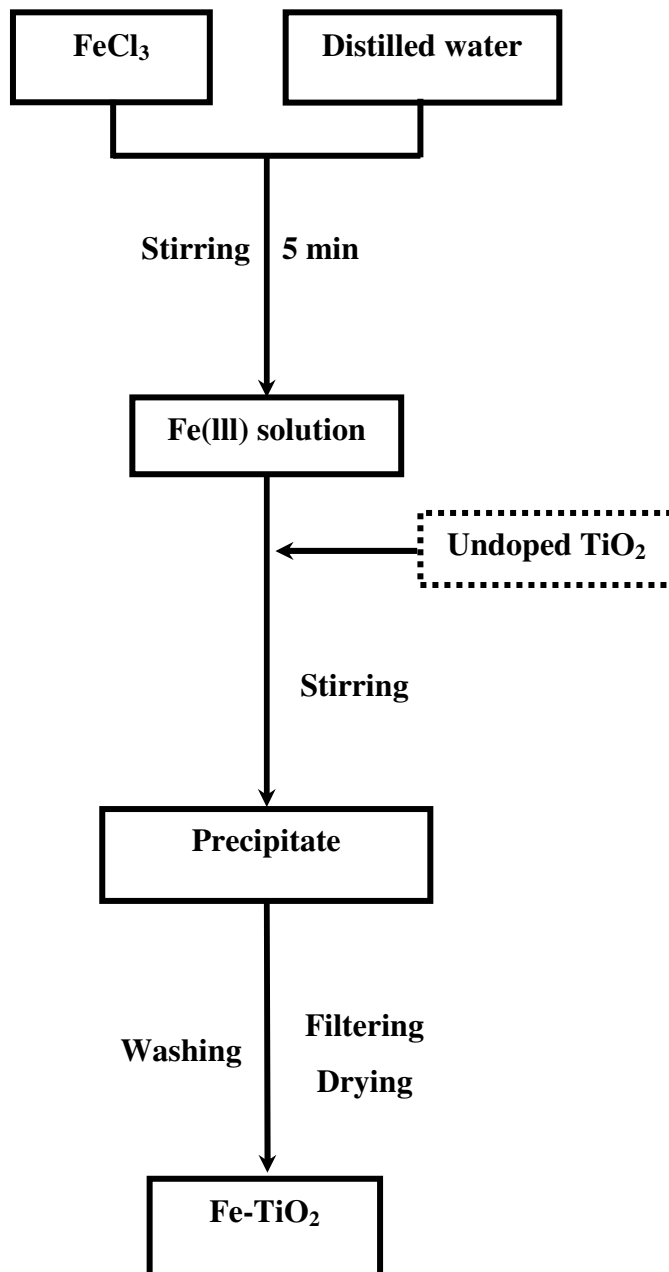


Figure 10 Flow chart of the preparation of Fe-TiO₂ powder by impregnation method.

2.3.2 Characterization of undoped TiO₂ and trivalent (Cr, Fe) doped TiO₂

2.3.2.1 X-ray powder diffractometer (XRD)

The XRD technique was used to study crystalline phase to identify and confirms structure of titanium dioxide samples. The XRD spectra of undoped and trivalent ion (Cr, Fe) doped titanium dioxide were acquired at the Scientific Equipment Center, Prince of Songkla University, Hat Yai, Songkhla, Thailand, with the Philips PW 3710 powder diffractometer (PHILIPS X'Pert MPD) using Cu K α radiation and equipped with a Ni filter over the range of $2\theta = 5-90^\circ$ at room temperature.

2.3.2.2 Diffuse reflectance spectroscopy (DRS)

Diffused reflectance studies were performed on a UV-vis absorption spectrophotometer (UV-2401) in the scan range 200-800 nm with a 2.0 nm slit width and using barium sulphate (BaSO₄) as reference sample. The information absorption edge, band gap energy, and the type of band to band transition of TiO₂ can be obtained from these spectra.

2.3.2.3 Electron spin resonance spectroscopy (ESR)

The ESR technique was used to study and confirm the presence of metal ions into TiO₂ samples. The ESR spectra of undoped and trivalent ion (Cr, Fe) doped titanium dioxide were acquired with an ESR spectrometer: JEOL model JES-RE2X, in the range of 8.8-9.6 GHz. at the Scientific and Technological Research Equipment Centre, Chulalongkorn University, Bangkok, Thailand.

2.3.2.4 Scanning electron microscopy (SEM)

The external morphology of all TiO₂ samples were observed on a SEM: JEOL JSM-5800LV and JSM-5200 scanning electron microscope (SEM) using high vacuum mode with secondary electron image conditions and electron micrograph technique. All data were acquired by the Scientific Equipment Center, Prince of Songkla University, Hat Yai, Songkhla, Thailand.

2.3.2.5 Transmission electron microscopy (TEM)

The morphology of materials on an atomic scale with resolution larger than 2 Å was acquired by a TEM: JEOL JSM 2010 transmission electron microscope (TEM) using high voltage condition about 200 kV and electron micrograph technique. All data were acquired by the Scientific Equipment Center, Prince of Songkla University, Hat Yai, Songkhla, Thailand.

2.3.2.6 Wavelength dispersive x-ray fluorescence spectrometer (XRF)

X-ray fluorescence spectrometry technique was used to confirm the presence of metal ions on the surface of samples using WDXRF, PW2400, Philips, the Netherlands. All data were acquired by the Scientific Equipment Center, Prince of Songkla University, Hat Yai, Songkhla, Thailand.

2.3.2.7 Fourier-transformed infrared spectrophotometry (FT-IR)

Infrared spectrophotometry technique was used to identify the functional groups present on the sample surface in diffused reflectance mode at 4,000-400 cm^{-1} by FT-IR : Spectrum GX, Perkin Elmer, U.S.A., using KBr as blank.

2.3.2.8 Surface area / pore size

The specific surface area and pore size were measured by the BET method (Coulter, model SA3100, U.S.A) with N_2 chemisorptions. All data were acquired at the Department of Chemical Engineering, Faculty of Engineering, Prince of Songkla University, Hat Yai, Songkhla, Thailand.

2.3.2.9 Photoluminescence spectroscopy (PL)

The PL technique was used to determine the band gap energy of TiO_2 samples. PL spectra were recorded in the range 200-800 nm at room temperature in air by LS55 Photoluminescence spectrofluorimeter with the excitation and emission slit widths 5 and 7.5 nm, respectively.

2.3.3 Optimum condition for preparation TiO₂ samples

The optimum condition for preparation of undoped and trivalent (Cr, Fe) doped TiO₂ were determined by studying the effect of dopant concentrations, doping time, and drying temperature.

2.3.3.1 Dopant concentrations

The effect of dopant concentrations was studied by varying dopant concentrations in the range of 0.05-0.2 mol%. The samples that showed highest photocatalytic efficiency was selected.

2.3.3.2 Doping duration

The effect of doping duration was carried out by stirring time and stirring speed. For the preparation of trivalent (Cr, Fe) doped TiO₂ by incipient wetness impregnation method, 5 g of undoped TiO₂ was added into beaker with the required volume of Cr(III) or Fe(III) solution at room temperature and stirred for 0.5, 1, 2, and 3 h. Furthermore, in each case, stirring speed was also investigated by using 300, 400, and 500 rpm.

2.3.3.3 Drying temperature and drying duration

The effect of drying temperature and drying duration were investigated by varying temperature in the range 80, 105, and 150 °C which, in each case, the drying time was varied: 12, 24, and 36 h.

2.3.4 Photocatalytic degradation of MB by undoped TiO₂ and trivalent (Cr, Fe) doped TiO₂

2.3.4.1 Preparation of calibration graph

The calibration graph is used to find the concentration of MB at any stages during the experiment. In this work, the concentrations of standard MB solutions were 1.0×10^{-6} M to 1.0×10^{-3} M. In order to construct a reliable standard calibration graph of MB, the working concentrations were divided into three ranges: 1.0×10^{-6} M to 1.0×10^{-5} M, 1.0×10^{-5} M to 1.0×10^{-4} M, and 1.0×10^{-4} M to 1.0×10^{-3} M.

2.3.4.2 The experiments for photocatalytic degradation of MB by undoped TiO₂ and trivalent (Cr, Fe) doped TiO₂ comparing with the commercial TiO₂ powders.

In the photocatalysis studies, 0.05 g of each TiO₂ sample was placed in an Erlenmeyer flask which contained measured volume of MB solution (100 mL of 2.5×10^{-5} M). The mixture was then stirred for 1 h in the dark to reach the adsorption equilibrium in tightly closed wooden compartment (0.75m x 0.75m x 0.75m) to avoid interference from ambient light. The suspension mixture then was irradiated with UV-light (20 watts blacklight F20T12-BLB, G.E., U.S.A.) or visible light (18 watts fluorescence TL-D 18W/54-765, PHILIPS, the Netherlands.) and magnetically stirred 5 or 12 h, for UV or visible light, respectively. At given irradiation time intervals (every 1 h), 5 ml of MB solution samples were collected. The degradation of MB solutions was analyzed from the changes in absorbance of the absorption maximum at 665 nm using UV-vis spectrophotometer (UV-VIS: SPECORD S100, Analytik Jena, Germany).

In the comparison studies of the commercial TiO₂, anatase (Carlo Erba) and Degussa P25 (Degussa AG), the same experimental set up was employed as given above.

2.3.4.3 The experiments for the effect of various parameters on photocatalytic activities of undoped TiO₂ and trivalent (Cr, Fe) doped TiO₂

The effect of an initial MB dye concentration was investigated in the range of 1.0×10^{-5} M to 7.5×10^{-4} M. The effect of pH was investigated by varying the pH of MB solutions in the range 3 to 9 by adding dilute aqueous solution of HCl or NaOH.

Chapter 3

Results

3.1 Syntheses and characterizations of undoped and trivalent (Cr, Fe) doped TiO₂ powders

3.1.1 Syntheses of undoped and trivalent (Cr, Fe) doped TiO₂ powders

(1) Undoped TiO₂

In the present study, undoped TiO₂ powder was synthesized from reaction between TiCl₄ and diluted NH₃ solution via base-catalyzed sol-gel method. Undoped TiO₂ exists as a white powder solid as shown in Figure 11.



Figure 11 The photograph of undoped TiO₂ powder.

(2) Trivalent (Cr, Fe) doped TiO₂

TiO₂ doped with Cr(III), and Fe(III), designated as Cr-TiO₂ and Fe-TiO₂, respectively, were prepared by incipient wetness impregnation processes, using aqueous solution of CrCl₃•6H₂O and FeCl₃ as the dopant sources, respectively. The light-brownish and greenish powders of Fe-TiO₂ and Cr-TiO₂ are shown in Figure 12(a) and 12(b), respectively.

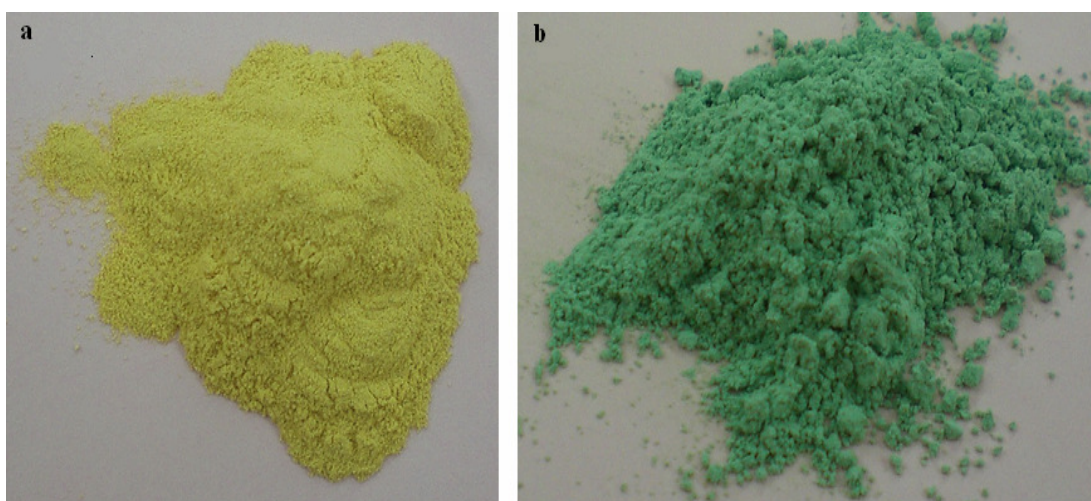


Figure 12 The photographs of doped TiO₂ powders; (a) Fe-TiO₂, and (b) Cr-TiO₂.

3.1.2 Characterizations of undoped and trivalent (Cr, Fe) doped TiO₂ powders

(a) X-ray powder diffraction (XRD)

XRD measurements were carried out with the Philips PW 3710 powder diffractometer (PHILIPS X'Pert MPD, the Netherlands) using CuK_α radiation ($\lambda = 1.5406 \text{ \AA}$) and equipped with a Ni filter over the range of $2\theta = 5\text{-}90^\circ$ at room temperature and compared with the original commercial TiO₂ powders. The identification of a species from its powder diffraction pattern is based upon the position of the lines (in terms of 2θ) and their relative intensities (Skoog and Leary, 1992). XRD patterns of undoped, doped-TiO₂, and commercial TiO₂ samples are

shown in Figure 13. Only flat base lines were detected in all synthetic TiO₂ samples, Figure 13(a)-(g), confirming the amorphous nature of these samples. No XRD diffraction pattern peaks of the dopants could be observed possibly due to quantity of the metal ions doped to TiO₂ was too small to be detected by XRD (Lee, *et al.*, 2001; Yuan, *et al.*, 2007). The commercial Degussa P25, Figure 13(h), shows pattern of both anatase ($2\theta = 25.4^\circ$) and rutile ($2\theta = 27.5^\circ$) phases in the ratio of *ca.* 4:1, calculated by the intensities obtained from the area of the most intense diffraction peaks of these two modifications, whereas the commercial anatase, Figure 13(i), shows only anatase phase, $2\theta = 25.4^\circ$, of TiO₂ in the sample. The weak diffraction peaks appear around $2\theta = 3-5^\circ$ in all samples were due to the signal of XRD instrument.

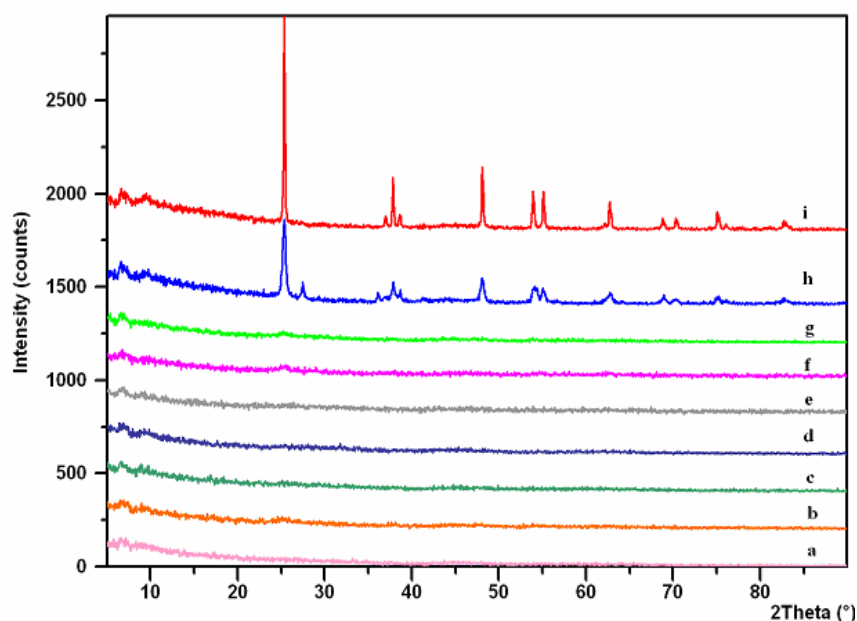


Figure 13 X-ray diffraction patterns for (a) undoped TiO₂, (b) 0.05Fe-TiO₂, (c) 0.1Fe-TiO₂, (d) 0.2 Fe-TiO₂, (e) 0.05Cr-TiO₂, (f) 0.1Cr-TiO₂, (g) 0.2 Cr-TiO₂, (h) Degussa P25, and (i) anatase TiO₂.

The data of the crystalline phase present in each sample in all synthesized TiO₂ and commercial samples are shown in Table 5.

Table 5 The crystalline phase of synthesized TiO₂ and commercial.

TiO₂ samples	Crystalline phase
Undoped TiO₂	Amorphous
Fe(III) doped TiO₂ 0.05Fe-TiO₂ 0.1Fe-TiO₂ 0.2Fe-TiO₂	Amorphous Amorphous Amorphous
Cr(III) doped TiO₂ 0.05Cr-TiO₂ 0.1Cr-TiO₂ 0.2Cr-TiO₂	Amorphous Amorphous Amorphous
Commercial TiO₂ Anatase (Carlo Erba) Degussa P25	Anatase Anatase + Rutile

(b) Diffuse reflectance spectroscopy (DRS)

Diffused reflectance studies were performed on a UV-vis absorption spectrophotometer, UV 2401, in the scan range 200-800 nm with a 2.0 nm slit width and using BaSO₄ as reference sample. Diffuse reflectance spectrum of undoped TiO₂ is shown in Figure 14. Figure 15 shows diffuse reflectance spectra of doped TiO₂, Fe-TiO₂ and Cr-TiO₂; and Figure 16 shows diffuse reflectance spectra of commercial TiO₂ samples, anatase and Degussa P25.

The band gap energies of all TiO₂ samples were determined from their diffuse reflectance spectra and calculated according to the equation:

$$E_g = h \frac{C}{\lambda} = \frac{1240}{\lambda} \quad \text{.....(12)}$$

where E_g is the band gap energy (eV), h is the Planck's constant (6.63×10^{-34} J.s), c is the light velocity (3.0×10^8 m s⁻¹), and λ is the wavelength at onset of absorption (nm) determined by the linear extrapolation of the steep part of the UV absorption toward the baseline.

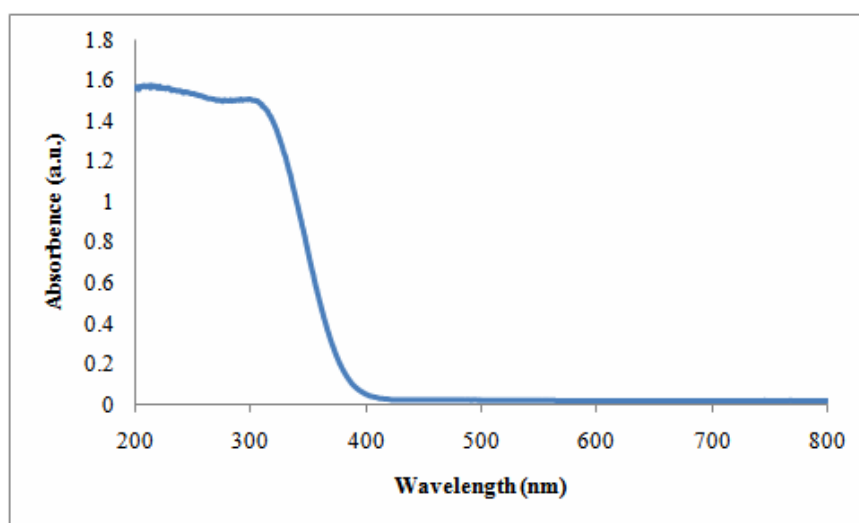


Figure 14 DRS spectrum of undoped TiO₂.

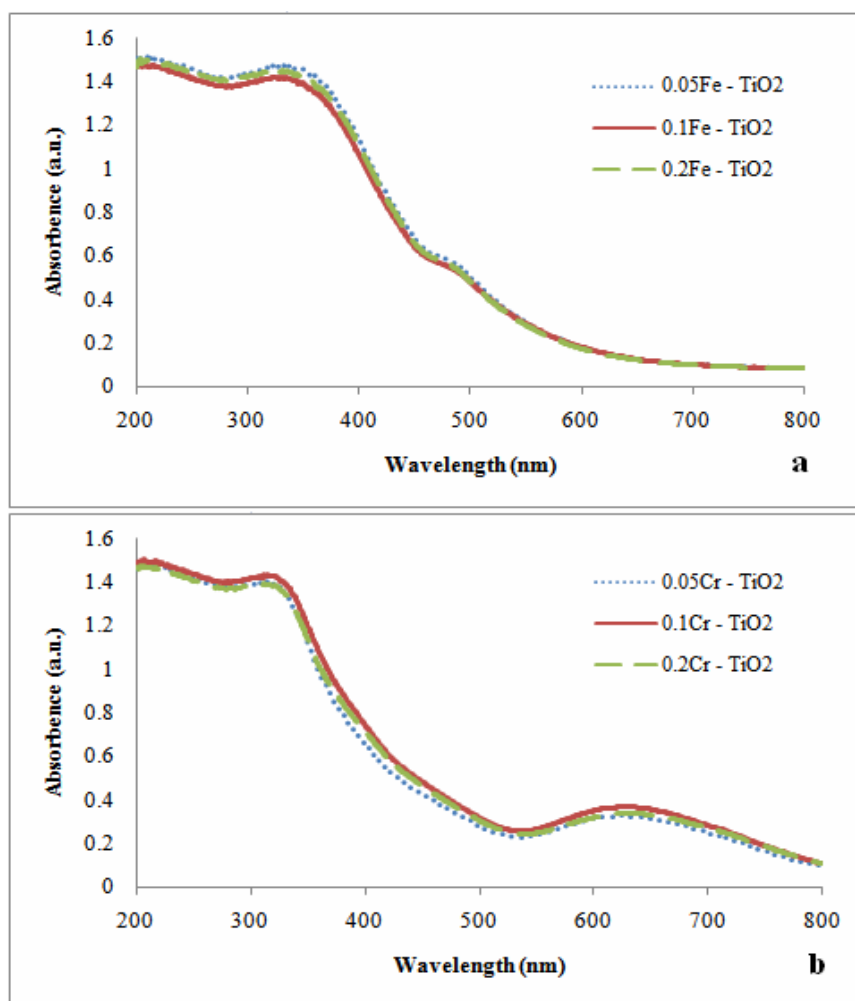


Figure 15 DRS spectra of doped TiO₂; (a) Fe-TiO₂, (b) Cr-TiO₂.

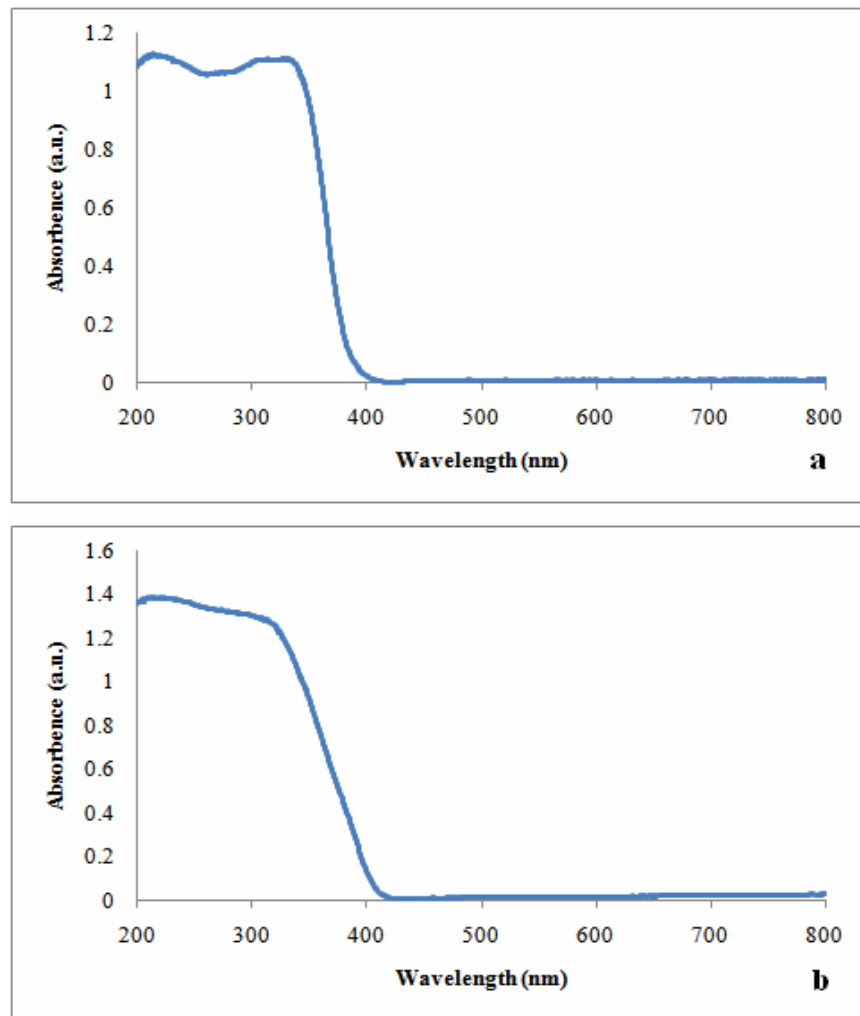


Figure 16 DRS spectrum of commercial TiO₂; (a) anatase, and (b) Degussa P25.

In order to establish the type of band-to-band transition in these synthesized particles, the absorption data were fitted to equation for both indirect and direct band gap transitions (Kumar, *et al.*, 2000).

Direct semiconductors are characterized by the minimum of the lowest conduction band positioned in k space directly under the maximum of the highest valence band. The absorption coefficient (α) near the absorption edge for direct interband transition is given by;

$$\alpha = B_d(h\nu - E_g)^{1/2} / h\nu \quad \text{.....(13)}$$

where α is the absorption coefficient (cm^{-1}), B_d is the absorption constant for a direct transition, $h\nu$ is the energy of excitation, E_g is the band gap energy (Serpone, *et al.*, 1995).

For indirect semiconductors, the minimum of the lowest conduction band is shifted relative to the maximum of the highest valence band and the lowest-energy interband transition must then be accompanied by photon excitation. Indirect interband transitions are characterized by the stronger energy dependence of the absorption coefficient (α) nearer the absorption edge than the otherwise the case for direct transition. The equation for indirect transition is given by;

$$\alpha = B_i(h\nu - E_g)^2 / h\nu \quad \text{.....(14)}$$

where B_i is the absorption constant for an indirect transition.

The absorption coefficient (α) for reflectivity measurements could be calculated by the following equation (Zhao, *et al.*, 1991);

$$\alpha = \frac{A}{d_s} \quad \text{.....(15)}$$

where A is the measured absorbance and d_s is the thickness of sample in DRS cell (0.4 cm).

The value of E_{phot} extrapolated to $\alpha = 0$ gives an absorption energy, which corresponds to band gap energy (E_g). Thus, the plot of $(\alpha E_{phot})^2$ versus E_{phot} and $(\alpha E_{phot})^{1/2}$ versus E_{phot} should determine the nature of the transition in the sample and are shown in Figures 17 and 18, respectively. The data of the wavelength at onset of absorption and the band gap energy which calculated from equations (12) - (14) of all TiO_2 samples are shown in Table 6.

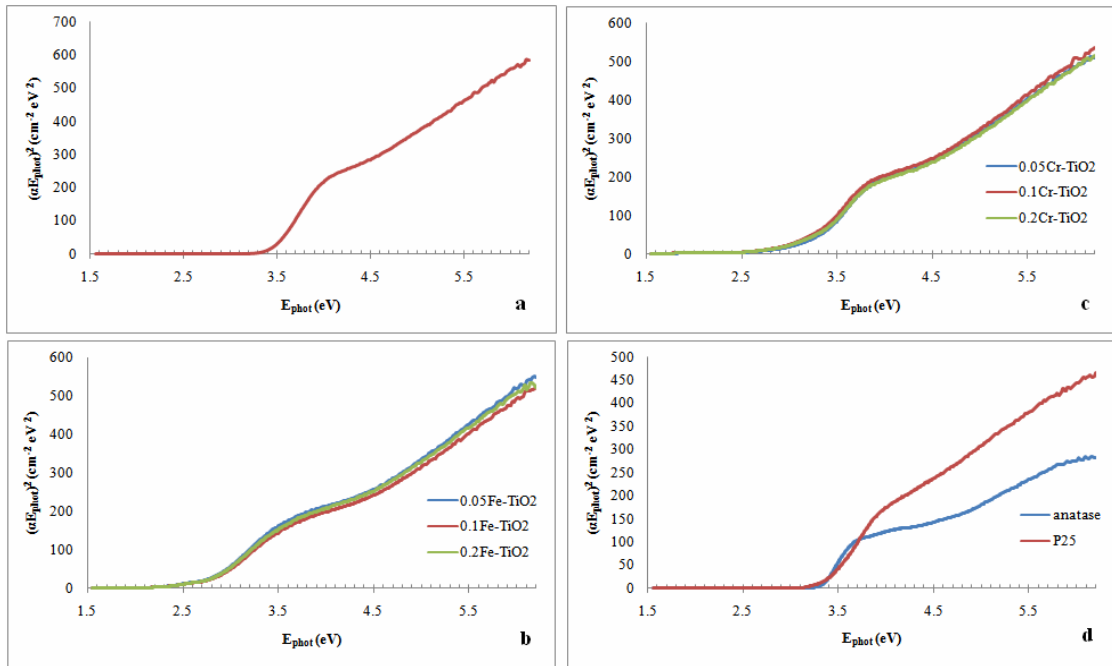


Figure 17 Plot of $(\alpha E_{phot})^2$ versus E_{phot} for a direct transition of TiO₂ samples; (a) undoped TiO₂, (b) Fe-TiO₂, (c) Cr-TiO₂, and (d) commercial TiO₂.

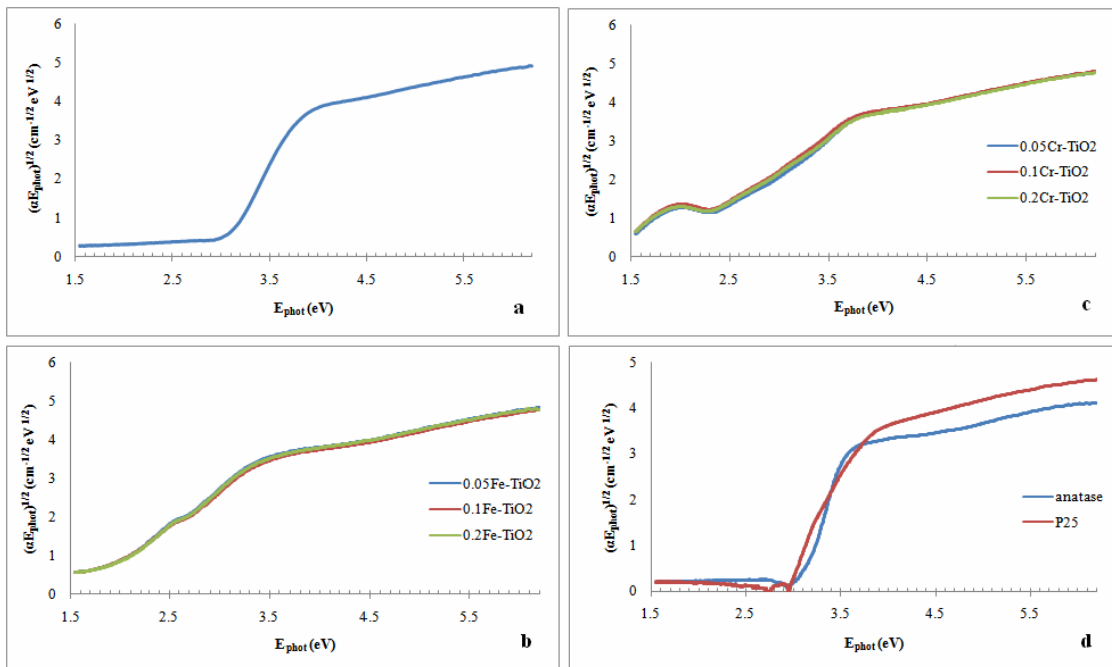


Figure 18 Plot of $(\alpha E_{phot})^{1/2}$ versus E_{phot} for an indirect transition of TiO₂ samples; (a) undoped TiO₂, (b) Fe-TiO₂, (c) Cr-TiO₂, and (d) commercial TiO₂.

Table 6 The wavelength at onset of absorption and the band gap energy of all TiO₂ samples.

TiO ₂ sample	λ_{onset} of absorption (nm)	Band gap energy (eV)		
		Equation 12	Direct	Indirect
Undoped TiO₂	378	3.28	3.46	3.01
Fe(III) doped TiO₂				
0.05Fe-TiO₂	498	2.49	3.20	1.79
0.1Fe-TiO₂	496	2.50	3.18	1.82
0.2Fe-TiO₂	497	2.49	3.22	1.80
Cr(III) doped TiO₂				
0.05Cr-TiO₂	426	2.91	2.72	2.22
0.1Cr-TiO₂	434	2.86	2.80	2.20
0.2Cr-TiO₂	432	2.87	2.75	2.20
Commercial TiO₂				
Anatase	385	3.22	3.30	3.12
Degussa P25	394	3.15	3.25	2.97

(c) Photoluminescence spectroscopy (PL)

Commonly, the band gap energy of semiconductor materials such as ZnO, TiO₂, and CdS can be measured using PL technique as described by Gfroerer, and Liqiang *et al.* (Gfroerer, 2000; Liqiang, *et al.*, 2006). In this work, this method was used to determine and confirm the band gap energies of all TiO₂ samples with LS55 spectrofluorimeter. The pre-scan spectra of TiO₂ samples were obtained in full range of monochromator limits from 200-800 nm with the excitation and emission slit widths at 5 and 7.5 nm, respectively. Figures 19 and 20 show the PL spectrum of undoped TiO₂ and commercial TiO₂ powders, anatase and Degussa P25, respectively, while those of the doped samples are shown in Figure 21.

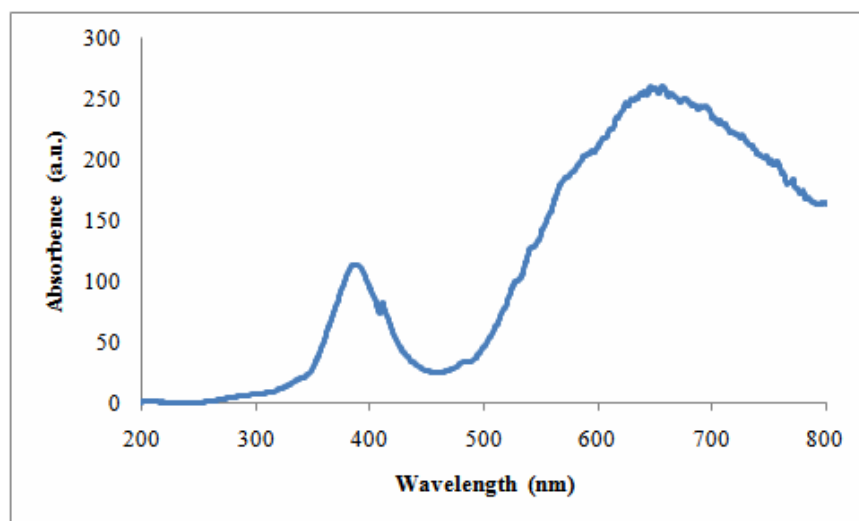


Figure 19 Shows PL spectrum of undoped TiO₂.

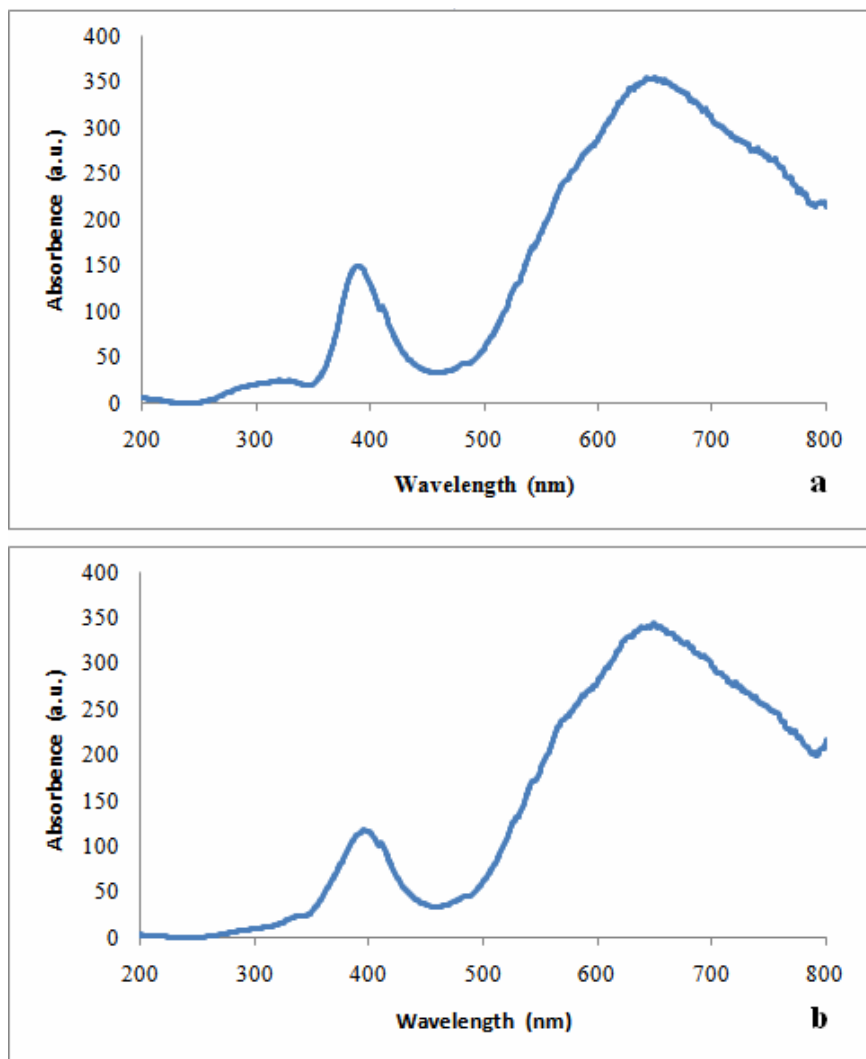


Figure 20 Show PL spectrum of commercial TiO₂ powders, (a) anatase, and (b) Degussa P25.

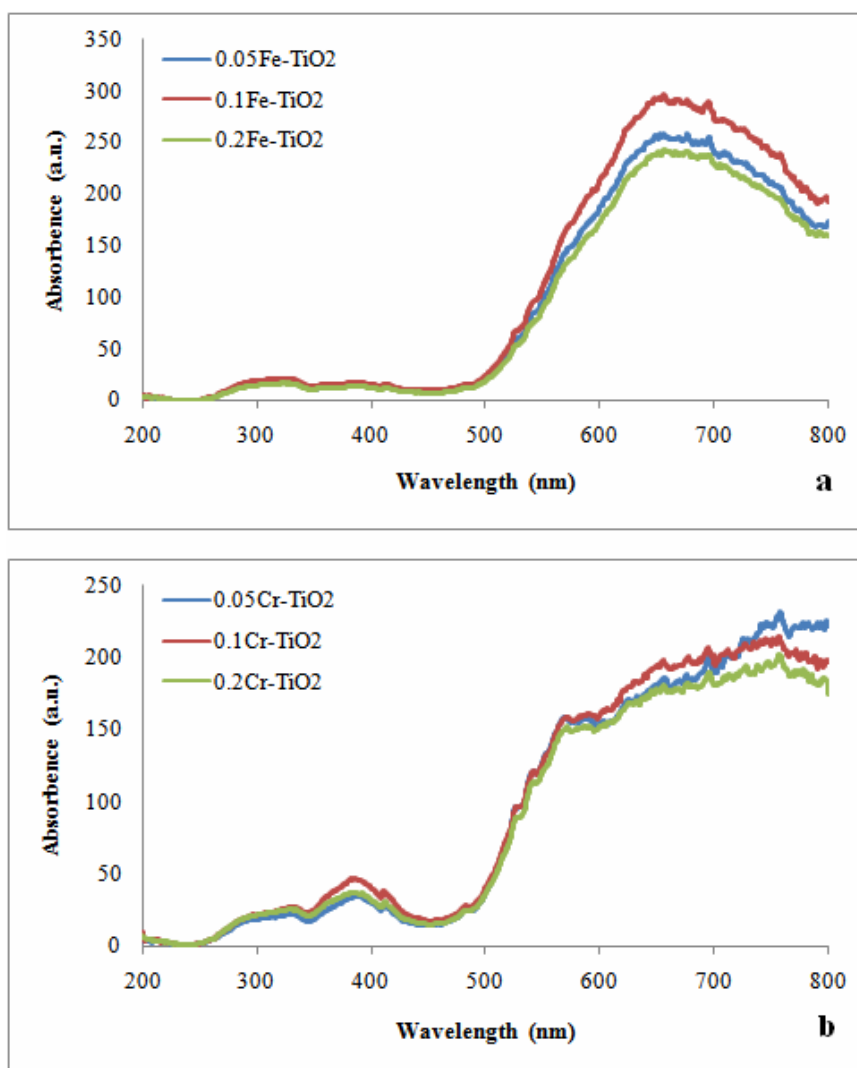


Figure 21 Show PL spectra of doped TiO₂; (a) Fe-TiO₂, and (b) Cr-TiO₂.

(d) Fourier-transformed infrared spectroscopy (FT-IR)

Fourier-transformed spectroscopy is a measurement technique whereby spectra are collected based on measurements of the temporal coherence of a radiative source, using time-domain measurements of the electromagnetic radiation or other type of radiation. It can be applied to a variety of types of spectroscopy including optical spectroscopy, infrared spectroscopy (FTIR), and electron spin resonance spectroscopy. Infrared spectroscopy is a technique for determining the functional groups within the compounds. The FT-IR spectrum range of the usage in the mid-infrared region, which covers the frequency from 400 to 4,000 cm^{-1} (Skoog and

Leary, 1992). The FT-IR spectra of undoped TiO_2 , doped TiO_2 (Fe-TiO_2 and Cr-TiO_2), and commercial TiO_2 (anatase and Degussa P25), are shown in Figures 22-26, respectively. The assigned modes of functional groups corresponding to Figures 22–24 listed in Tables 7. Table 8 lists the assigned modes of the functional groups that are responsible for vibration bands of the commercial TiO_2 .

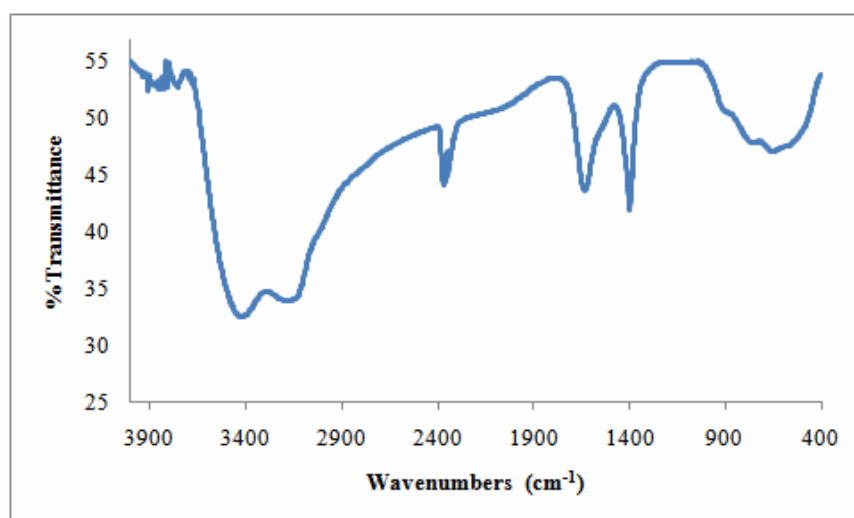


Figure 22 FT-IR spectrum of undoped TiO_2 .

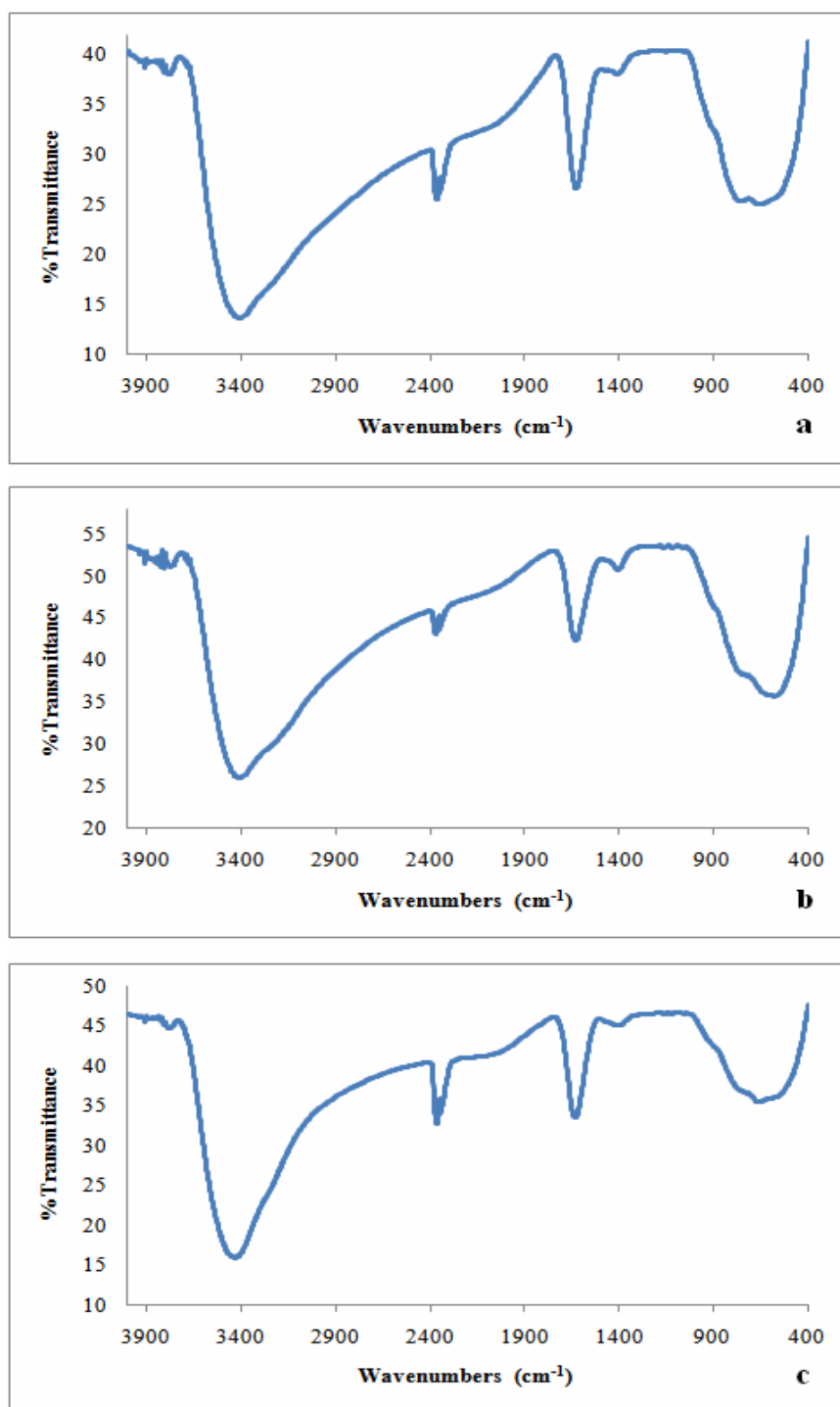


Figure 23 FT-IR spectrum of Fe(III) doped TiO₂ powders; (a) 0.05Fe-TiO₂, (b) 0.1Fe-TiO₂, and (c) 0.2Fe-TiO₂.

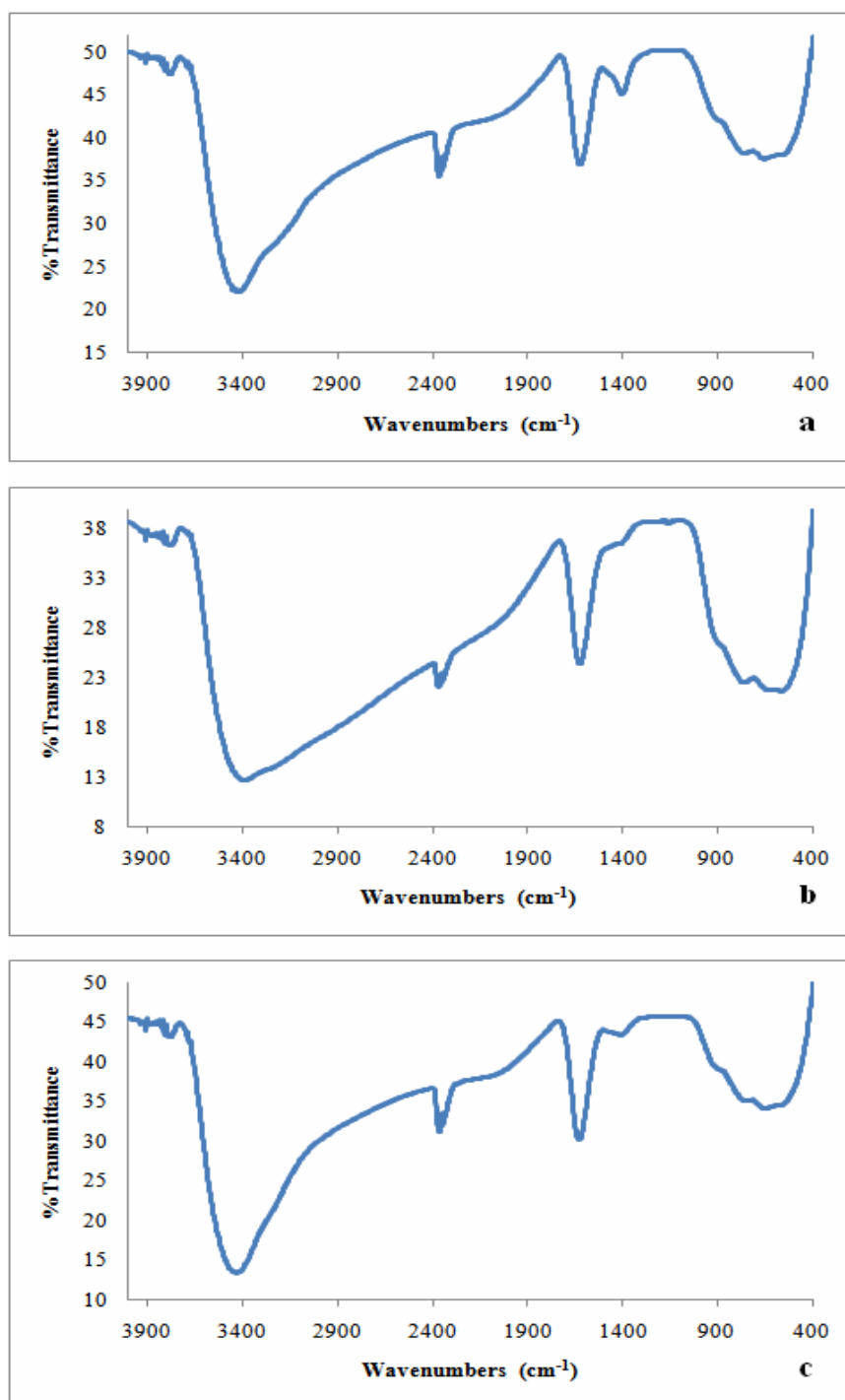


Figure 24 FT-IR spectrum of Cr(III) doped TiO₂ powders; (a) 0.05Cr-TiO₂, (b) 0.1Cr-TiO₂, and (c) 0.2Cr-TiO₂.

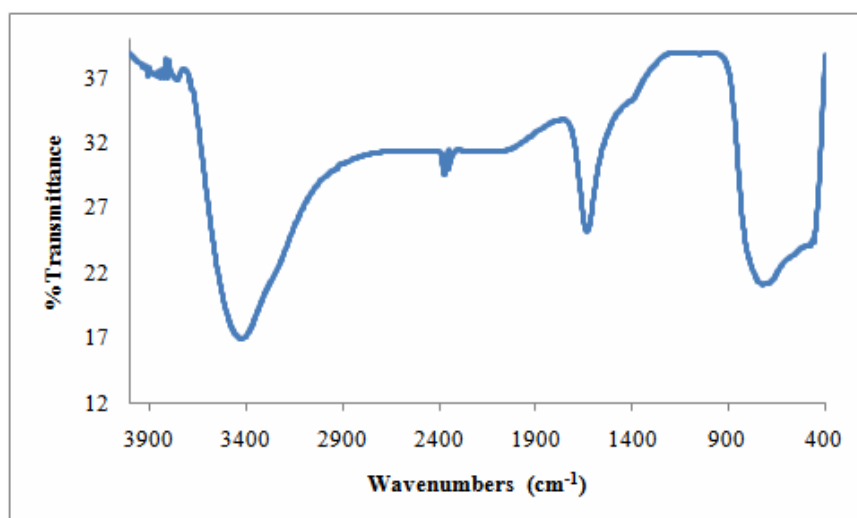


Figure 25 FT-IR spectrum of commercial TiO₂ powder, anatase.

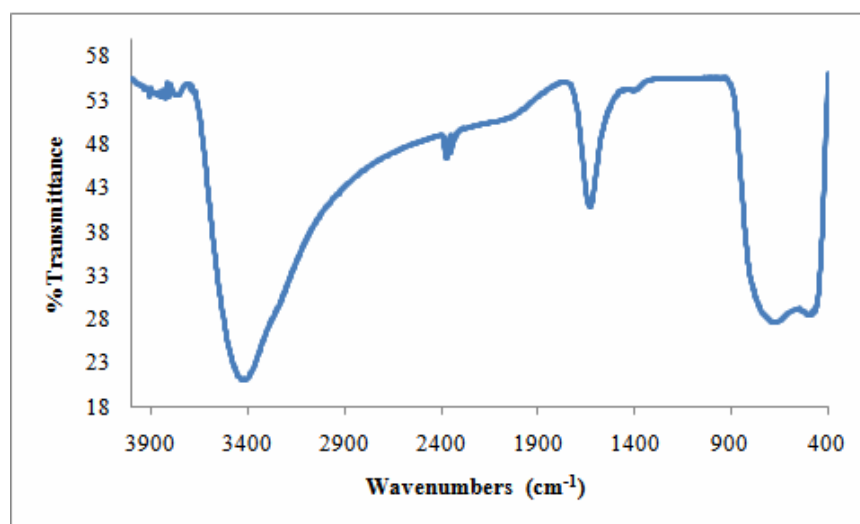


Figure 26 FT-IR spectrum of commercial TiO₂ powder, Degussa P25.

Table 7 Assignment of the FT-IR bands of synthetic TiO₂.

TiO ₂ sample	Wavenumbers (cm ⁻¹)	Assignment	Functional groups/Molecule	Reference
Undoped TiO ₂	3,500 – 3,000 2,375 1,630 1,398 Below 800	ν_{OH} and ν_{NH} ν_{CO} δ_{OH} δ_{NH} $\nu_{\text{Ti-O}}$	H ₂ O and NH ₄ ⁺ CO ₂ OH groups NH ₄ ⁺ groups Ti-O bond	Wang, <i>et al.</i> , 2000 Nakamoto, 1970 Youn, <i>et al.</i> , 1999 Youn, <i>et al.</i> , 1999 Velasco, <i>et al.</i> , 1999
0.05Fe-TiO ₂	3,500 – 3,000 2358 1607 1401 Below 800	ν_{OH} and ν_{NH} ν_{CO} δ_{OH} δ_{NH} $\nu_{\text{Ti-O}}$	H ₂ O and NH ₄ ⁺ CO ₂ OH groups NH ₄ ⁺ groups Ti-O bond	Wang, <i>et al.</i> , 2000 Nakamoto, 1970 Youn, <i>et al.</i> , 1999 Youn, <i>et al.</i> , 1999 Velasco, <i>et al.</i> , 1999
0.1Fe-TiO ₂	3,500 – 3,000 2364 1627 1401 Below 800	ν_{OH} and ν_{NH} ν_{CO} δ_{OH} δ_{NH} $\nu_{\text{Ti-O}}$	H ₂ O and NH ₄ ⁺ CO ₂ OH groups NH ₄ ⁺ groups Ti-O bond	Wang, <i>et al.</i> , 2000 Nakamoto, 1970 Youn, <i>et al.</i> , 1999 Youn, <i>et al.</i> , 1999 Velasco, <i>et al.</i> , 1999
0.2Fe-TiO ₂	3,500 – 3,000 2358 1633 1406 Below 800	ν_{OH} and ν_{NH} ν_{CO} δ_{OH} δ_{NH} $\nu_{\text{Ti-O}}$	H ₂ O and NH ₄ ⁺ CO ₂ OH groups NH ₄ ⁺ groups Ti-O bond	Wang, <i>et al.</i> , 2000 Nakamoto, 1970 Youn, <i>et al.</i> , 1999 Youn, <i>et al.</i> , 1999 Velasco, <i>et al.</i> , 1999

Table 7 Continued.

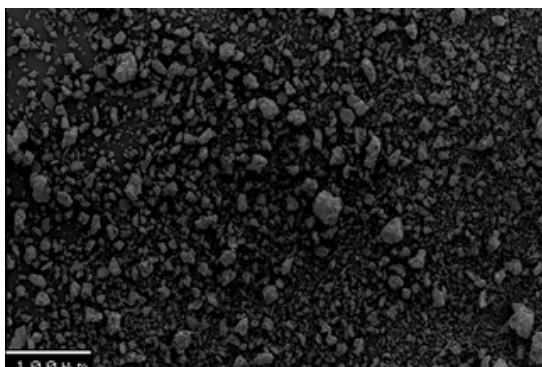
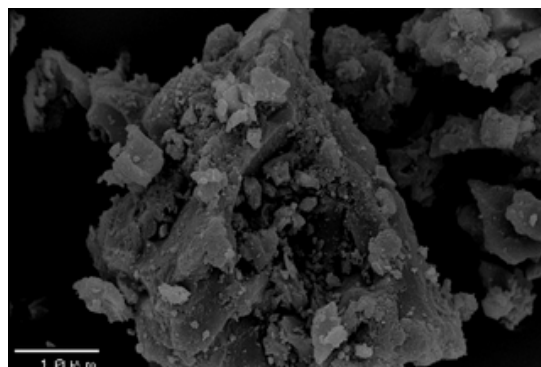
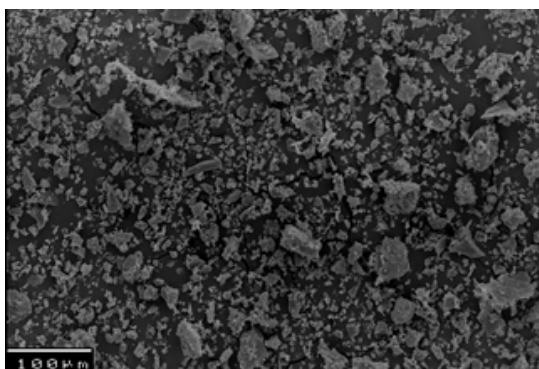
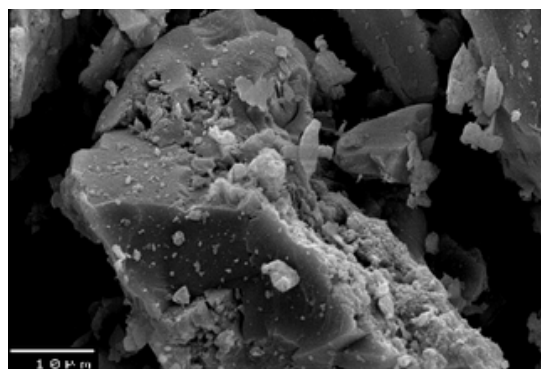
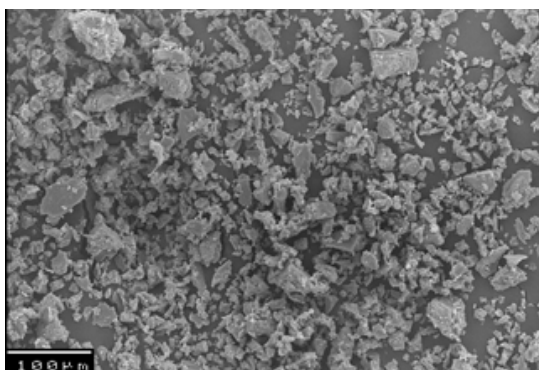
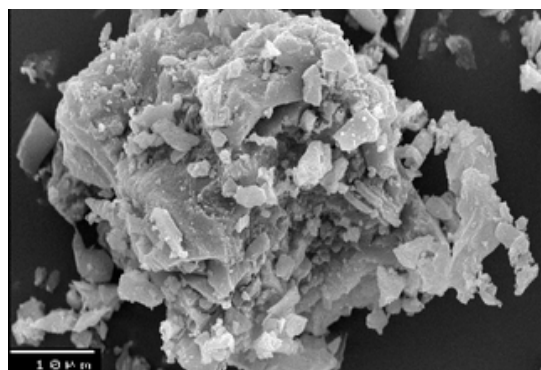
TiO ₂ sample	Wavenumbers (cm ⁻¹)	Assignment	Functional groups/Molecule	Reference
0.05Cr-TiO ₂	3,500 – 3,000 2,364 1624 1404 Below 800	ν_{OH} and ν_{NH} ν_{CO} δ_{OH} δ_{NH} $\nu_{\text{Ti-O}}$	H ₂ O and NH ₄ ⁺ CO ₂ OH groups NH ₄ ⁺ groups Ti-O bond	Wang, <i>et al.</i> , 2000 Nakamoto, 1970 Youn, <i>et al.</i> , 1999 Youn, <i>et al.</i> , 1999 Velasco, <i>et al.</i> , 1999
0.1Cr-TiO ₂	3,500 – 3,000 2,358 1,622 1402 Below 800	ν_{OH} and ν_{NH} ν_{CO} δ_{OH} δ_{NH} $\nu_{\text{Ti-O}}$	H ₂ O and NH ₄ ⁺ CO ₂ OH groups NH ₄ ⁺ groups Ti-O bond	Wang, <i>et al.</i> , 2000 Nakamoto, 1970 Youn, <i>et al.</i> , 1999 Youn, <i>et al.</i> , 1999 Velasco, <i>et al.</i> , 1999
0.2Cr-TiO ₂	3,500 – 3,000 2358 1627 1406 Below 800	ν_{OH} and ν_{NH} ν_{CO} δ_{OH} δ_{NH} $\nu_{\text{Ti-O}}$	H ₂ O and NH ₄ ⁺ CO ₂ OH groups NH ₄ ⁺ groups Ti-O bond	Wang, <i>et al.</i> , 2000 Nakamoto, 1970 Youn, <i>et al.</i> , 1999 Youn, <i>et al.</i> , 1999 Velasco, <i>et al.</i> , 1999

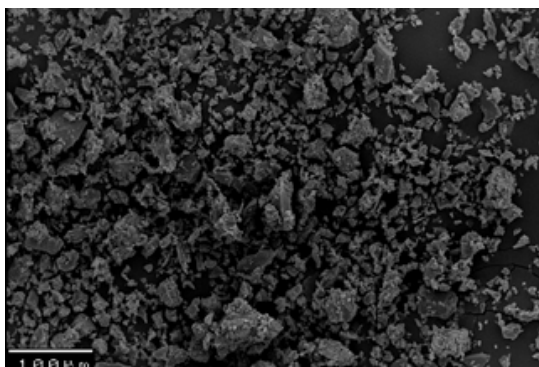
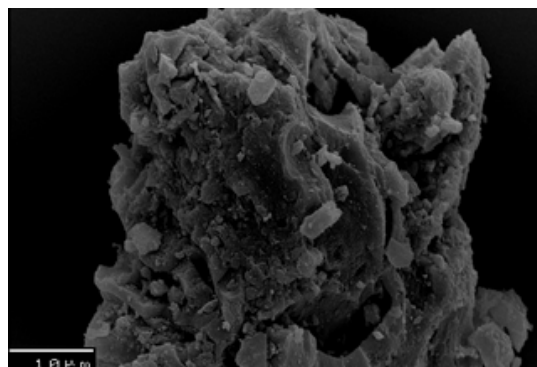
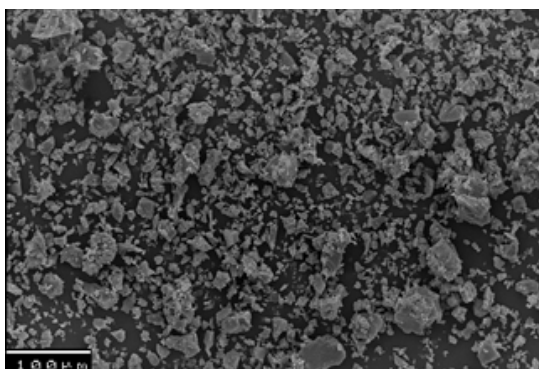
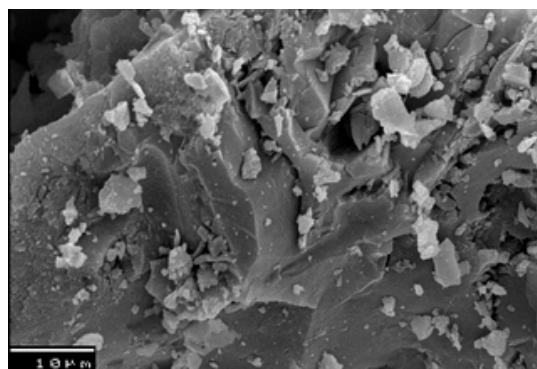
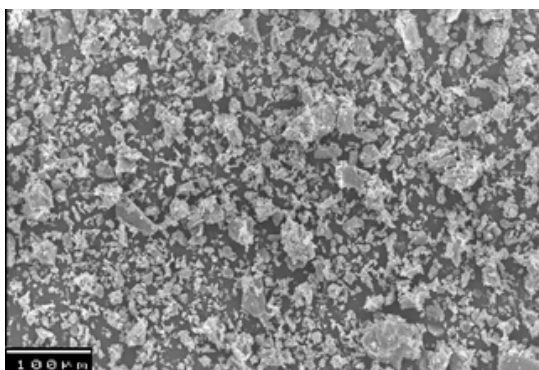
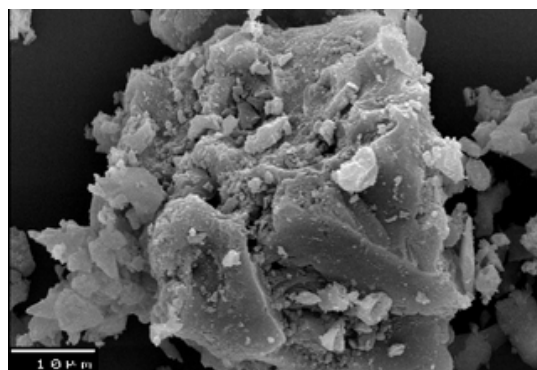
Table 8 Assignment of the FT-IR bands of commercial TiO₂.

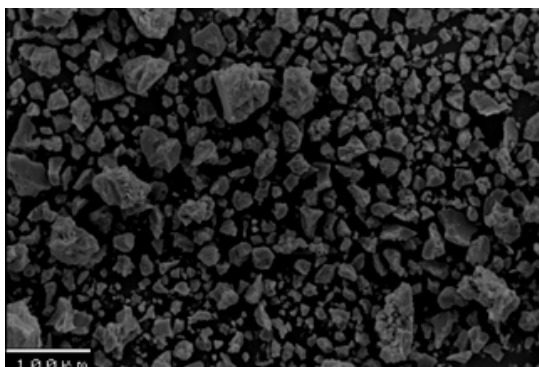
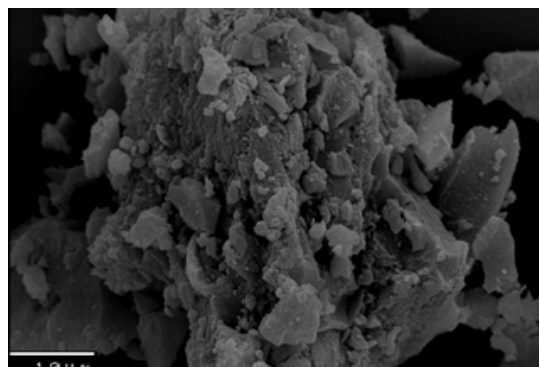
TiO ₂ sample	Wavenumbers (cm ⁻¹)	Assignment	Functional groups/Molecule	Reference
Anatase	3,500 – 3,200	ν_{OH} and ν_{NH}	H ₂ O and NH ₄ ⁺	Wang, <i>et al.</i> , 2000
	2375	ν_{CO}	CO ₂	Nakamoto, 1970
	1633	δ_{OH}	OH groups	Youn, <i>et al.</i> , 1999
	710	$\nu_{\text{Ti-O}}$	TiO ₂	Zhang, <i>et al.</i> , 2001
Degussa P25	3,500 – 3,200	ν_{OH} and ν_{NH}	H ₂ O and NH ₄ ⁺	Wang, <i>et al.</i> , 2000
	2375	ν_{CO}	CO ₂	Nakamoto, 1970
	1633	δ_{OH}	OH groups	Youn, <i>et al.</i> , 1999
	682	$\nu_{\text{Ti-O}}$	TiO ₂ (anatase)	Zhang, <i>et al.</i> , 2001
	503	$\nu_{\text{Ti-O}}$	TiO ₂ (rutile)	Zhang, <i>et al.</i> , 2001

(e) Scanning electron microscopy (SEM)

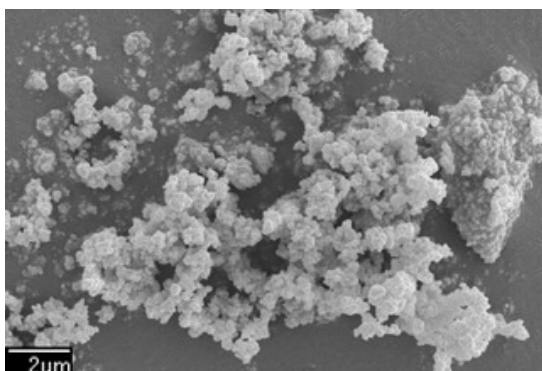
SEM is a type of electron microscope that images the sample surface by scanning it with a high-energy beam of electrons in a raster scan pattern. This technique was used to investigate the surface morphology of TiO₂ samples, undoped, doped, and commercial TiO₂. In this work, SEM images were carried out by SEI mode with 20-25 kV. The SEM images of undoped TiO₂, doped TiO₂ (Fe-TiO₂ and Cr-TiO₂), and the commercial TiO₂ (anatase and Degussa P25) powders are shown in Figures 27-31, respectively.

(a) Undoped TiO_2 x 200(b) Undoped TiO_2 x 2,000**Figure 27** SEM images of undoped TiO_2 .(a) 0.05Fe- TiO_2 x 200(b) 0.05Fe- TiO_2 x 2,000(c) 0.1Fe- TiO_2 x 200(d) 0.1Fe- TiO_2 x 2,000

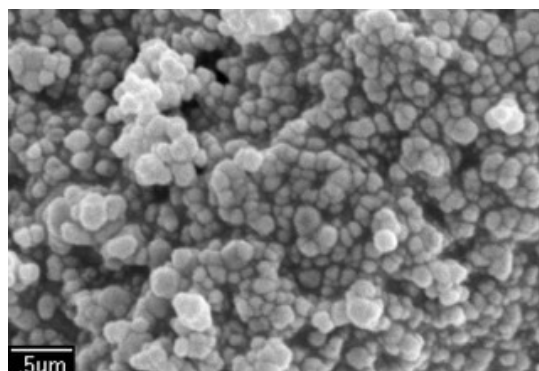
(e) 0.2Fe-TiO_2 x 200(f) 0.2Fe-TiO_2 x 2,000**Figure 28** SEM images of Fe(III) doped TiO_2 .(a) 0.05Cr-TiO_2 x 200(b) 0.05Cr-TiO_2 x 2,000(c) 0.1Cr-TiO_2 x 200(d) 0.1Cr-TiO_2 x 2,000

(e) 0.2Cr-TiO₂ x 200(f) 0.2Cr-TiO₂ x 2,000**Figure 29** SEM images of Cr(III) doped TiO₂.

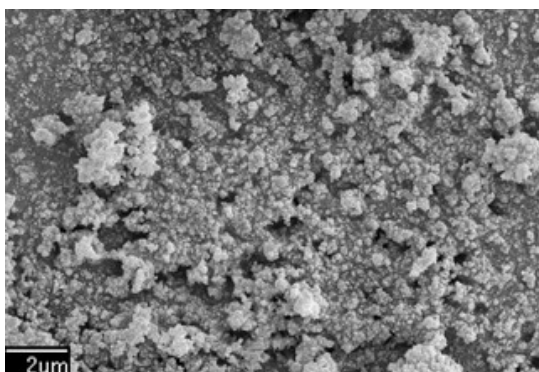
(a) Anatase x 7,500



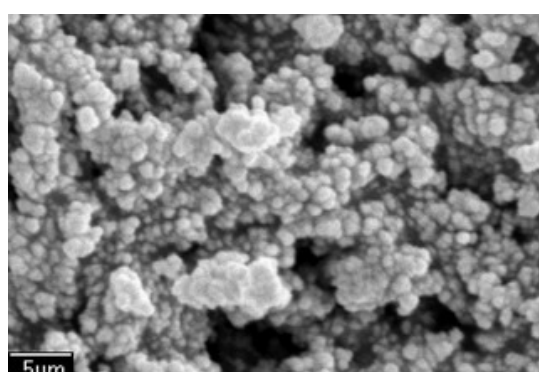
(b) Anatase x 30,000

**Figure 30** SEM images of commercial TiO₂ (anatase).

(a) Degussa P25 x 7,500



(b) Degussa P25 x 30,000

**Figure 31** SEM images of commercial TiO₂ (Degussa P25).

(f) Transmission electron microscopy (TEM)

TEM technique is used to estimate the particle size and texture of crossed section particles. TEM micrograph was carried out using transmission electron microscope, model JEM-2010, with 160 kV. The TEM micrographs of undoped TiO_2 , doped TiO_2 (Fe- TiO_2 , and Cr- TiO_2), and the commercial TiO_2 (anatase and Degussa P25) are shown in Figures 32-34, respectively.

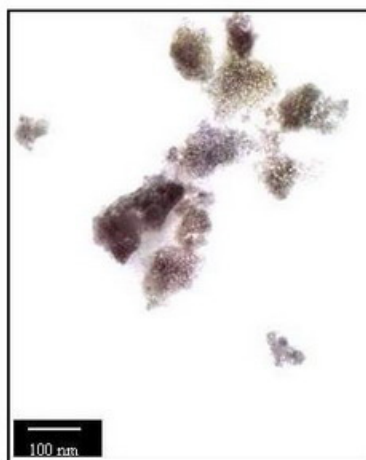


Figure 32 TEM micrograph of undoped TiO_2 at $\times 80,000$.

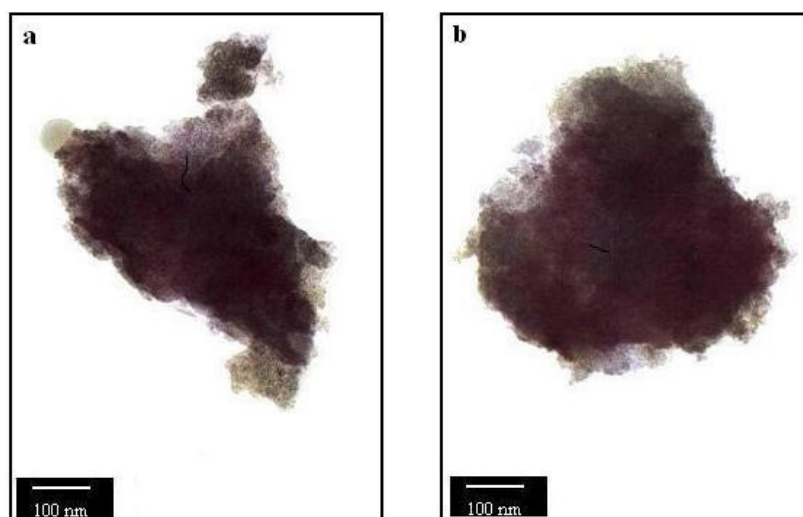


Figure 33 TEM micrographs at $\times 80,000$ of doped TiO_2 ; (a) Fe- TiO_2 , and (b) Cr- TiO_2 .

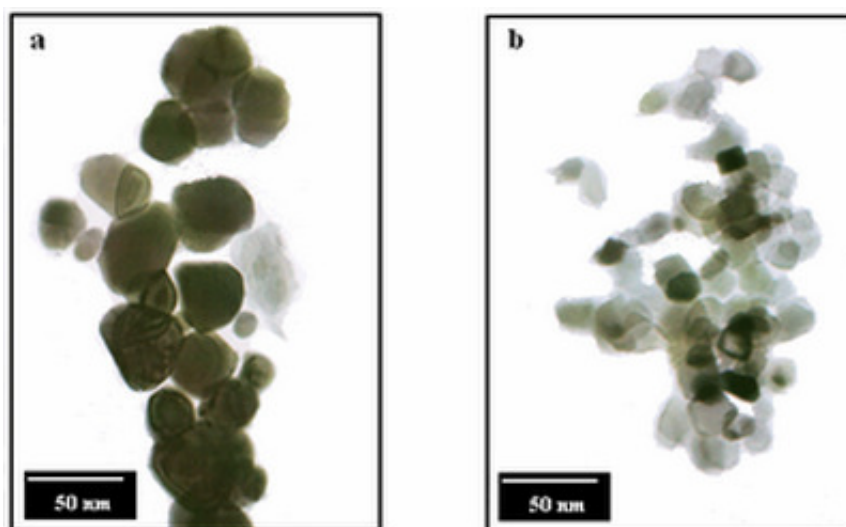


Figure 34 TEM micrographs at $\times 80,000$ of commercial TiO_2 ; (a) anatase, and (b) Degussa P25.

(g) Surface area / pore size

The surface area is an average measurement of the external surface of a large number of particles and expressed in term of the area per unit mass (m^2/g). There are two main analysis techniques for measuring surface area; gas adsorption and gas permeability. In this work gas adsorption surface area analysis was used.

The gas adsorption approach starts with a clean surface achieved through vacuum or inert gas bake-out. The clean powder surface is exposed to varying partial pressures of known adsorbing vapors. A measurement is made from the amount of gas adsorbed on the powder surface versus the partial pressure. The measurement is often referred to as the BET specific surface area after Brunauer, Emmett and Teller who developed the concept in 1938 (Brunauer, *et al.*, 1938).

Under equilibrium, the rate of adsorption equals the rate of evaporation. Letting P equals the partial pressure of adsorbate, P_0 equals the saturation pressure of adsorbate (which depends on the gas and temperature), X equals the amount of gas adsorbed at a pressure P , X_m equals the monolayer capacity of the powder (the amount of gas necessary to form a uniform surface coating one atomic layer thick), and C equal a constant relating to the adsorption enthalpy, gives

$$\frac{P}{X(P_0 - P)} = \frac{1}{X_m C} + \frac{C-1}{X_m C} \frac{P}{P_0} \quad \text{.....(16)}$$

The linear relation between the term on the left of equal sign and the partial pressure ratio P/P_0 is noted. This is the BET equation, and is generally valid for powders in the range P/P_0 from 0.05 to 0.30. Equation (16) can be rewritten in a general form as,

$$\frac{P}{X(P_0 - P)} = B + A \frac{P}{P_0} \quad \text{.....(17)}$$

where

$$X_m = \frac{1}{A + B} \quad \text{.....(18)}$$

Giving A as the slope and B as the intercept of the linear equation. Finally, the surface area is calculated as

$$S = \frac{X_m N_0 A_0}{wM} \quad \text{.....(19)}$$

Using M as the molecular weight of adsorbate, A_0 as the average occupational areas of an adsorbate molecule, N_0 as Avogadro's number, and w as the sample weight.

Surface area and porosity of all TiO_2 samples, undoped, doped, and commercial TiO_2 , are shown in Table 9 and Table 10, respectively. Moreover, the porosity studies of synthesized samples are shown in Figures 35-40.

Table 9 Surface area of all TiO₂ samples.

TiO₂ sample	Surface area^a (m²/g)
Undoped TiO₂	484.73
Fe-TiO₂	
0.05 Fe-TiO₂	351.23
0.1 Fe-TiO₂	459.55
0.2 Fe-TiO₂	405.21
Cr-TiO₂	
0.05Cr-TiO₂	457.10
0.1Cr-TiO₂	456.62
0.2Cr-TiO₂	470.11
Commercial TiO₂^b	
Anatase	9.65
Degussa P25	51.41

^a Data were determined by using SA3100, Coulter.

^b Data by Choychangtong, 2004.

Table 10 Porosity of all TiO₂ samples.

TiO ₂ sample	Pore volume (%) for pore diameter (nm)								Porosity (mL/g)
	<6	6-8	8-10	10-12	12-16	16-20	20-80	>80	
Undoped TiO₂	64.99	11.67	3.72	3.13	2.60	2.42	8.30	3.17	0.08571
0.05Fe- TiO₂	62.02	13.25	4.30	3.86	3.57	3.25	7.44	2.32	0.15409
0.1Fe- TiO₂	66.95	9.28	3.21	3.10	3.13	2.65	8.43	3.25	0.08372
0.2Fe- TiO₂	64.14	9.60	3.28	3.28	3.54	3.50	9.39	3.27	0.11248
0.05Cr- TiO₂	62.92	12.33	5.01	4.42	3.81	3.02	6.72	1.77	0.11424
0.1Cr- TiO₂	58.99	11.77	4.90	4.06	3.62	2.92	9.72	4.01	0.08019
0.2Cr- TiO₂	64.75	9.90	3.60	3.57	3.48	3.14	9.01	2.56	0.08372
Anatase^a	2	1	1	1	1	1	15	78	0.019
P25^a	5	3	2	2	3	4	38	43	0.235

^a Data by Choychangtong, 2004.

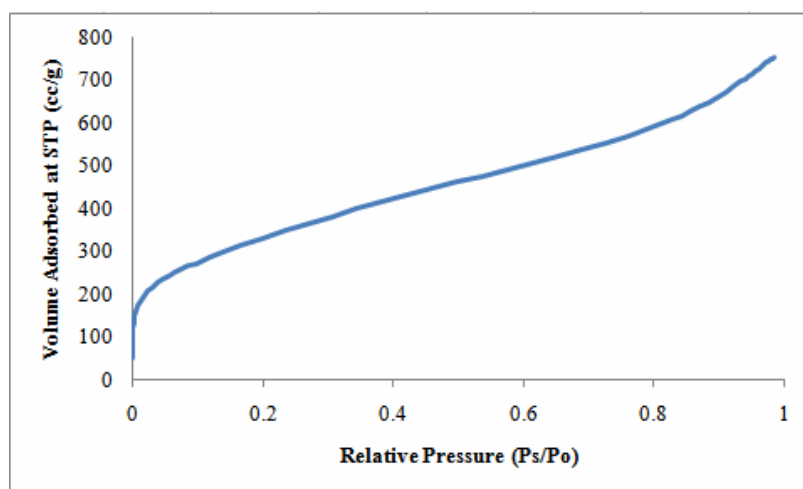


Figure 35 N₂ adsorption isotherm of undoped TiO₂.

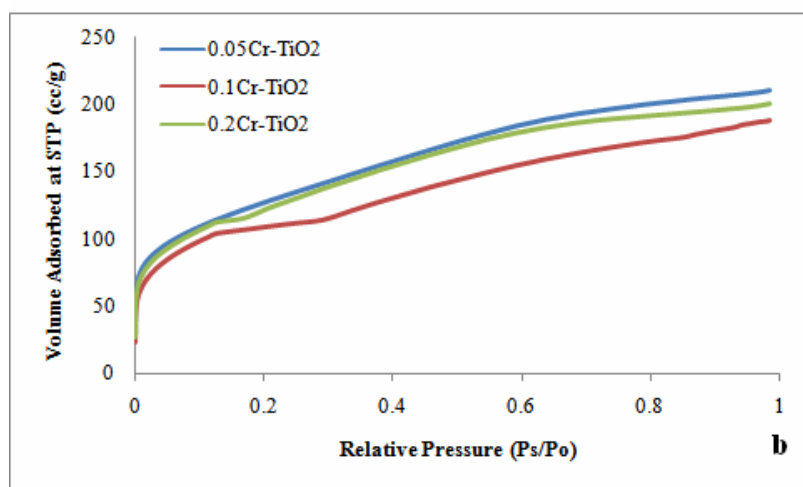
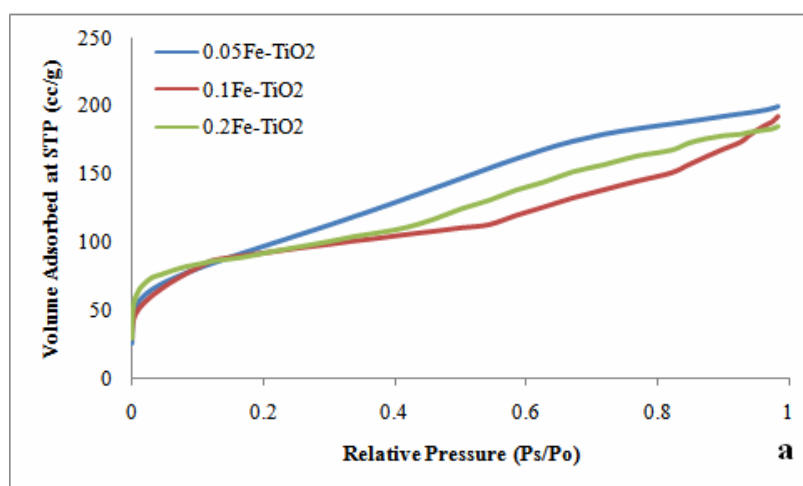


Figure 36 N₂ adsorption isotherm of doped TiO₂; (a) Fe-TiO₂, and (b) Cr-TiO₂.

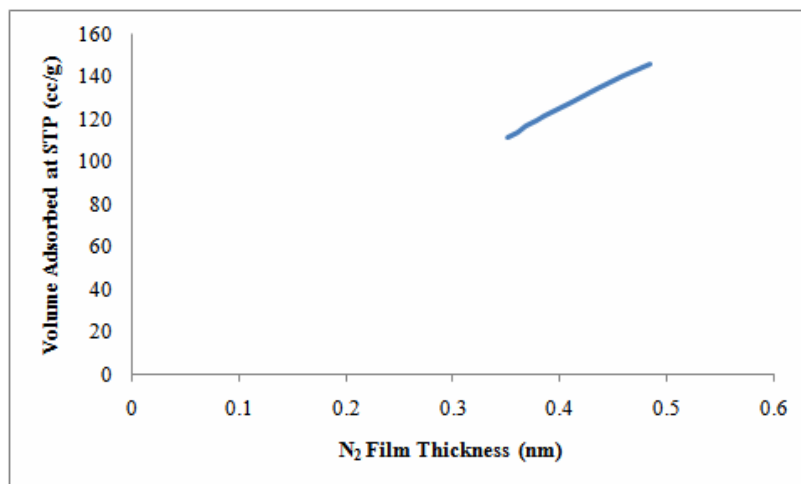


Figure 37 T-plot of N₂ adsorption isotherm of undoped TiO₂.

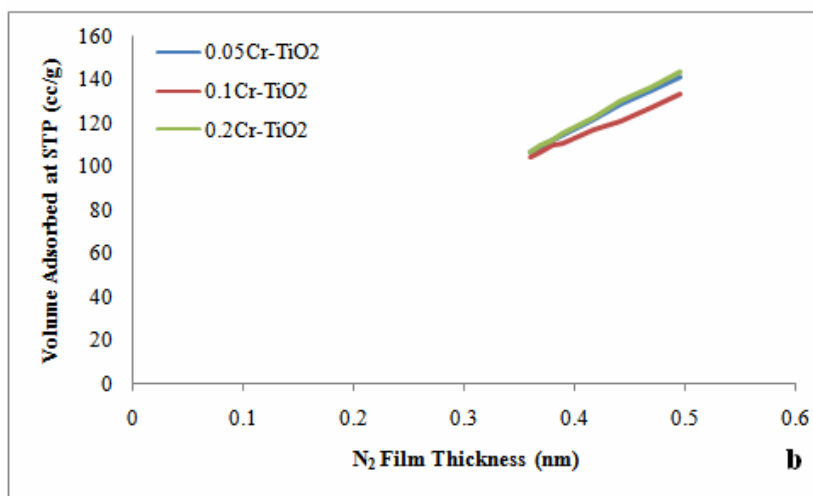
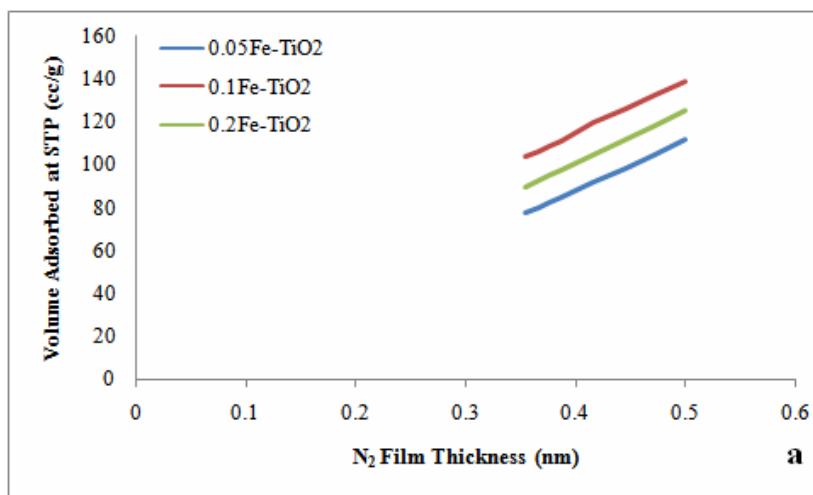


Figure 38 T-plot of N₂ adsorption isotherm of doped TiO₂; (a) Fe-TiO₂, and (b) Cr-TiO₂.

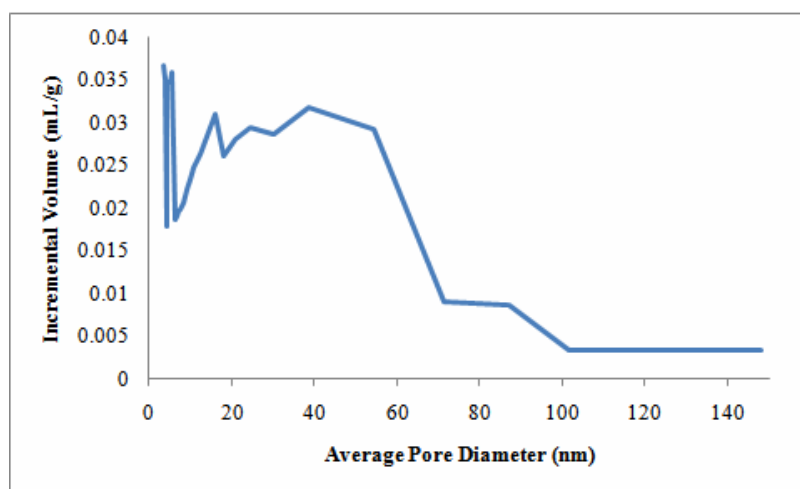


Figure 39 Pore size distribution curve of undoped TiO₂.

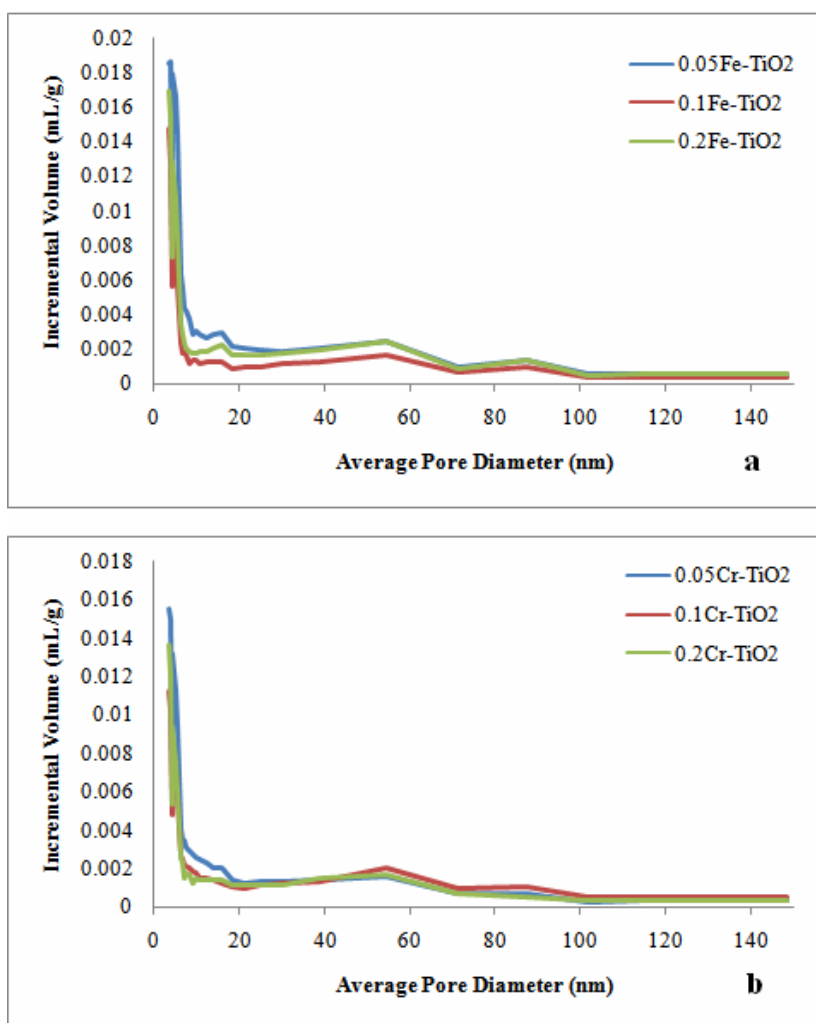


Figure 40 Pore size distribution curve of doped TiO₂; (a) Fe-TiO₂, and (b) Cr-TiO₂.

(h) Electron spin resonance spectroscopy

Electron spin resonance (ESR) or electron paramagnetic resonance (EPR) spectroscopy is a technique for studying chemical species that have one or more unpaired electrons, such as organic and inorganic free radicals, inorganic complexes possessing a transition metal ion or metal oxide material. ESR spectroscopy is a very powerful and sensitive method for the characterization of the electronic structures of materials with unpaired electrons. There is a variety of ESR techniques, each with its own advantages. In continuous wave ESR (CW-ESR), the sample is subjected to a continuous beam of microwave irradiation of fixed frequency and the magnetic field is swept. Different microwave frequencies may be used and they are denoted as S-band (3.5 GHz), X-band (9.25 GHz), K-band (20 GHz), Q-band (35 GHz) and W-band (95 GHz). Other techniques, such as electron nuclear double resonance (ENDOR) and electron spin echo envelope modulation (ESEEM) spectroscopies, record in essence the NMR spectra of paramagnetic species. Electron spin resonance has been applied for the characterization of transition metal ions that are present in the lattice and on the surface, coordinated to lattice oxygen atoms or to extra-lattice ligands (Weckhuysen, *et al.*, 2004).

The ESR spectrum was obtained from JEOL, JES-RE2X model at room temperature with ES-IPRIT software, in the original single TE₀₁₁ cylindrical cavity, and X-band microwave frequency (8.8-9.6 GHz). The ESR spectra of undoped TiO₂ and doped TiO₂ (Fe-TiO₂ and Cr-TiO₂) are shown in Figures 41-42, respectively. Table 11 lists assigned peak corresponding to ESR spectra of synthesized TiO₂ samples.

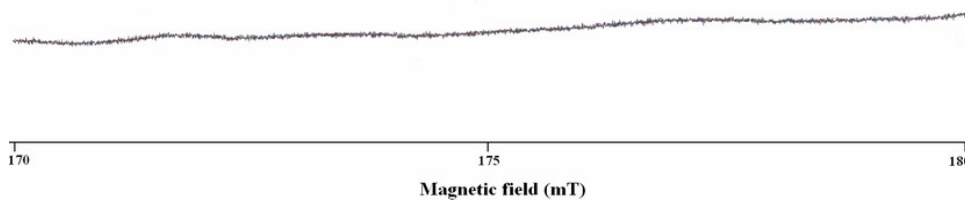


Figure 41 ESR spectrum of undoped TiO₂.

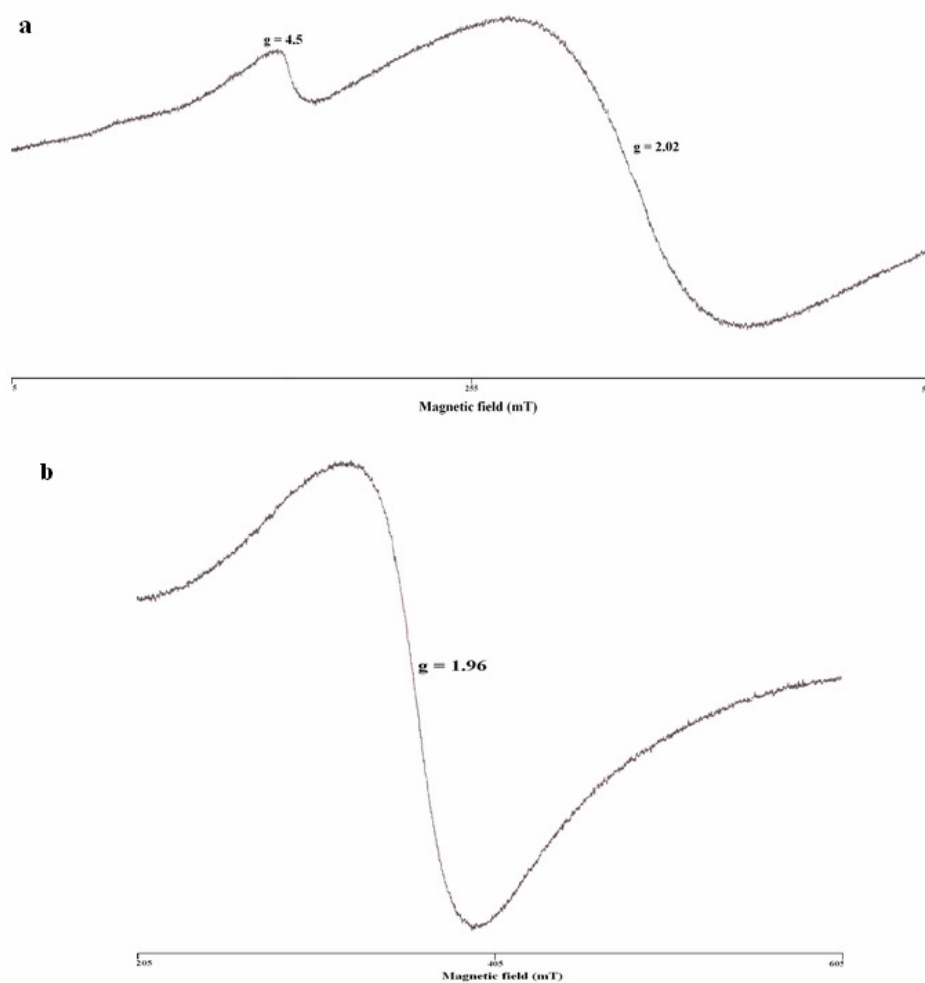


Figure 42 ESR spectra of doped TiO₂; (a) Fe-TiO₂, and (b) Cr-TiO₂.

Table 11 ESR signal of synthesized TiO₂ samples.

TiO ₂ sample	g value	Assignment	Reference
Undoped TiO ₂	-	Pure TiO ₂	Coronado and Soria, 2007
Fe(III) doped TiO ₂	2.02, 4.50	Fe(III) in TiO ₂ lattice	Tong, <i>et al.</i> , 2008
Cr(III) doped TiO ₂	1.96	Cr(III) in TiO ₂ lattice	Fabielle, <i>et al.</i> , 2008

(i) X-ray fluorescence spectrometer

X-ray fluorescence (XRF) is the emission of characteristic "secondary" (or fluorescent) X-rays from a material that has been excited by bombarding with high-energy X-rays or gamma rays. The phenomenon is widely used for elemental analysis and chemical analysis, particularly in the investigation of metals, glass, ceramics and building materials, and for research in geochemistry, forensic science and archaeology. In this work, XRF was used to confirm the deposition of metal ions and to determine the quantity of the ions in TiO₂ samples. In determining the quantities of Fe(III) and Cr(III) coexisted with TiO₂, the standard addition was used and the results are shown in Table 12.

Table 12 Percentage of Fe(III) and Cr(III) amount in doped TiO₂.

TiO ₂ sample	Amount of metal ions in TiO ₂ (mol%)	
	Preparation	Found
Fe-TiO₂		
0.05Fe-TiO ₂	0.05	0.032
0.1Fe-TiO ₂	0.10	0.075
0.2Fe-TiO ₂	0.20	0.125
Cr-TiO₂		
0.05Cr-TiO ₂	0.05	0.034
0.1Cr-TiO ₂	0.10	0.062
0.2Cr-TiO ₂	0.20	0.115

3.1.3 Optimum conditions for preparation TiO₂ samples

The optimum conditions for preparation of undoped and trivalent (Cr, Fe) doped TiO₂ were determined by studying the effect of dopant concentrations, doping time, and drying temperature. The results can be divided into two cases; (1) undoped TiO₂ and (2) trivalent (Cr, Fe) doped TiO₂. The optimum conditions of both cases were determined based on the degradation efficiency of MB aqueous solution at 2.5×10^{-5} M.

(a) Optimum conditions for preparation of undoped TiO₂

In this work, undoped TiO₂ product exists in an amorphous form. The major factor that affects the phase of product is the drying temperature. Therefore, the effect of drying temperature and drying duration were studied. In the drying step of undoped TiO₂ syntheses, the sample was dried at various temperatures as well as duration of drying and the data are shown in Table 13.

Table 13 Drying temperature, drying duration and phase of undoped TiO₂.

Method	Drying temperature (°C)	Drying duration (h)	Phase ^a
A	80	36	Amorphous
B	105	24	Amorphous
C	150	12	Amorphous + anatase

^aDetermined by XRD

The undoped products from A, B, C methods showed no significant difference in decolorization efficiency with complete decolorizations were reached in

less than 1 h. The method B, however, was selected as optimal condition for preparation because of its pure phase obtained in shorter time.

(b) Optimum conditions for preparation of trivalent (Cr, Fe) doped TiO_2

In the preparation of trivalent (Cr, Fe) doped TiO_2 , various factors (doping concentrations, doping duration, stirring speed) that can affect the product qualities were evaluated based on degradation efficiency of MB under UV irradiation. Figures 43-45 show the effect of these factors in the preparation of trivalent (Cr, Fe) doped TiO_2 .

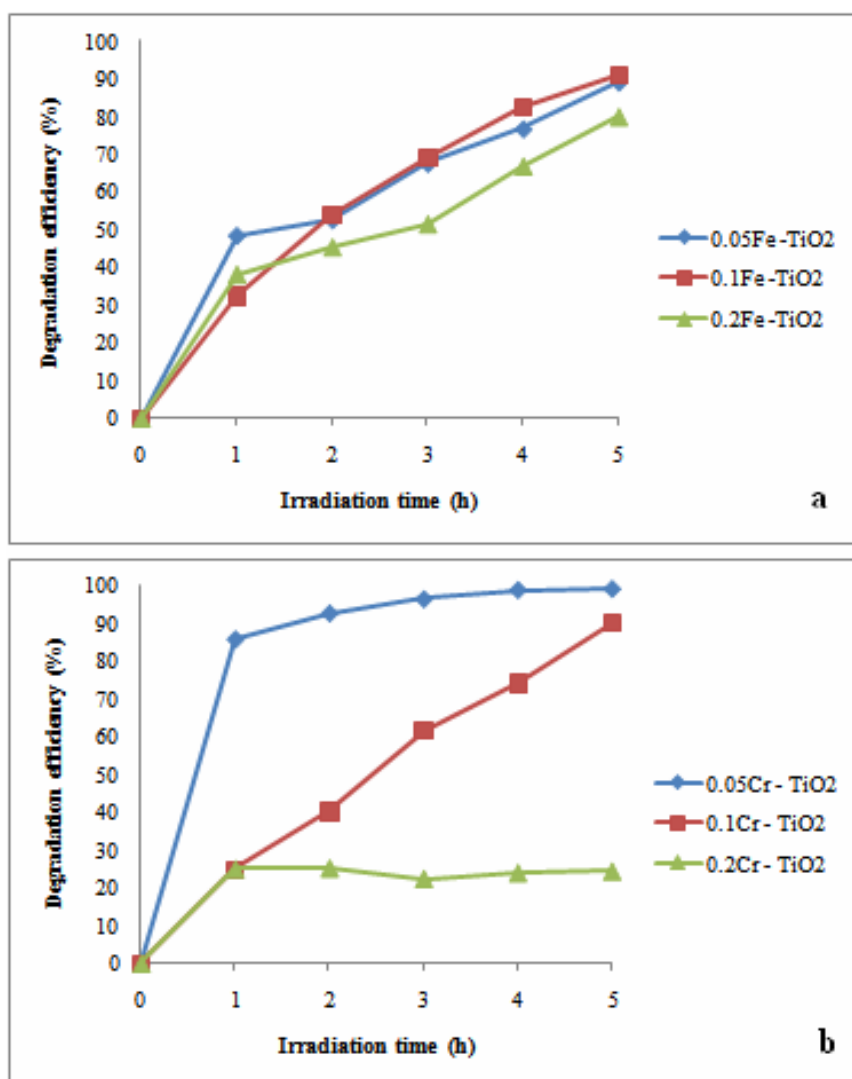


Figure 43 Effect of dopant concentrations in the preparation of doped TiO₂; (a) Fe-TiO₂, and (b) Cr-TiO₂.

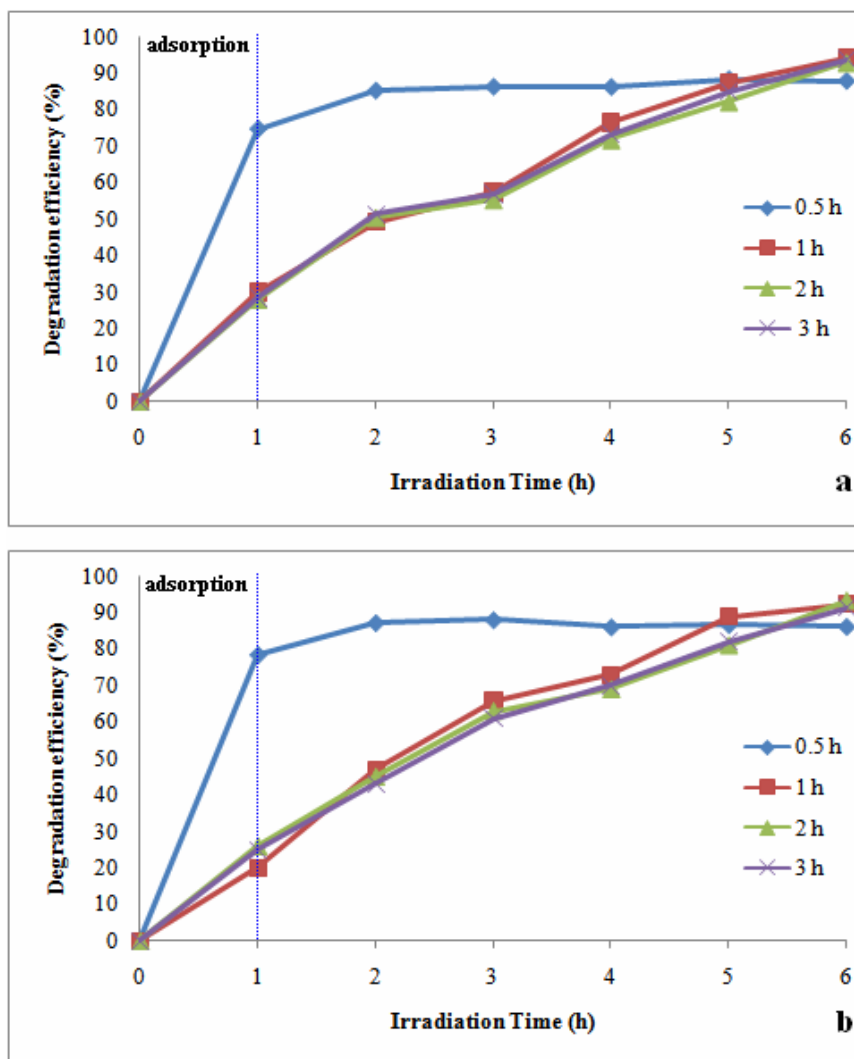


Figure 44 Effect of doping duration in the preparation of doped TiO₂; (a) Fe-TiO₂, and (b) Cr-TiO₂.

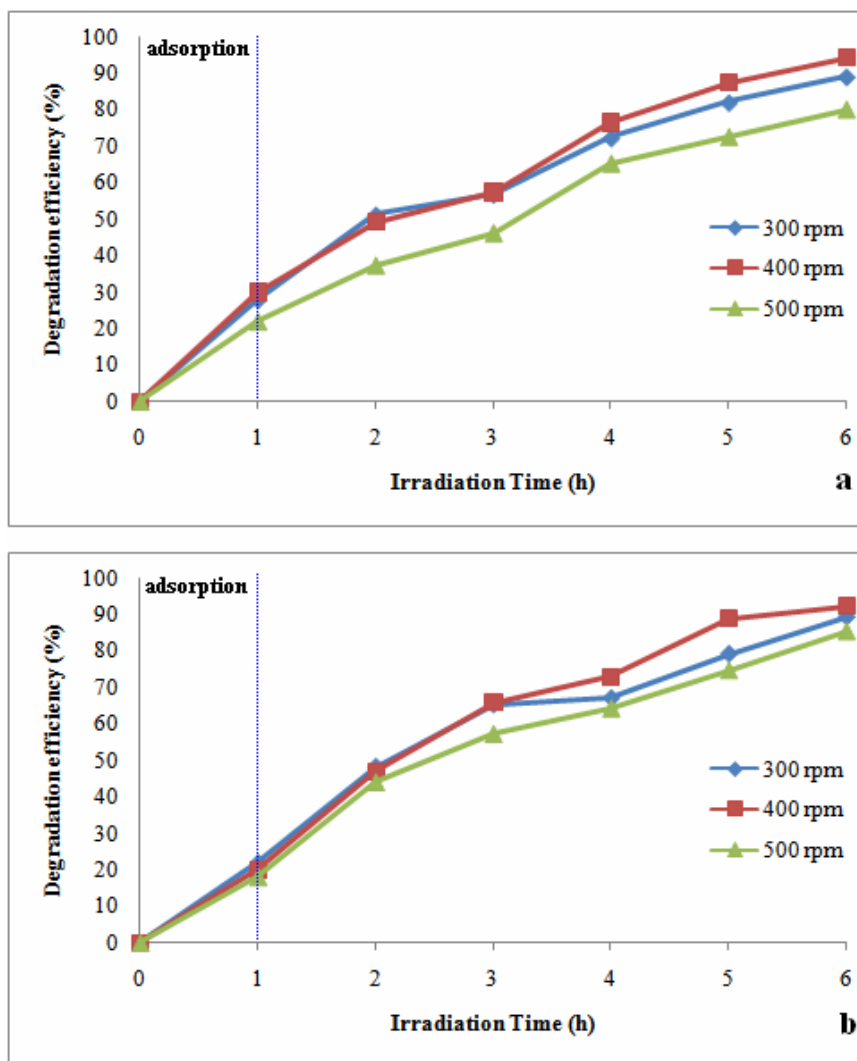


Figure 45 Effect of stirring speed in the preparation of doped TiO₂; (a) Fe-TiO₂, and (b) Cr-TiO₂.

From Figures 43-45, the optimum conditions for the preparation of trivalent (Cr, Fe) doped TiO₂ were studied from the ones that gave product showing greatest degradation efficiencies. These conditions were 0.1 mol% dopant concentration, 1 h doping duration, and 400 rpm stirring speed.

3.2 Photocatalytic activities of MB by undoped TiO₂, trivalent (Cr, Fe) doped TiO₂, and commercial TiO₂

In this work, the photocatalytic activities of TiO₂ samples were evaluated using MB as a model organic dye compound under UV and visible light irradiation.

3.2.1 Preparation of calibration graph

MB concentrations were measured by using the standard calibration graph. The concentration of standard MB solutions were prepared in the range 1.0×10^{-6} M to 1.0×10^{-3} M. In order to construct reliable standard calibration graph of MB, the concentrations were divided into three ranges: 1.0×10^{-6} M to 1.0×10^{-5} M, 1.0×10^{-5} M to 1.0×10^{-4} M, and 1.0×10^{-4} M to 1.0×10^{-3} M. The absorbance of MB solution was measured with SPECORD S100 spectrophotometer at $\lambda = 665$ nm. The standard calibration graphs of MB in these ranges are shown in Figures 46-48.

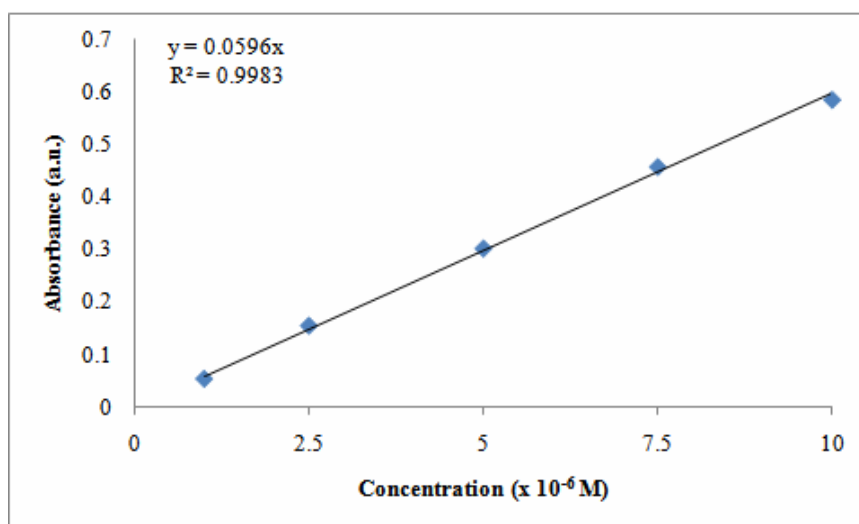


Figure 46 The standard calibration graph of MB solution in the range of 1.0×10^{-6} M to 1.0×10^{-5} M.

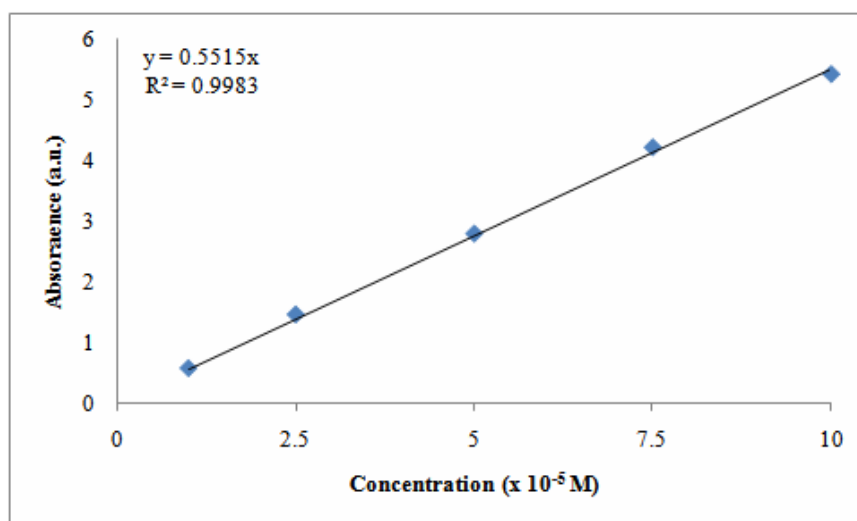


Figure 47 The standard calibration graph of MB solution in the range of 1.0×10^{-5} M to 1.0×10^{-4} M.

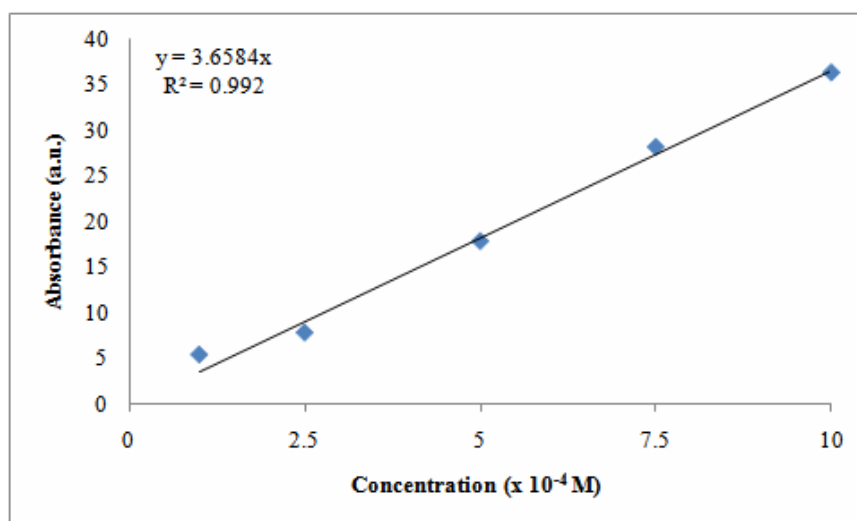


Figure 48 The standard calibration graph of MB solution in the range of 1.0×10^{-4} M to 1.0×10^{-3} M.

3.2.2 The experiments for photocatalytic degradation of MB by undoped TiO₂ and trivalent (Cr, Fe) doped TiO₂ powders

Degradation of MB solution was divided into 2 cases: (1) undoped TiO₂, and (2) trivalent (Cr, Fe) doped TiO₂. Each case can be divided further into 3 sub-cases: (a) the adsorption study, (b) the photocatalytic activity under UV irradiation, and (c) the photocatalytic activity under visible light irradiation. In the adsorption case, 0.05 g of each TiO₂ sample was placed in an Erlenmeyer flask which contained 100 mL of MB solution the mixture was then continuously stirred in the closed wooden compartment to avoid interference from ambient light until the end of experiment, 5 h. At time intervals (every 1 h), 5 ml of MB solution samples were collected. The degradation of MB solutions was analyzed from the changes in absorbance of the absorption maximum at 665 nm using UV-Vis spectrophotometer. For the photoreaction cases, the same amount of reactants were used in the same reaction compartment. Before switching on the lamp, the mixture was stirred for 1 h in the dark to reach the adsorption equilibrium. Then the light source was switched on (UV or visible light) and magnetically stirred for 5 h (UV) or 12 h (visible light). After that, 5 ml of MB solution was taken out every interval time for analysis and the concentration was read off from the calibration graph. The percentage of MB decolorized (adsorption study) or degraded (photocatalytic study) was determined from the following equation;

$$\% \text{ of MB decolorized (or degraded)} = \frac{C_0 - C_t}{C_0} \times 100 \quad \text{.....(20)}$$

where C₀ is the initial concentration of MB solution and C_t is the concentration of MB solution at specific time interval when the aliquot was collected.

(1) The case of undoped TiO₂

(a) The adsorption study of undoped TiO₂

The decolorization of MB solution at various concentrations by undoped TiO₂ is shown in Figure 49 and Table 14.

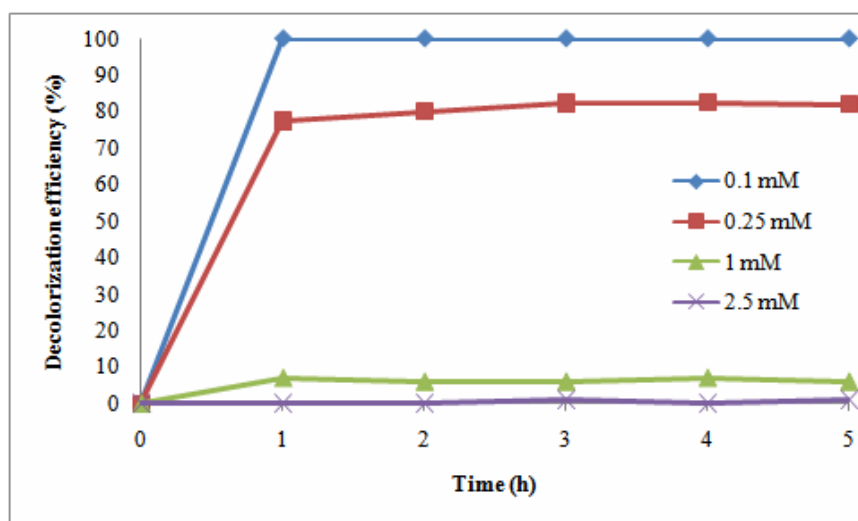


Figure 49 Decolorization of MB by undoped TiO₂ at various concentrations (selected data from Table 14).

Table 14 The percentage of MB decolorization by undoped TiO₂ at various concentrations.

MB concentration	Decolorization efficiency (%) at adsorption time (h)				
	1	2	3	4	5
1 μ M	100	100	100	100	100
2.5 μ M	100	100	100	100	100
10 μ M	100	100	100	100	100
25 μ M	100	100	100	100	100
0.1 mM	100	100	100	100	100
0.25 mM	77.53	80.16	82.42	82.53	82.07
1 mM	7.13	6.34	6.68	7.07	7.88
2.5 mM	0	0	0.53	0.24	0.45

Complete decolorizations of MB by undoped TiO₂ were obtained in 1 h. when the dye concentrations were low (below 0.1 mM). This decolorization resulted solely from adsorption only. At higher concentrations (0.25 mM and up) which exceed the adsorption saturation point the % decolorization decreased as an intense color of dye still remained in solution.

(b) The photocatalytic activity of undoped TiO₂ under UV irradiation

The photocatalytic study of undoped TiO₂ under UV light irradiation was investigated with MB concentrations in the range 0.25-2.5 mM. The degradation efficiencies at three concentrations (included adsorption) are shown in Figure 50.

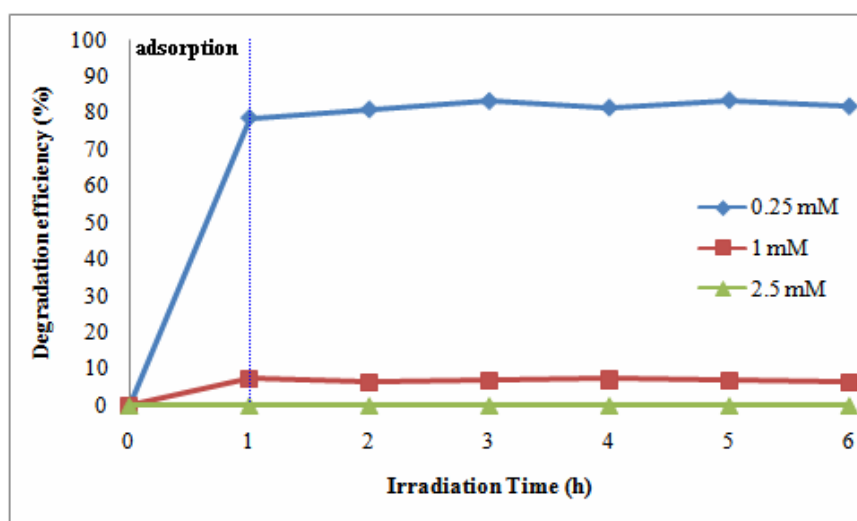


Figure 50 Photocatalytic activity of undoped TiO₂ under UV irradiation at high MB concentrations.

(c) The photocatalytic activity of undoped TiO₂ under visible light irradiation

The degradation efficiencies of undoped TiO₂ under visible light irradiation (included adsorption) are shown in Figure 51. The same experimental conditions as in case (b) above were used.

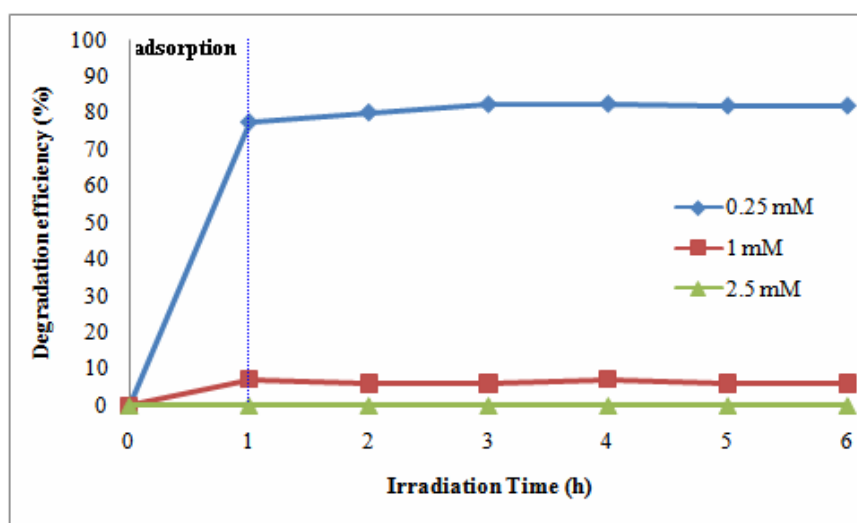


Figure 51 Photocatalytic activity of undoped TiO₂ under visible light irradiation at high MB concentrations.

It is clear, from Figures 50-51, that undoped TiO₂ did not show the photoactivity both under UV and visible light in all investigated concentrations.

(2) The case of trivalent (Cr, Fe) doped TiO₂

MB solution at one concentration, 2.5×10^{-5} M, was used in the experiments to assess the efficiencies of the doped TiO₂ samples in decolorization of dye either by adsorption or by photocatalytic degradation.

(a) Adsorption study for trivalent (Cr, Fe) doped TiO₂

The color of MB solution can fade away by adsorption onto the TiO₂ surface. Decolorization efficiencies of doped TiO₂, Fe-TiO₂ and Cr-TiO₂ are shown in Figures 52 and 53, respectively.

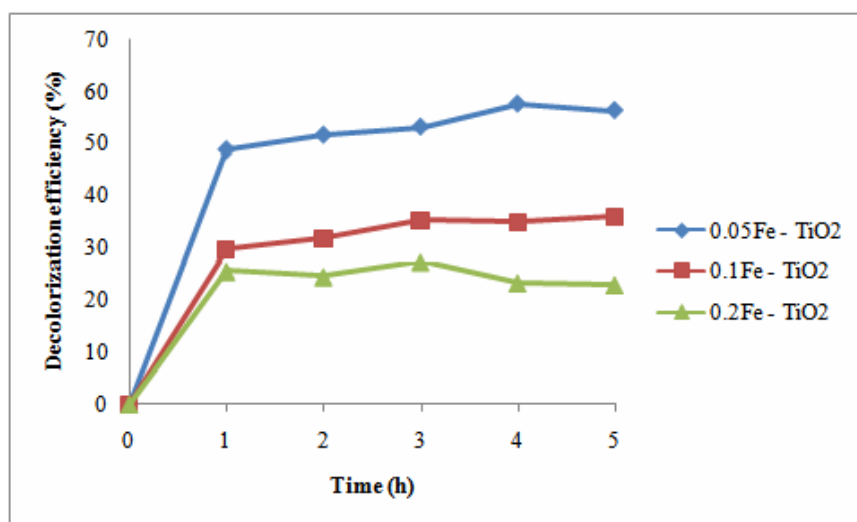


Figure 52 Decolorization efficiency of MB by Fe-TiO₂ (adsorption).

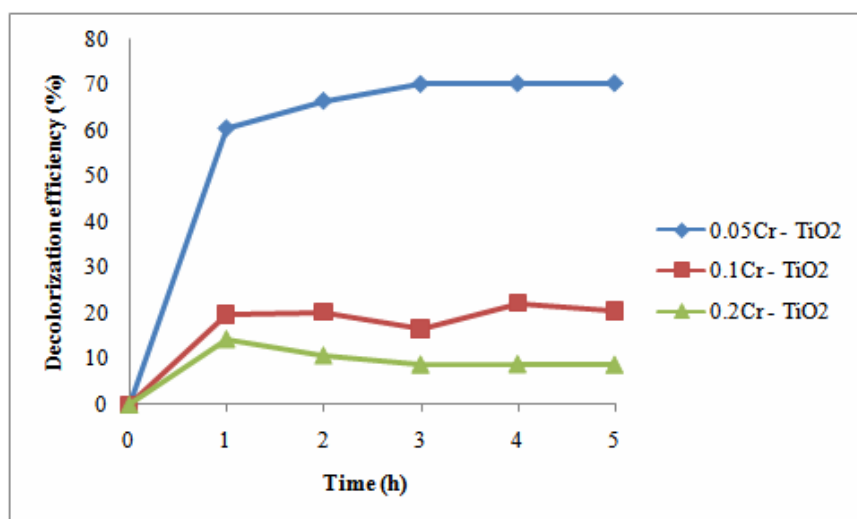


Figure 53 Decolorization efficiency of MB by Cr-TiO₂ (adsorption).

Figures 52 and 53 show the effect of varying amount of dopant in range 0.05-0.2 mol%. Decolorization in this experiment was due to loss of dye molecules from solution phase as they were adsorbed onto the TiO_2 surface. The results showed that the decolorization efficiency of MB dye decreased when doping amount increased.

(b) The photocatalytic activity of trivalent (Cr, Fe) doped TiO_2 under UV irradiation

Degradation efficiencies of doped TiO_2 , Fe- TiO_2 and Cr- TiO_2 , under UV irradiation (included adsorption) are shown in Figures 54 and 55, respectively.

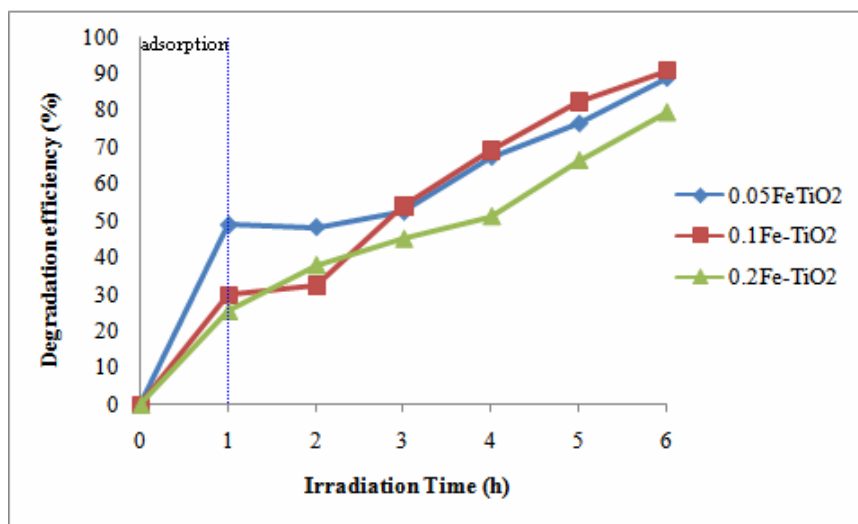


Figure 54 Degradation efficiency of MB by Fe- TiO_2 under UV irradiation.

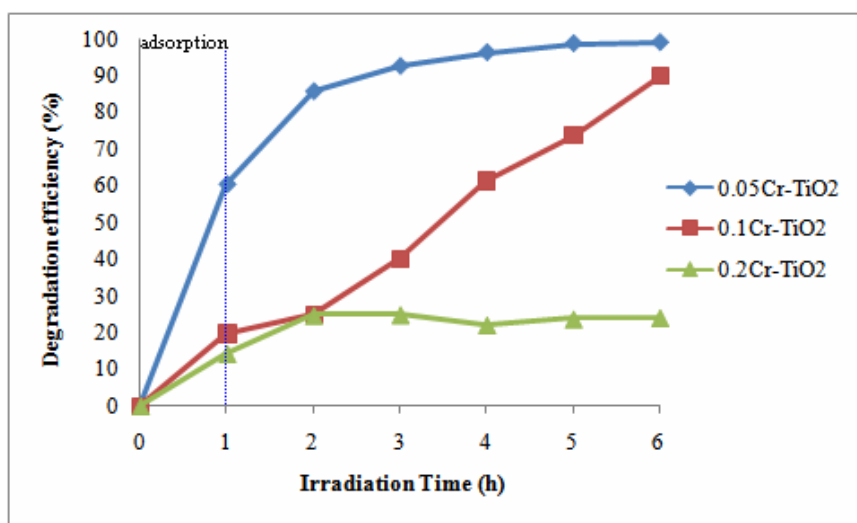


Figure 55 Degradation efficiency of MB by Cr-TiO₂ under UV irradiation.

(c) The photocatalytic activity of trivalent (Cr, Fe) doped TiO₂ under visible light irradiation

Degradation efficiencies of doped TiO₂, Fe-TiO₂ and Cr-TiO₂, under visible light irradiation (included adsorption) are shown in Figures 56 and 57, respectively.

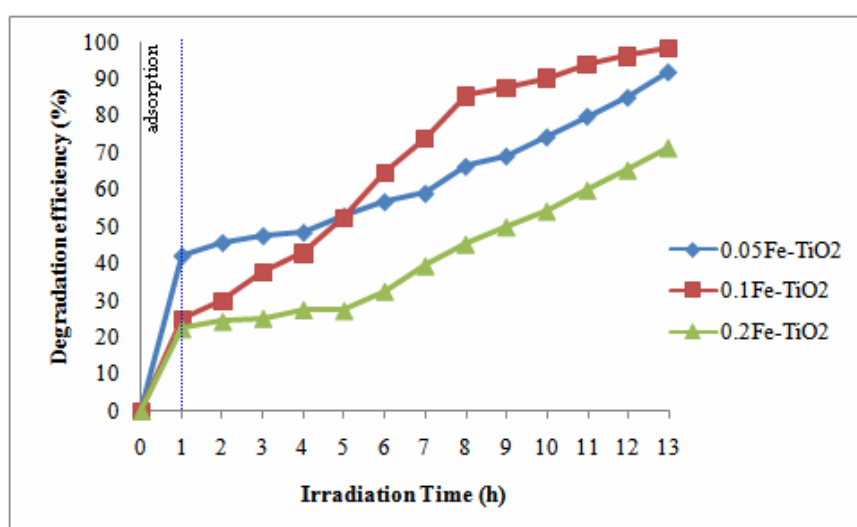


Figure 56 Degradation efficiency of MB by Fe-TiO₂ under visible light irradiation.

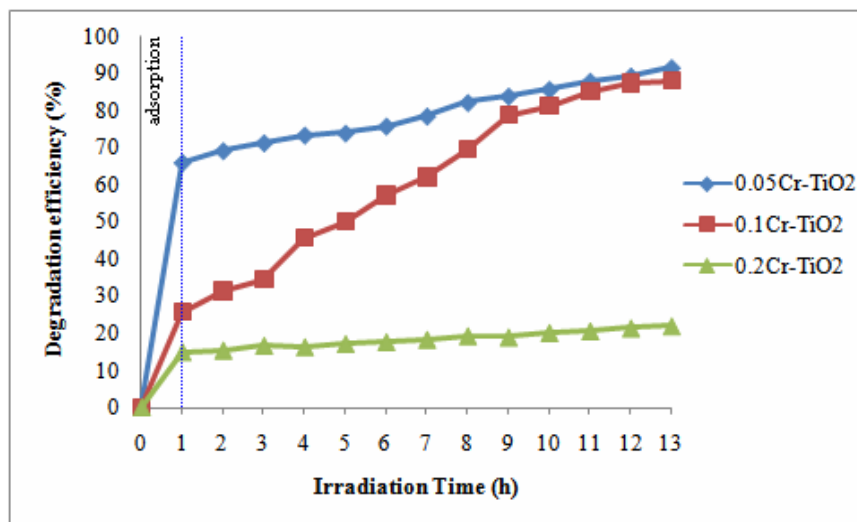


Figure 57 Degradation efficiency of MB by Cr-TiO₂ under visible light irradiation.

From the data shown in Figures 54-57, the 0.1 mol% doped samples of both Fe(III) and Cr(III) showed the most improvement in % degradation (after 1 h adsorption) than the other two doping values. Therefore, the 0.1Fe-TiO₂ and 0.1Cr-TiO₂ were selected as the best doping ratio and were used in the following studies in comparison with commercial TiO₂, anatase and Degussa P25.

3.2.3 Comparative photocatalytic studies of trivalent (Cr, Fe) doped TiO₂ with commercial TiO₂ powders.

As mentioned above, the 0.1 mol% is the best doping concentration for both Fe(III) and Cr(III). These doped samples, 0.1Fe-TiO₂ and 0.1Cr-TiO₂, were then put to test for photocatalytic efficiencies in direct comparison with the commercial samples, anatase and Degussa P25, under UV and visible light irradiation. The results from these comparative studies are shown in Figures 58 and 59, respectively.

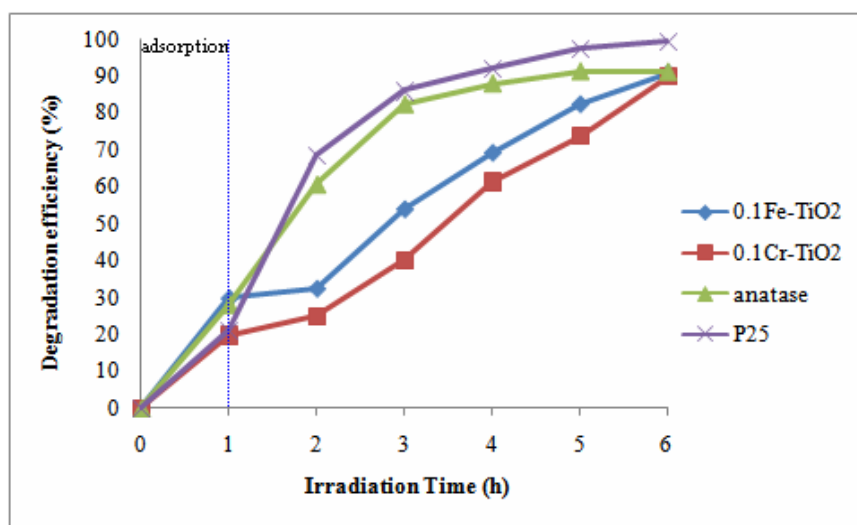


Figure 58 Comparative degradation efficiencies of MB by 0.1Fe-TiO₂, Cr-TiO₂ and commercial TiO₂ under UV irradiation.

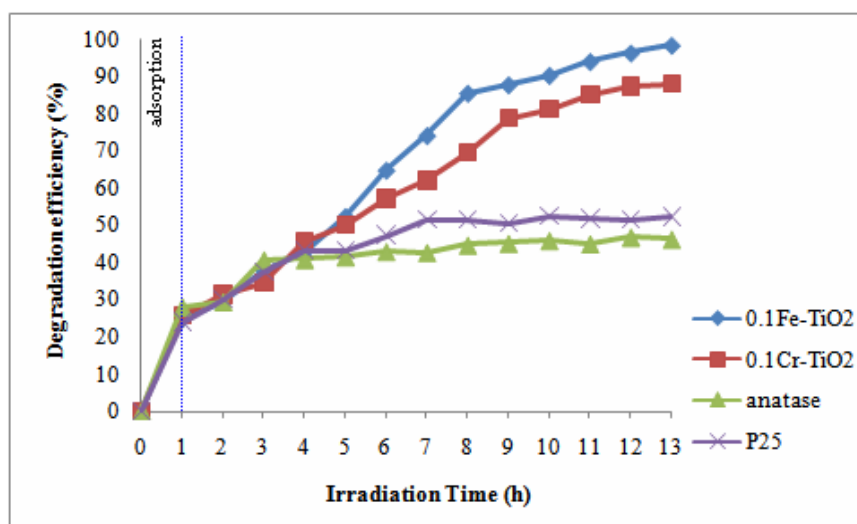


Figure 59 Comparative degradation efficiencies of MB by 0.1Fe-TiO₂, Cr-TiO₂ and commercial TiO₂ under visible light irradiation.

Chapter 4

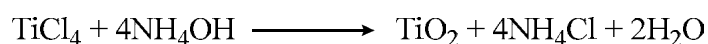
Discussions

4.1 Synthesis and characterizations of TiO₂ powders

4.1.1 Synthesis of undoped and trivalent (Cr, Fe) doped TiO₂ powders

(1) Undoped TiO₂

In the present study, undoped TiO₂ powder was synthesized from reaction between TiCl₄ and diluted NH₃ solution via base-catalyzed sol-gel method. During the reaction process, white precipitate formed and large amount of white smoke due to the formation of HCl were observed. The synthesis can be described by the following chemical reaction (Kanna, 2002);

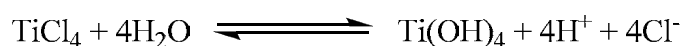


In general, the sol-gel process consists of two sub-reactions, hydrolysis and condensation reactions. The hydrolysis reaction leads to the formation of original nuclei of TiO₂ whereas the condensation reaction leads to the growth of network system of original nuclei (Kumar, *et al.*, 1999).

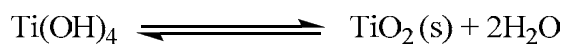
Zhang, *et al.*, (2000) suggested that the equilibrium between the hydrolysis reaction and condensation reaction possibly made the formation of TiO₂ in rutile phase possible, after the neutralization of ammonia solution, the equilibrium between the hydrolysis and condensation was broken and the condensation reaction or the growth rate was possible to accelerate for the formation of anatase phase (Zhang, *et al.*, 2000). According to Tang, *et al.*, (2002) the formation of anatase and rutile TiO₂ is determined by the hydrolysis and condensation reactions. If the condensation starts before completion of hydrolysis, either amorphous or anatase TiO₂ will form. And also, in neutral and basic conditions, condensation starts before complete hydrolysis, while acid condition promotes the hydrolysis and decreases the condensation (Tang, *et al.*, 2002).

Generally, NH_4OH most likely dissociates to NH_3 and H_2O than NH_4^+ and OH^- (Leblanc, *et al.*, 1978). In the present work, the synthesis of TiO_2 route base-catalyzed sol-gel method can be explained in term of the hydrolysis and the condensation reactions as (Suwanachawalit, 2005);

The hydrolysis reaction



The condensation reaction



The resulting powder existed in an amorphous form because the condensation started before completion of the hydrolysis (Tang, *et al.*, 2002). Along the hydrolysis reaction, white smoke of HCl and heat occurred. Then the thermal from hydrolysis reaction accelerated condensation reaction. The reaction was carried out at low temperature, in the ice-bath, to avoid and reduce the strong reactions between TiCl_4 and NH_4OH .

(2) Trivalent (Cr, Fe) doped TiO_2

TiO_2 doped with $\text{Fe}(\text{III})$ and $\text{Cr}(\text{III})$, namely Fe-TiO_2 and Cr-TiO_2 , were prepared by incipient wetness impregnation processes, using aqueous solution of $\text{CrCl}_3 \cdot 6\text{H}_2\text{O}$ and FeCl_3 as the dopant sources, respectively. The light-brownish and greenish powders of Fe-TiO_2 and Cr-TiO_2 , respectively, resulted after the doping process.

4.1.2 Characterizations of TiO₂ powders

(a) X-ray powder diffractometer (XRD)

XRD patterns of undoped, doped, and commercial TiO₂ samples are shown in Figure 13. Only flat base lines were detected in all synthetic TiO₂ samples, confirming the amorphous nature of these samples. No XRD diffraction pattern peaks of the dopants could be observed possibly due to quantity of the metal ions doped to TiO₂ was too small to be detected by XRD (Lee, *et al.*, 2001; Yuan, *et al.*, 2007). The commercial Degussa P25 shows pattern of both anatase ($2\theta = 25.4^\circ$) and rutile ($2\theta = 27.5^\circ$) phases in the ratio of *ca.* 4:1, calculated by the intensities obtained from the area of the most intense diffraction peaks of these two modifications, whereas the commercial anatase shows only anatase phase, $2\theta = 25.4^\circ$, of TiO₂ in the sample. The results from XRD technique confirmed that the synthesized, undoped TiO₂, sample existed in an amorphous form, and doping with trivalent (Cr, Fe) dopants did not affect the phase of products.

Generally, phase transformation of TiO₂ predominately takes place by the thermal processes. Huang, *et al.*, (1997) studied the phase transformation of TiO₂ in thermal process by using TGA/DTA technique and suggested that xerogel TiO₂ began to change to an amorphous TiO₂ around 90 °C and completely changed to an amorphous TiO₂ at 180 °C. If the thermal was added continuously, the amorphous form changed to anatase form in the range 380-430 °C, moreover, if heating up further the anatase could be changed to the rutile phase around 588 °C but was not complete even when heated up to 800 °C (Huang, *et al.*, 1997).

(b) Diffuse reflectance spectroscopy (DRS)

UV-vis spectroscopy has been used to characterize the bulk structure of TiO₂. TiO₂ is a semiconducting oxide with easily measured optical band gap. UV-vis diffuse reflectance spectroscopy is used to probe the band structure or molecular energy levels in the materials since UV-vis light excitation creates photo-generated electron and holes (Reddy, *et al.*, 2001).

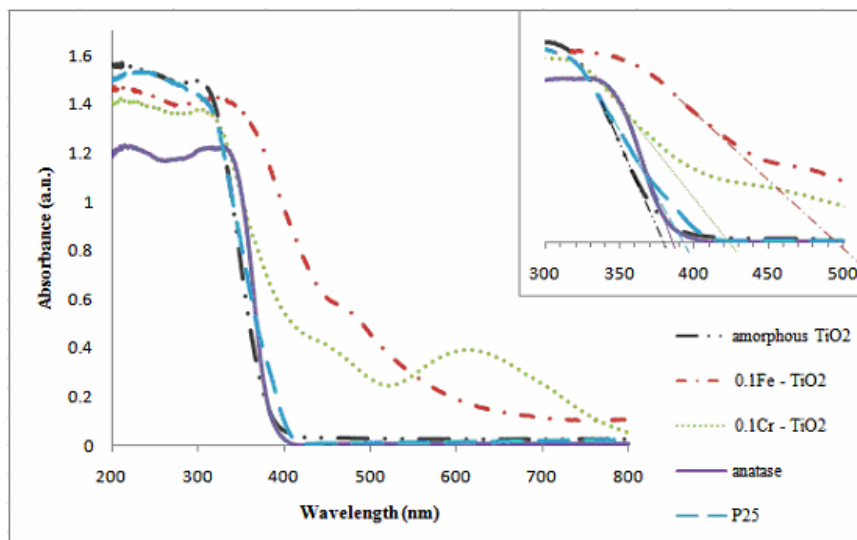


Figure 60 DRS spectra of undoped, doped, and commercial TiO₂. Inset: λ_{onset} of absorption of TiO₂ samples.

Figure 60 shows the UV-vis diffuse reflectance spectra of synthetic TiO₂ samples, together with the commercial materials, anatase (Carlo Erba) and Degussa P25. The absorption edge of undoped TiO₂ is found to be at the shorter wavelength than that of other samples. It is evident that undoped TiO₂ has no adsorption in the visible light region (>400 nm) whereas trivalent (Cr, Fe) doped TiO₂ displays a wide absorption band in the range 400-700 nm. When transition metal ions are present in the system, their characteristic d-d absorptions can be used to confirm their presence and charges. In the case of Cr-TiO₂, the absorption around 450 nm is due to the charge transfer band Cr(III) → Ti(IV) or ${}^4A_{2g} \rightarrow {}^4T_{1g}$ of Cr(III) in an octahedral environment and the broad absorption band from 620 to 800 nm is due to ${}^4A_{2g} \rightarrow {}^4T_{2g}$ d-d transitions of Cr(III) (Zhu, *et al.*, 2006). For the Fe-TiO₂, a broad absorption peak around 520 nm can be assigned to the absorption of Fe(III) in octahedral symmetry (Lee, *et al.*, 2001). Besides being useful in helping characterization the transition metal ions, the extended absorbance of TiO₂ samples into the visible region provides a possibility for enhancing the photocatalytic behavior of TiO₂ for solar energy application.

Undoped TiO₂ shows significantly higher band gap energy than doped TiO₂ samples, however, doped TiO₂ powders, Cr-TiO₂ and Fe-TiO₂ show

bathochromic shift of light absorption compared with undoped TiO₂, e.g. the onset of absorbance of 0.1Fe-TiO₂ and 0.1Cr-TiO₂, extended to 496 and 434 nm, respectively.

Because of the difference in the particle size of synthesized TiO₂ and commercial product, it is clear that the band gap energy of synthesized TiO₂ should be larger than those commercial products. It had been known and demonstrated by many that the properties of nanosized particles depend very sensitively on the particle size. This is the so-called “quantum size effect”. As the diameter of crystallite approaches the exciton Bohr diameter, a splitting of the energy bands into discrete quantized energy level occur, it leads to a blue-shift in the absorption spectrum due to increased band gap nonlinear optical properties (Reddy, *et al.*, 2001). Thus, it means that as the particle size decreases the band gap energy increases vice versa. In order to determine the nature of the band gap and the type of band-to-band transition in synthesized TiO₂, either indirect or direct transition one has to consider the expression for the variation of the absorption coefficient with energy. Figures 17 and 18 show the plot of $(\alpha E_{phot})^2$ versus E_{phot} for a direct transition and $(\alpha E_{phot})^{1/2}$ versus E_{phot} for an indirect transition, respectively. The value of E_{phot} extrapolated to $\alpha = 0$ gives an absorption energy which corresponds to a band gap energy (E_g). As seen in Figure 17 for direct transition, undoped TiO₂ shows a perfect fit and the extrapolation yields an E_g value of 3.46 eV. Similarly, the commercial sample: anatase and Degussa P25 show an E_g value of 3.30 and 3.25 eV, respectively, which the trivalent (Cr, Fe) doped TiO₂ samples show an E_g values in the range 3.20-3.22 eV and 2.72-2.80 eV for Fe-TiO₂ and Cr-TiO₂, respectively. Comparison of an E_g values between direct method and equation (12), the results are significantly difference which could be attributed to particle size of the samples. Serpone *et al.*, (1995) had established the mechanism believed being operatively in nanophase TiO₂. These authors had attributed the spectral blue shifts due to quantum size effects in TiO₂ colloids as a result of direct transitions (Serpone, *et al.*, 1995). In this work, doped TiO₂ shows red-shifted spectral compared with undoped sample possibly explained by the same reason. Figure 18 shows the $(\alpha E_{phot})^{1/2}$ versus E_{phot} of all TiO₂ samples. The value of E_g was estimated from the $\alpha = 0$ extrapolation as 3.01 eV for the undoped TiO₂, 3.12, and 2.97 eV for the commercial anatase and Degussa P25, respectively. For the doped TiO₂, Fe-TiO₂ and

Cr-TiO₂, the extrapolation yields E_g values in the range 1.79-1.82 eV and 2.20-2.22 eV, respectively. Both direct and indirect methods did not agree well with E_g values calculated from equation (12).

(c) Photoluminescence spectroscopy

Photoluminescence spectroscopy is a contactless, nondestructive method of probing the electronic structure of materials. Light is directed onto a sample, where it is absorbed and imparts excess energy into the material in a process called photo-excitation. One way this excess energy can be dissipated by the sample is through the emission of light, or luminescence. In the case of photo-excitation, this luminescence is called photoluminescence (PL). The intensity and spectral content of this PL is a direct measure of various important material properties such as band gap determination, impurity levels and defect detection, recombination mechanisms. Generally, photo-excitation causes electrons within the material to move into permissible excited states. When these electrons return to their equilibrium states, the excess energy is released and may include the emission of light (a radiative process) or may not (a nonradiative process). The energy of the emitted light (photoluminescence) relates to the difference in energy levels between the two electron states involved in the transition between the excited state and the equilibrium state. The quantity of the emitted light is related to the relative contribution of the radiative process (Gfroerer, 2000).

The PL technique has been widely used to investigate the structure and properties of the active sites on the surface of metal oxides and zeolites, because of its high sensitivity and non-destructive character. Also, the PL technique has been useful in the field of photocatalysis over semiconductors for understanding the surface processes. PL spectrum is an effective way to study the electronic structure, optical and photochemical properties of semiconductor materials, by which information such as surface oxygen vacancies and defects, as well as the efficiency of charge carrier trapping, immigration and transfer can be obtained. Therefore, it is of great significance for environmental photocatalysis. It is well known that the PL signals of semiconductor materials result from the recombination of photo-induced charge

carriers. In general, the lower the PL intensity, the lower the recombination rate of photo-induced electron - hole pairs, and the higher the photocatalytic activity of semiconductor photocatalysts. However, the photocatalytic activity of semiconductor photocatalysts can increase as the PL intensity becomes stronger. These results seem to be incompatible. In fact, the inherent relationships between the PL spectrum and photocatalytic activity are determined mainly by the attributes of the PL signal. To the best of our knowledge, despite some work about the PL spectra and photocatalytic activity, papers devoted solely to a systematic description of the PL technique of semiconductor nanomaterials have seldom been reported, especially about the relationships between the PL intensity and the photocatalytic activity on the basis of PL attributes (Gfroerer, 2000).

From Figures 19-21 which show the PL spectra of some TiO₂ samples, the band gap energies can be calculated by using equation (12), the results are shown in Table 15.

Table 15 Band gap energies of some TiO₂ samples obtained from PL.

TiO ₂ sample	λ_{\max} (nm)	Band gap energy (eV)
Undoped TiO ₂	388	3.20
Fe-TiO ₂	-	-
Cr-TiO ₂	-	-
Anatase	390	3.18
Degussa P25	396	3.13

- Cannot be determined

The normal pre-scan spectrum of TiO₂ shows two major bands around 400 nm (intrinsic band gap) and the range 500-800 nm (defects on surface). The λ_{\max} of absorption was used to determine band gap energy of each sample by using equation (12). The doped TiO₂ samples show different patterns from undoped and commercial TiO₂ powders that they do not show distinct peak for calculation of the band gap energy, so determination and confirmation of the band gap energy of doped TiO₂, Fe-TiO₂ and Cr-TiO₂, with PL are not possible. It has been pointed out that the intensity of PL spectrum corresponds to the photoactivity under UV irradiation (Kim, *et al.*, 2006). According to the Fe(III) dopant series, the 0.1 mol% showed highest PL intensity and also the greatest in photoactivities. Moreover, in Cr(III) dopant series, 0.1 mol% exhibited the same result.

(d) Fourier-transformed infrared spectroscopy (FT-IR)

The infrared spectra of all TiO₂ samples, undoped, doped, and commercial, in the range 4,000-400 cm⁻¹ are shown in Figures 22-26. The broad band around 3,425 cm⁻¹ corresponds to the stretching vibration of OH groups linking with titanium atoms (Ti-OH) and the band at 1,630 cm⁻¹ is the flexion vibration of OH group in adsorbed water (Wang, *et al.*, 2000; Kangle, *et al.*, 2009). These results confirm the presence of hydroxyl group in the structure of all synthetic TiO₂ samples. The adsorbed water and hydroxyl group are crucial to the photocatalytic reactions since they react with photo-excited holes on the catalyst surface to produce hydroxyl radicals, which are powerful oxidant (Kangle, *et al.*, 2009). Near this band at 3,050 cm⁻¹, a shoulder was generated by an asymmetric vibration mode of the residual ammonium ions. The broad band below 800 cm⁻¹ is attributed to the Ti-O stretching vibrations of TiO₂ phase. For commercial anatase TiO₂ a broad band at 710 cm⁻¹ is the confirmation of anatase phase (Zhang *et al.*, 2001). Degussa P25, consisting of both anatase and rutile, shows the bands at 682 and 503 cm⁻¹ due to the crystalline phases of anatase and rutile, respectively (Zhang *et al.*, 2001). The sharp band around 1,400 cm⁻¹ is the stretching bond of N-H from residual precursor while the band around 2,350 cm⁻¹ is CO₂ (Nakamoto, 1970; Belver, *et al.*, 2006).

(e) Scanning electron microscopy (SEM)

The SEM study gives only the information about the morphology and aggregation of particle. From SEM images of this study, which are shown in Figures 27-29, for undoped TiO₂, Fe-TiO₂, and Cr-TiO₂, respectively. The results appear in lower aggregation of spherical shape of particle. The dopants did not affect to the morphology and aggregation of samples, no obvious difference in SEM images between undoped and doped TiO₂ powders. The morphology of commercial TiO₂; anatase and Degussa P25 are shown in Figures 30 and 31, respectively. It could be seen that the habit of the commercial specimens are perfect spherical shape, compared with the synthetic TiO₂.

The roughness morphology of all synthetic TiO₂ powders, especially undoped TiO₂, is the nature of an amorphous form. The preparation technique is one of the main factor that has effect on the morphologies of samples. Zhang, *et al.*, (2007) synthesized the hydrated titania via two routes, either slow evaporation or rapid precipitation. The authors suggested that if the reaction occurred through a slow process an aggregation of TiO₂ forms rather spherical shape and the amount of water do not affect the shape of amorphous TiO₂ (Zhang and Maggard, 2007).

Shown in Figure 61, SEM analyses of amorphous TiO₂ reveal increasing particle sizes and aggregation for increasing amounts of ethanol used in the slow preparation step 2, 5, 10, and 20 mL for Figure (a)-(d), respectively. The larger particles result from the increased time for ethanol evaporation, but the different sizes do not affect the total amount of water in TiO₂ particles.

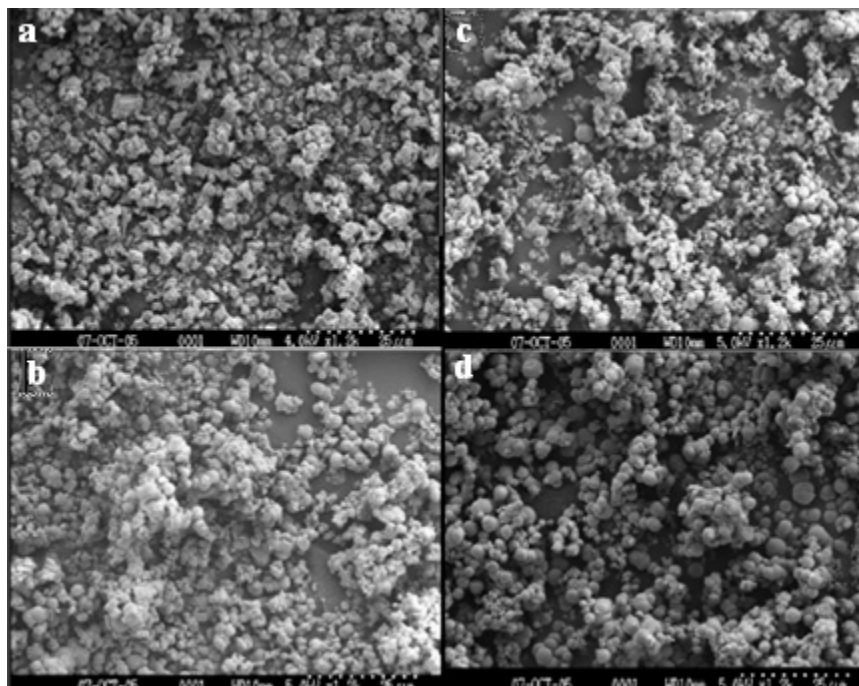


Figure 61 SEM images of TiO_2 from the study of Zhang et al., 2007.

(f) Transmission electron microscopy (TEM)

The exact microstructure of synthesized TiO_2 could be investigated by TEM. The micrographs of all TiO_2 are shown in Figures 32-34, for undoped, doped, and commercial samples, respectively. There is no obvious different in the pattern of undoped and doped TiO_2 . However, the particle size of the doped samples seems to increase slightly as seen by the deposition of the dopant particles on the surface of amorphous TiO_2 . Commercial samples show a small spherical shape with diameter *ca.* 60 nm and 30 nm, for anatase and Degussa P25, respectively.

(g) Surface area / pore size

The specific surface areas of undoped TiO_2 , trivalent (Cr, Fe) doped TiO_2 , and commercial TiO_2 samples are shown in Table 9. In order to compare this value, other samples of TiO_2 were also subjected to the same measurement under the same conditions, such as the commercially available anatase from Carlo Erba, and the Degussa P25. It can be seen in Table 9 that both synthesized TiO_2 , undoped and trivalent (Cr, Fe) doped TiO_2 , have higher surface area than commercial TiO_2 due to

lower crystallinity of the synthesized samples. Undoped TiO₂ sample shows the highest surface area with value of 484.73 m²/g. The larger surface area of sample could be attributed to highly network system from condensation reaction which is caused by the high volume of water in amorphous sample (Zhang *et al.*, 2001).

The porous nature of synthesized TiO₂ was studied by nitrogen adsorption isotherm. In order to utilize the information within the adsorption isotherms, it is necessary to inspect the shape of physisorption isotherm and the identification of the principle mechanism of adsorption. The majority of physisorption isotherms could be grouped into six types, as shown in Figure 62 and Table 16.

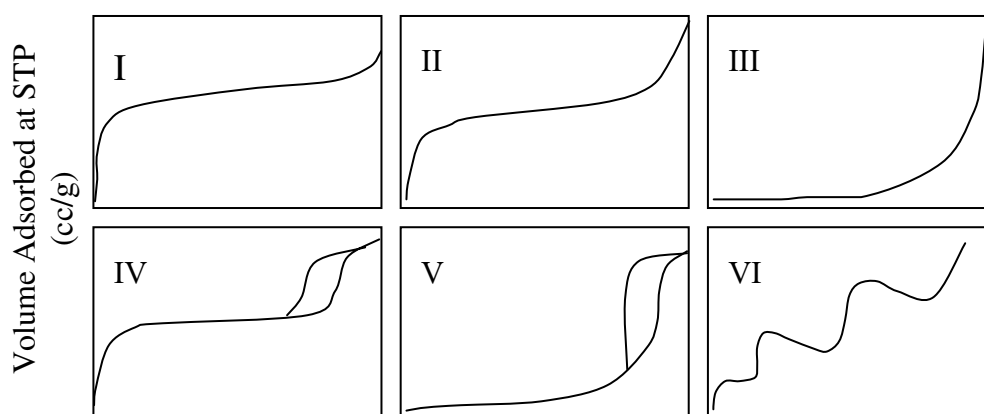


Figure 62 IUPAC classification of adsorption isotherms (Ryu, *et al.*, 1999).

Table 16 IUPAC classification of the pore (Khalil, *et al.*, 2001).

Porosity type	Size (d)
Ultramicropores	< typical molecule diameter of the adsorptive about 0.6 nm
Micropores	$d < 2$ nm
Mesopores	$2 \text{ nm} < d < 50 \text{ nm}$
Macropores	$d > 50 \text{ nm}$

The Type I isotherm is given by microporous solids. The very steep region at low P/P_0 is due to the filling of very narrow pores and limiting uptake is dependent on the accessible micropore volume rather than on the internal surface area.

The Type II isotherm is normally given by a non-porous solids which unrestricted monolayer-multilayer adsorption can occur.

The Type III isotherm is generally associated with weak adsorbent - adsorbate and relatively strong adsorbate - adsorbate interactions. In this case cooperative effects lead to the development of patches of multilayer before a uniform monolayer has been formed.

Type IV isotherm with hysteresis loop is the characteristic features of the adsorbate - adsorbate interactions which is associated with capillary condensation. Some microporous or mesoporous solids are amongst the few adsorbents to give Type V isotherm.

The Type VI isotherm is relatively rare, it presents stepwise multilayer adsorption on a uniform non-porous surface. (Ryu, *et al.*, 1999).

The nitrogen adsorption isotherms for undoped and doped TiO_2 samples are shown in Figures 35 and 36, respectively. The isotherms corresponding to the undoped sample is of Type I (BDDT classification) (Ryu *et al.*, 1999), indicating that the pore size is in the microporous region. For Fe- TiO_2 and Cr- TiO_2 , the isotherm is of Type I. Except for 0.1Fe- TiO_2 where the isotherm is a combination of Type I and IV (BDDT classification) with two distinct regions; at low relative pressure, the isotherm exhibits high adsorption, indicating that the sample contains micropore (Type I). However, at high relative pressure, the curve exhibits the presence of mesopores (Type IV). In this study, the hysteresis loop in the isotherm could not be determined due to the limited capability of the equipment (SA3100 coulter) which was not equipped to determine the desorption study. The present of micropore could be checked by plotting the adsorbed layer called “*t*-plot” as seen in Figures 37 and 38 for undoped and doped TiO_2 , respectively. It seems that for the synthetic powders the linear section does not pass the origin, suggesting that it contains not only mesopore but also micropore (Khalil, *et al.*, 2001).

The pore size distributions of synthesized TiO₂ are shown in Figures 39 and 40 for undoped and doped TiO₂ samples, respectively. The undoped sample shows bimodal pore size distribution consisting of intra-particle pores (5-10 nm) and larger inter-particle pores (10-100 nm). Usually, there are two types of pores present in the bimodal pore size distribution. One is made from the intra-aggregated pores at lower P/P₀ range (the pores within the hard aggregates) and the other is larger inter-aggregated pores in the higher P/P₀ range arising from hard aggregated (the void between hard aggregates) (Yu, *et al.*, 2003). For doped TiO₂ samples, it exhibits also bimodal pore size distribution due to still of an amorphous phase.

(h) Electron spin resonance spectroscopy (ESR)

The ESR spectra of undoped TiO₂ and doped powders, Fe-TiO₂, Cr-TiO₂, are shown in Figures. 41 and 42, respectively. Spectrum of Fe-TiO₂, Figure 42(a), shows an intense signal at $g = 2.02$ and a weak signal at $g = 4.50$. These two signals can be assigned to Fe(III) substituted for Ti(IV) in the TiO₂ lattice and to Fe(III) substituted in the lattice adjacent to a charge-compensating oxide anion vacancy, respectively (Tong, *et al.*, 2008). For chromium, the chromium ion usually has three oxidation states with unpaired spin: Cr(V) ($3d^1$, $^2D_{3/2}$), Cr(III) ($3d^3$, $^4F_{3/2}$), and Cr(I) ($3d^5$, $^6S_{5/2}$), all are active to ESR with Cr(III) is the most stable paramagnetic species. The ESR spectrum of Cr-TiO₂ exhibited a signal at a $g = 1.96$, Figure 42(b). This signal can be attributed to the presence of Cr(III) in octahedral coordination (Fabielle, *et al.*, 2008). Only a flat base line was observed for the undoped TiO₂, Figure 37. Therefore, in addition to the UV-vis absorption data, the ESR data also clearly support both the successful doping of Fe(III) and Cr(III) to the amorphous TiO₂ and the assignment of +3 charge to both ions.

(i) X-ray fluorescence spectrometer (XRF)

The XRF study gives both qualitative and quantitative information about the detection of each element on the surface of as-prepared TiO₂ samples. The amount of dopants in the doped samples were determined quantitatively with XRF using the standard addition method. Table 12 shows the percentage of dopants amount

exist in undoped TiO₂. The standard curves were constructed using Fe₂O₃ and Cr₂O₃ for Fe(III) and Cr(III) dopant, respectively.

4.1.3 Optimal conditions for preparation of TiO₂ samples

(1) Optimal conditions for preparation of undoped TiO₂

In the preparation of undoped, amorphous TiO₂, the major factor that affects the phase of product is the drying temperature. Therefore, the effect of drying temperature and drying duration were studied. In the drying step of undoped TiO₂ synthesis, the sample was dried at various temperatures as well as varying duration of drying and the data are shown in Table 13.

The undoped products from A, B, C methods showed no significant difference in decolorization efficiency with complete decolorizations were reached in less than 1 h. For the method C, using 180 °C and 18 h for prepare undoped TiO₂, the XRD spectrum revealed the present of small amount of anatase phase. Both the method A and B showed pure amorphous TiO₂. The method B was selected as optimal condition for preparation because of its pure phase obtained in shorter time.

(2) Optimal conditions for preparation of trivalent (Cr, Fe) doped TiO₂

In the preparation of trivalent (Cr, Fe) doped TiO₂, various factors (doping concentrations, doping duration, stirring speed) that can affect the product qualities were evaluated based on degradation efficiency of MB under UV irradiation. Figures 43-45 show the effect of these factors in the preparation of trivalent (Cr, Fe) doped TiO₂.

From Figure 43, doping concentrations were varied from 0.05-0.2 mol%. Degradation efficiency of MB was investigated based on the difference of percentage at 1 h and 5 h of UV irradiation, 0.1 mol% was selected for optimal doping concentrations of both Fe-TiO₂ and Cr-TiO₂. For the latter, 0.05 mol%, although, shows better efficiency at 5 h UV irradiation, but that result was influenced from adsorption behavior.

From Figure 44, doping durations were varied from 0.5-3 h. The MB degradation results at 1-3 h doping durations showed no significant difference in degradation efficiency. Although at 0.5 h doping durations showed higher degradation efficiency than others but that result was influenced from the adsorption behavior of samples.

From Figure 45, the effect of stirring speed was varied from 300-500 rpm. The results showed little difference in degradation efficiency. The order of efficiency is 400 rpm > 300 pm > 500 rpm.

As mention above, the optimum conditions for the preparation of trivalent (Cr, Fe) doped TiO₂ were studied from the one that gave product showing greatest degradation efficiencies. These conditions were 0.1 mol% dopant concentration, 1 h doping duration, and 400 rpm stirring speed.

4.2 Photocatalytic activities of MB by undoped TiO₂ and trivalent (Cr, Fe) doped TiO₂ in comparison with commercial TiO₂

The degradation of MB was investigated by using undoped, as-prepared trivalent (Cr, Fe) doped TiO₂ with/without UV and visible light irradiation. In this study, UV source was the 20 watt blacklight tube, which emits UV light in the range 346-395 nm with a maximum at 366 nm (Randorn, *et al.*, 2004). The visible light source was 18 watts fluorescence tubes. In order to accurately assessing the degradation efficiency, adsorption and photo-degradation under UV and visible light irradiation were studied.

4.2.1 Adsorption study

The adsorption is the main mechanism for decolorizing of MB dye molecules by amorphous metal oxide because its surface area is larger than the crystalline phase. The decolorization efficiency was calculated by using equation (20) and are shown in Figures 49, 52, and 53, for undoped, Fe-TiO₂, and Cr-TiO₂ samples, respectively. The results indicated that adsorptability of undoped TiO₂ decreased when doped with Fe(III) or Cr(III) and dramatically decreased with increasing

dopants amount. According to doping concentrations, in the case of 0.05 mol% adsorbability only slightly decreased compared with undoped powders and further decrease was observed at 0.2 mol% dopant.

4.2.2 Photocatalytic studies with UV irradiation

As mentioned above, of the three doping concentrations, the 0.1 mol% of each dopant showed the highest efficiency in decolorizing the dye solutions. This doping concentration was then selected for further studies. Results of photocatalytic studies are shown in Figure 59 where the efficiencies of the 0.1 mol% doped samples are shown along with the two commercial samples, anatase and Degussa P25. The latter two had been known for their good photocatalytic property under UV light and it is confirmed again in this experiment where their graphs went up steeply, in Figure 63, and reached their corresponding saturation points in about 5 h. The P25 sample showed slightly better performance than anatase as its graph was constancy, but slightly, higher than that of anatase throughout the course. Under the same conditions the 0.1 mol% doped samples, 0.1Fe-TiO₂ and 0.1Cr-TiO₂, also showed photocatalytic activity as their graphs also went up but not as steep as the commercial ones. The efficiencies of doped samples, however, caught up with anatase performance at the end of 5 h. Without UV light, the photocatalytic power of the doped samples diminished as their graphs remained flat at the same level as the adsorption-desorption equilibrium in the dark. This is a strong evidence to support our claim that the doping can turn the previously photocatalytic inert amorphous TiO₂ to photocatalytic active.

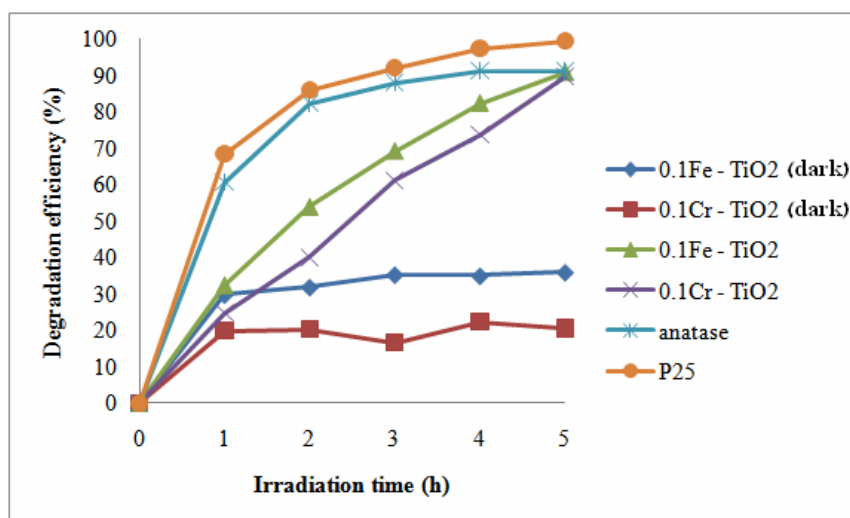
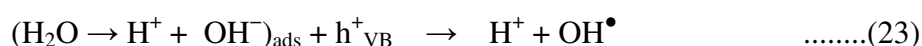
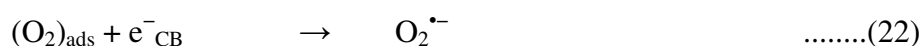
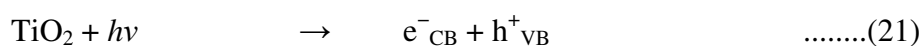
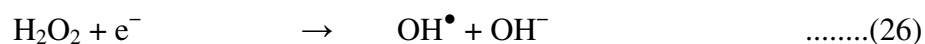
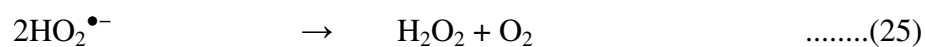
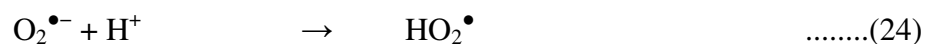


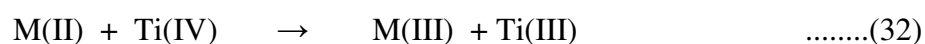
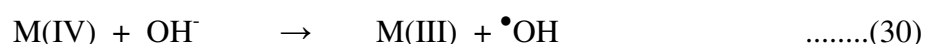
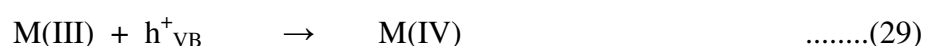
Figure 63 Comparison the degradation of MB by TiO₂ samples under UV irradiation.

In the case of commercial TiO₂, which show good photocatalytic activity, UV light irradiation of the catalysts generates electron - hole pairs ($e^-_{CB} - h^+_{VB}$), equation (21), or alternatively may be visualized as localized electrons (Ti^{3+}) and holes (O^- and/or $\bullet OH$ radicals). Some of these electron-hole pairs disappeared by recombination on bulk TiO₂, while other electrons and holes diffused to the surface of TiO₂ catalysts to react with various hydrocarbons (Houas, *et al.*, 2001; Ampo, *et al.*, 2003). In the case of the simple photocatalytic reaction, i.e., with UV light, the degradation of MB should go through the interaction with the electron - hole pair as usual. In equation (22), $(O_2)_{ads}$, O_2 that was present in the system and was adsorbed onto the surface of the catalyst, reacts with e^-_{CB} to become the superoxide anion – a precursor to equations (24) - (26). In the bleaching of MB, equation (27), $R = MB$ and since MB has a cationic fragment it should be favorably adsorbed to the negative sites of the TiO₂ surface and subsequently attacked by the very active $\bullet OH$ moiety, leading to the destruction of the MB molecule. MB molecule can also be destroyed by reacting directly with the positive hole (h^+_{VB}) as shown in equation (28) (Random, *et al.*, 2004).





For doped TiO₂, Fe-TiO₂, and Cr-TiO₂, the beneficial effect of metal ions under UV irradiation should be explained by considering the efficient separation of photoexcited electrons and holes. Cr(III) can act as photogenerated hole trappers (equations (29) and (30)), due to the energy level for Cr(III)/Cr(IV) above the valence band edge of anatase TiO₂ (Choi, *et al.*, 1994). The trapped holes in Cr(IV) can migrate to the surface and reacts with adsorbed hydroxyl ion to produce hydroxyl radicals. While, Fe(III) can act as both hole and/or electron trappers (equations (29) and (31)). According to crystal field theory, Fe(II) (equation (31)), is relatively unstable due to the loss of exchange energy on going from d⁵ (half-filled high spin) to d⁶ and tends to return to Fe(III) (d⁵). However, the Fe(II)/Fe(III) energy level lies close to Ti(III)/Ti(IV) level, as a consequence of this proximity, the trapped electron in Fe(II) can be easily transferred to the neighboring surficial Ti(IV) (Choi, *et al.*, 1994).



In another word, dopants, Cr(III) and Fe(III), promote the separation of photogenerated holes and electrons at a low concentration, which benefit the photocatalytic reaction, however, the reaction between electrons and metal ions are quickly increased at higher concentration of dopants, which is disadvantageous to photocatalytic reaction (Choi, *et al.*, 1994; Zhu, *et al.*, 2006). Thus, photocatalytic degradation of MB under UV irradiation showed the fastest reaction rate for 0.1 mol% doping concentration for both Fe-TiO₂ and Cr-TiO₂.

4.2.3 Photocatalytic studies with visible light

It is well known that commercial TiO_2 , especially anatase and Degussa P25, are useful as photocatalysts, however, there is still a problem that photocatalytic efficiency is rather low since TiO_2 is active only under ultraviolet light (UV) because of its wide band gap, ~ 3.2 eV for anatase and ~ 3.1 eV for Degussa P25, corresponding to 388 and 400 nm, respectively, and high rate of recombination of photogenerated electron - hole pairs resulting in low photo quantum efficiency.

Photocatalytic activities of the doped TiO_2 samples under visible light irradiation are shown in Figure 59. The commercial samples are included and readily seen that they did not show photocatalytic activity under visible light. The irradiation time had to be extended to 12 h to complete the decolorization. During the first 5 h the reaction was rather slow after which it increased dramatically. The 0.1Fe-TiO_2 exhibited better photocatalytic activity than 0.1Cr-TiO_2 , approximately 20 %. There are three main causes that may explain the difference observed in the photocatalytic activity of the two doped TiO_2 samples. Firstly, Fe(III) had the similar radius to the Ti(IV) and can present itself comfortably in the bulk of TiO_2 . Secondly, owing to the similar energy level of Fe(II)/Fe(III) and Ti(III)/Ti(IV), see Figure 64, electrons trapped by Fe(III) could readily transit to sideward Ti(IV) and improves the separation of photoproduced electron-hole pairs. Lastly, although Fe(III) and Cr(III) have similar energy levels in the TiO_2 lattice, similar ionic radii and identical oxidation states, it is quite possible that the differences in photocatalytic activity of Fe(III) and Cr(III) doped TiO_2 are linked to the difference in the diffusion lengths of the minority carriers (2 pm for Fe(III) vs. 0.2 pm for Cr(III)) (Choi, *et al.*, 1994; Yuan, *et al.*, 2007).

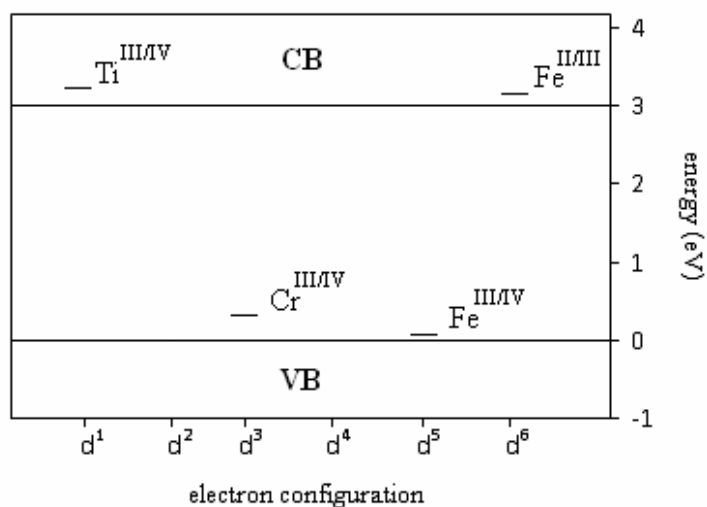


Figure 64 Energy levels of impurity ions in TiO₂, adapted from Mizushima *et al.*, 1972.

4.2.4 Kinetics of photocatalytic reactions

It is well established that photocatalytic decomposition of the organic molecules, or MB in our case, follows the Langmuir-Hinshelwood kinetics as

$$\ln\left(\frac{C_0}{C_t}\right) = k.t \quad \text{.....(33)}$$

where C_0 is an initial concentration of MB, C_t is the concentration of MB at time t , and k is the observed first-order rate constant (Baiju, *et al.*, 2007; Kontos, *et al.*, 2005).

The kinetics data of two doped and two commercial samples were plotted using equation (33) showing good straight lines as shown in Figure 65. All four samples showed first-order behavior when irradiated with UV light, Figure 65(a). As mentioned above, the two commercial samples, P25 and anatase, did not show photocatalytic activity when irradiated with visible light, hence, only the graphs of the two doped samples are shown in Figure 65(b).

The values of the rate constant, k , under UV and visible irradiation are listed in Table 17.

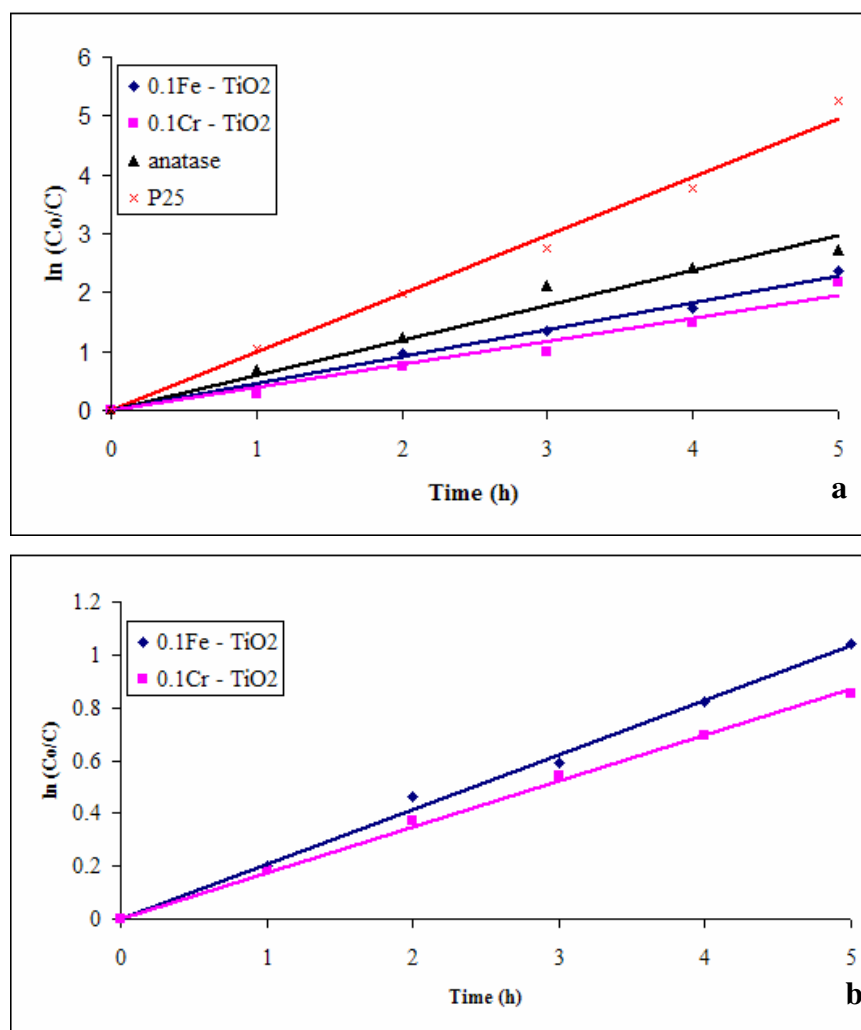


Figure 65 Kinetics plots of TiO₂ under (a) under UV light irradiation, and (b) visible light irradiation.

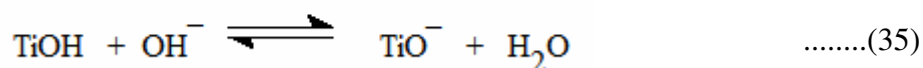
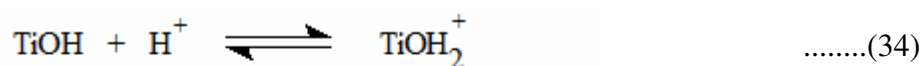
Table 17 The kinetics rate constants of TiO₂ samples under difference photocatalytic conditions.

sample	Rate constant (h ⁻¹)	
	UV	Visible
Fe-TiO ₂	0.4674	0.3099
Cr-TiO ₂	0.4300	0.1783
Anatase	0.6158	-
P25	0.9911	-

- cannot be determined

4.2.5 Effect of pH on the photocatalytic activity

In real life applications the photocatalyst may be used in environment with varying acidities, hence, all the TiO₂ samples were tested for their activities at varying pH values, 3, 5, and 9. The natural pH of MB aqueous solution in this work was 6.7. The influence of pH on the degradation of MB under UV and visible light irradiation of the doped samples are shown in Figures 66 and 67, respectively. The results showed that there was a strong dependence on the pH of the solution during the heterogeneous photo process. It is known that the metal oxide particles suspended in water behave similarly to diprotic acids. For TiO₂, the surface hydroxyl groups undergo two acid–base equilibria:



Generally, for charged substrates, a significant dependency of the photocatalytic degradation efficiency on the pH value was observed, since the overall surface charge and hence the adsorptive properties of TiO₂ particles depend strongly on the solution pH (Senthilkumar, *et al.*, 2005). The interpretation of pH effect on the photocatalytic process is very difficult because of its multiple roles such as electrostatic interactions between the semiconductor surface, solvent molecules,

substrate and charged radicals formed during the reaction process. With respect to the point of zero charge (pzc), the surface charge property of TiO_2 changes with the change of solution pH. The pH_{pzc} for TiO_2 has been reported in the range 6.25-6.90. Thus, the TiO_2 surface is positively charged in acidic medium ($\text{pH} < \text{pH}_{\text{pzc}}$), and negatively charged in alkaline medium ($\text{pH} > \text{pH}_{\text{pzc}}$) (Sun, et al., 2008).

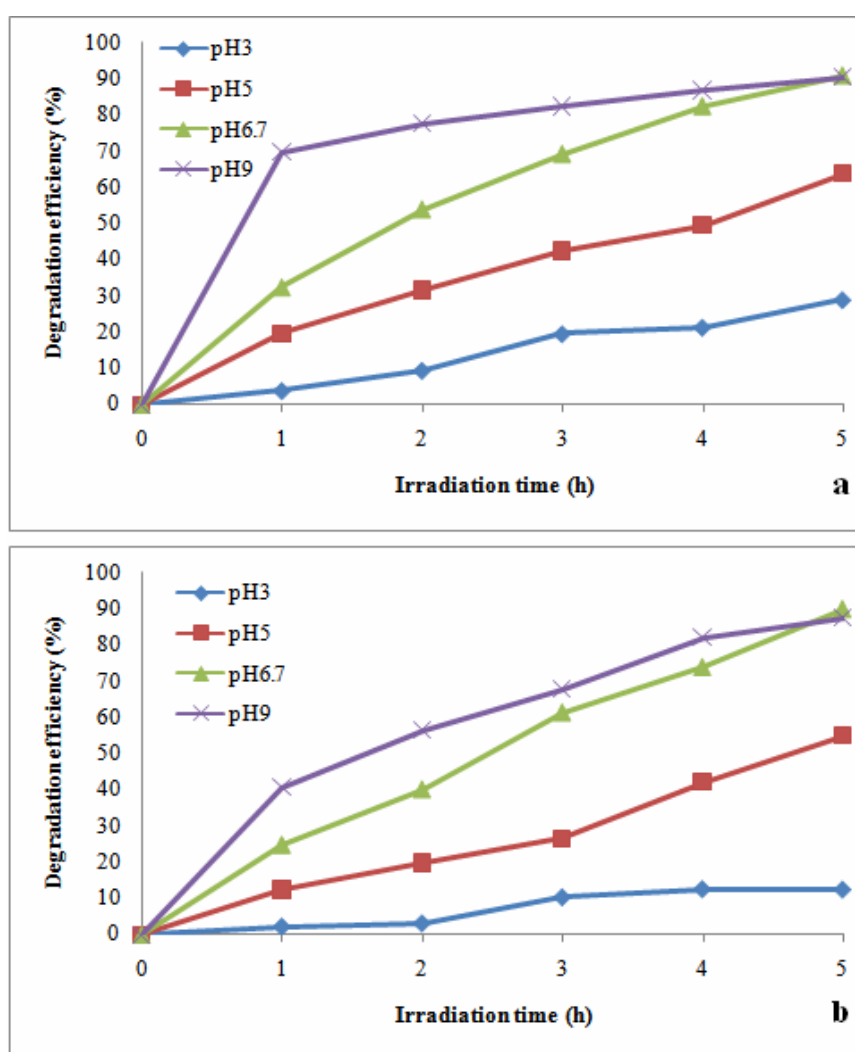


Figure 66 Effect of pH on photodegradation under UV light irradiation for (a) Fe-TiO₂, and (b) Cr-TiO₂.

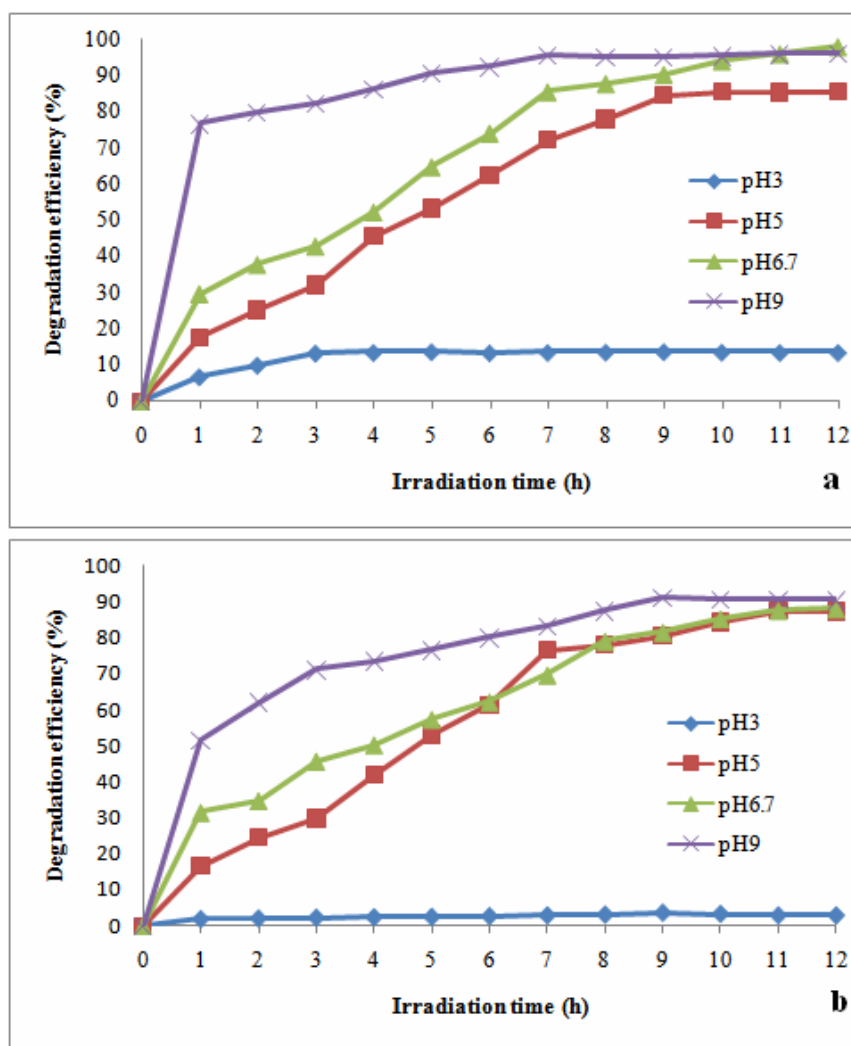


Figure 67 Effect of pH on photodegradation under visible light irradiation for (a) Fe-TiO₂, and (b) Cr-TiO₂.

From Figures 66 and 67, at pH below pH_{pzc} , the surface of TiO₂ acquires a positive charge which causes the electrostatic repulsion between the surface of TiO₂ and dye cation and retards the photodegradation activities. On the other hand, at pH above pH_{pzc} , the surface of TiO₂ is negative and electrostatic interaction between the negative surface and dye cation leads to strong adsorption with a corresponding high photodegradation activities reaching a maximum at pH 9. The order of activities is pH 9 > pH 6.7 > pH 5 > pH 3 under both UV and visible light irradiations.

Chapter 5

Conclusions

The synthesized TiO₂ in this work, undoped- and doped-TiO₂, were successfully prepared from two simple techniques. The undoped TiO₂ was prepared by using base-catalyzed sol-gel method without calcination, from reaction between TiCl₄ and diluted NH₃ solution. The trivalent (Cr, Fe) doped TiO₂ samples were prepared from incipient wetness impregnation, using CrCl₃•6H₂O and FeCl₃ as the dopant sources of Cr(III) and Fe(III), respectively. The amount of dopants were varied in three concentrations, 0.05, 0.1 and 0.2 mol%.

In our preparation the undoped TiO₂ is a pure amorphous form. Main factors that may have influence on the phase of sample are drying temperature and drying duration. Since, TiO₂ shows an amorphous character at low temperature and turns to the crystalline structure when temperature is increased (Huang, *et al.*, 1997). The optimum drying temperature and drying duration were obtained at 105 °C with 24 h. This condition yields pure amorphous phase in shorter time. The powder obtained from this method was used in the following steps.

In the preparation of trivalent (Cr, Fe) doped TiO₂, various factors were investigated based on the highest degradation efficiencies of MB aqueous solution. The optimum conditions for preparation of trivalent (Cr, Fe) doped TiO₂ are;

- i. Doping concentration : 0.1 mol%
- ii. Doping duration : 1 h
- iii. Stirring speed : 400 rpm

The obtained products were characterized by several techniques, such as XRD, XRF, ESR, DRS, SEM, TEM, BET, FT-IR, and UV-vis spectroscopy techniques. The XRD patterns of the synthesized TiO₂ indicated that both undoped- and doped-TiO₂ existed in an amorphous form. These samples have high surface area. The undoped TiO₂ showed slightly higher surface area than trivalent doped TiO₂ but the two doped samples, Fe(III) doped TiO₂ and Cr(III) doped TiO₂, have similar surface area. ESR and XRF techniques were used to confirmed that Cr(III) or Fe(III) were present in the doped products. Doping with Cr(III) or Fe(III) did not change the

phase of products, however, the band gap energies decreased from 3.2 eV (undoped TiO₂) to 2.5 eV and 2.8 eV for Fe-TiO₂ and Cr-TiO₂, respectively. This corresponds to the shift of absorption spectrum from near UV into visible region. The SEM and TEM images revealed the morphologies of products as non-uniform rough surfaces and the dopant contents did not affect the morphologies of samples.

The photocatalytic degradation of methylene blue was investigated by using these undoped- and trivalent (Cr, Fe) doped TiO₂ samples in comparison with the commercial TiO₂, anatase (Carlo Erba) and Degussa P25. As a result, these doped samples showed photocatalytic activity both under UV and visible light. Under UV irradiation, trivalent (Cr, Fe) doped TiO₂ could degrade dye solution as good as commercial anatase after 5 h which was slightly inferior to P25. Under visible light where both P25 and anatase were not active, the trivalent (Cr, Fe) doped TiO₂ samples still showed activity by degrading the dye solutions in 12 h. Moreover, the effect of dopant contents, the effect of initial concentration of MB, and the effect of pH of MB solution were studied. The results, at 0.1 mol% of each dopant showed the greatest photocatalytic activities in term of MB degradation. The photocatalytic activities of the trivalent (Cr, Fe) doped TiO₂ decreased when the initial concentration of MB increased, and at high pH, photocatalytic activities of the trivalent (Cr, Fe) doped TiO₂ were greater than at low pH. The results from this work show that doping with transition metal ions can turn the inert amorphous TiO₂ to become photocatalytically active. Considering the simplicity in preparation and low cost due to exclusion of calcination process, this should be an attractive choice to wastewater treatment industries.

References

- Alexiou, M. S. and Sermon, P. A. 1993. Aspects of the preparation of heterogeneous catalysts by impregnation. *Reaction Kinetics and Catalysis Letters*. 51, 1-7.
- Anpo, M., and Takeuchi, M. 2003. The design and development of highly reactive titanium oxide photocatalysts operating under visible light irradiation. *Journal of catalysis*. 216, 505-516.
- Anderson, C. and Brad, A. J. 1995. An improved photocatalyst of $\text{TiO}_2/\text{SiO}_2$ prepared by Sol-Gel synthesis. *The Journal of Physical Chemistry*. 99, 9882-9885.
- Aruna, S. T.; Tirosh, S. and Zaban, A. 2000. Nanosize rutile titania particle synthesis via a hydrothermal method without mineralizers. *Journal of Materials Chemistry*. 10, 2388-2391.
- Arana, J.; Diaz, O. G.; Saracho, M. M.; Dona Rodriguez, J. M.; Herrera Melian, J. A. and Pena, J. P. 2002. Maleic acid photocatalytic degradation using Fe-TiO₂ catalysts: Dependence of the degradation mechanism on the Fe catalysts content. *Applied Catalysis B: Environmental*. 36, 113-124.
- Baiju, K. V.; Shukla, S.; Sandhya, K. S.; James, J. and Warriar, K. G. K. 2007. Photocatalytic Activity of Sol-Gel-Derived Nanocrystalline Titania. *The Journal of Physical Chemistry C*. 111, 7612-7622.
- Balong, Z.; Baishun, C.; Keyu, S.; Shangjin, H.; Xiaodong, L.; Zongjie, D. and Kelian, Y. 2003. Preparation and characterization of nanocrystal grain TiO₂ porous microspheres. *Applied Catalysis B: Environmental*. 40, 253-258.

- Baran, W.; Makowski, A. and Wardas, W. 2008. The effect of UV radiation adsorption of cationic and anionic dye solutions on their photocatalytic degradation in the presence TiO_2 . *Dyes and Pigments*. 76, 226-230.
- Belver, C.; Bellod, R.; Fuerte, A. and Fernandez-Garcia, M. 2006. Nitrogen-containing TiO_2 photocatalysts Part 1: Synthesis and solid characterization. *Applied Catalysis B: Environmental*. 65, 301–308.
- Bizani, E.; Fytianos, K.; Poullos, I. and Tsiridis, V. 2006. Photocatalytic decolorization and degradation of dye solutions and wastewaters in the presence of titanium dioxide. *Journal of Hazardous Materials*. 136, 85-94.
- Bokhimi, A. M.; Novaro, O.; López, T.; Sánchez, E. and Gómez, R. 1995. Effect of hydrolysis catalyst on the Ti deficiency and crystallite size of sol-gel- TiO_2 crystalline phases. *Materials Research Society*. 10, 2788-2796.
- Brunauer, S.; Emmett, P. H.; and Teller, E. 1938. Adsorption of gases in multimolecular layers. *The Journal of the American Chemical Society*. 60, 309-319.
- Buchner, W.; Schliebs, S.; Winter, G., and Buchel. K. H. 1989. *Industrial Inorganic Chemistry*. New York : VCH.
- Carneiro, P. A.; Osugi, M. E.; Sene, J. J.; Anderson, M. A. and Boldrin Zanoni, M. V. 2004. Evaluation of color removal and degradation of a reactive textile azo dye on nanoporous TiO_2 thin-film electrodes. *Electrochimica Acta*. 49, 3807-3820.
- Chemat. 1998. Sol-Gel Technology. <http://www.chemat.com/4.tpl?cart=1235666467235414>. Chemat Technology, Inc. (accessed 24/02/09)

- Chiang, K.; Amal, R. and Tran, T. 2002. Photocatalytic degradation of cyanide using titanium dioxide modified with copper oxide. *Advances in Environmental Research*. 6, 471-485.
- Choi, W.; Termin, A. and Hoffmann, M. R. 1994. The role of metal ion dopants in quantum-sized TiO₂: correlation between photoreactivity and charge carrier recombination dynamics. *The Journal of Physical Chemistry*. 98, 13669-13679.
- Choychangtong, W. 2004. Synthesis and Characterization of Titanium Dioxide. Master of Science Thesis, Prince of Songkla University, Songkhla, Thailand.
- Clark, R. J. H. 1968. *The Chemistry of Titanium and Vanadium*. Amsterdam: Elsevier.
- Coronado, J. M. and Soria, J. 2007. ESR study of the initial stages of the photocatalytic oxidation of toluene over TiO₂ powders. *Catalysis Today*. 123, 37-41.
- Da browski, A. 2001. Adsorption-from theory to practice. *Advances in Colloid and Interface Science*. 93, 135-224.
- Di Paola, A.; Marci, G.; Palmisano, L.; Schiavello, M.; Uosaki, K.; Ikeda, S. and Ohtani, B. 2002. Preparation of polycrystalline TiO₂ photocatalysts impregnated with various transition metal ions: characterization and photocatalytic activity for the degradation of 4-Nitrophenol. *The Journal of Physical Chemistry B*. 106, 637-645.
- Ding, X. and Liu, X. 1997. Synthesis and microstructure control of nanocrystalline titania powders via a sol-gel process. *Materials Science and Engineering A*. 224, 210-215.

- Ding, Z.; Lu, G. Q. and Greenfield, P. F. 2000. Role of the crystallite phase of TiO₂ in heterogeneous photocatalysis for phenol oxidation in water. *The Journal of Physical Chemistry*. 104, 4815-4820.
- Duplyakin, V. K.; Belyi, A. S.; Rodionov, A. V. and Alfeev, V. S. 1991, New impregnation process for producing coated catalysts. *Chemistry and Technology of Fuels and Oils*. 27, 39-42.
- Escobar, J.; Reyes, J. D. and Viveros, T. 2000. Influence of the synthesis additive on the texture and structural characteristic of Sol-Gel Al₂O₃-TiO₂. *Industrial and Engineering Chemistry Research*. 39, 666-672.
- Fabielle, C. M.; Maria, C. C. and Alexandre, M. S. 2008. Use of TiO₂/Cr-MCM-41 molecular sieve irradiated with visible light for the degradation of thiophene in the gas phase. *Catalysis Today*. 133-135, 594-599.
- Faisal, F.; Abu Tariq, M. and Muneer, M. 2005. Photocatalysed degradation of two selected dyes in UV-irradiated aqueous suspensions of titania. *Dyes and Pigments*. 72, 233-239.
- Fan, X.; Chen, X.; Zhu, S.; Li, Z.; Yu, T; Ye, J. and Zou, Z. 2008. The structural, physical and photocatalytic properties of the mesoporous Cr-doped TiO₂. *Journal of Molecular Catalysis A: Chemical*. 284, 155-160.
- Fu, Y. and Viraraghavan, T. 2001. Fungal decolorization of dye wastewaters: a review. *Bioresource Technology*. 79, 251-262.
- Garfield, S. 2001. *Mauve: How One Man Invented a Color That Changed the World*. New York: Norton.

- Gfroerer, T. H. 2000. Photoluminescence in Analysis of Surfaces and Interfaces. In: Encyclopedia of Analytical Chemistry, R.A. Meyers Ed. John Willey & Sons Ltd, Chichester., pp 9209-9231.
- Gomes de Moraes, S.; Sanches Freire, R. and Duran, N. 2000. Degradation and toxicity reduction of textile effluent by combined photocatalytic and ozonation processes. *Chemosphere*. 40, 369-373.
- Harizanov, O.; Ivanova, T. and Harixanova, A. 2001. Study of sol-gel TiO₂ and TiO₂-MnO obtained from a peptized solution. *Materials Letters*. 49, 165-171.
- Houas, A.; Lachheb, H.; Ksibi, M.; Elaloui, E.; Guillard, C. and Hermann, J. M. 2001. Photocatalytic degradation pathway of methylene blue in water. *Applied Catalysis B: Environmental*. 31, 145-157.
- Huang, P. J.; Chang, H.; Yeh, C. T. and Tsai, C. W. 1997. Phase transformation of Y₂O₃ monitored by Thermo-Raman spectroscopy with TGA/DTA. *Thermochimica Acta*. 297, 85-92.
- Kangle, L.; Zuo, H.; Sun, J.; Deng, K.; Liu, S.; Li, X. and Wang, D. 2009. (Bi, C and N) codoped TiO₂ nanoparticles. *Journal of Hazardous Materials*. 161, 396–401.
- Kanna, M. 2002. Adsorption Behavior of Some Metal Ions on Titanium Dioxide Surface. Master of Science Thesis, Prince of Songkla University, Songkhla, Thailand.
- Kanna, M.; Wongnawa, S.; Sherdshoopongse, P. and Boonsin, P. 2005. Adsorption behavior of some metal ions on hydrated amorphous titanium dioxide surface. *Songklanakarin Journal of Science and Technology*. 27, 1017-1026.

- Khalil, T.; Abou El-Nour, F.; El-Gammal, B and Boccaccini. 2001. Determination of surface area and porosity of sol-gel derived ceramic powders in the system $\text{TiO}_2\text{-SiO}_2\text{-Al}_2\text{O}_3$. *Powder Technology*. 114, 106-111.
- Kim, H. R.; Lee, T. G. and Shul, Y.-G. 2007. Photoluminescence of La/Ti mixed oxides prepared using sol-gel process and their pCBA photodecomposition. *Journal of Photochemistry and Photobiology A: Chemistry*. 185, 156-160.
- Kontos, A. I.; Arabatzis, I. M.; Tsoukleris, D. S.; Kontos, A. G.; Bernard, M. C.; Petrakis, D. E. and Falaras, P. 2005. Efficient photocatalysts by hydrothermal treatment of TiO_2 . *Catalysis Today*. 101, 275-281.
- Kumar, S. R.; Suresh, C.; Vasudevan, A. K.; Suja, N. R. and Mukundan, P. 1999. Phase transformation in sol-gel titania containing silica. *Materials Letters*. 38, 161-166.
- Kumar, P. M.; Barinarayanan, S. and Sastry, M. 2000. Nanocrystalline TiO_2 studied by optical, FT-IR and X-ray photoelectron spectroscopy: correlation to presence of surface states. *Thin Solid Films*. 358, 122-130.
- LeBlanc, J. R.; Madhavan, S. and Porter, R.E. 1978. Ammonia. In: *Kirk-Othmer Encyclopedia of Chemical Technology*, 3rd Ed. Wiley-Interscience, New York., Vol. 2, pp 474.
- Lee, S.-H.; Kang, M.; Cho, S.M.; Han, G.Y.; Kim, B.-W.; Yoon, K.J. and Chung, C.-H. 2001. Synthesis of TiO_2 photocatalyst thin film by solvothermal method with a small amount of water and its photocatalytic performance. *Journal of Photochemistry and Photobiology A: Chemistry*. 146, 121-128.

- Li, J.; Liu, S.; He, Y. and Wang, J. 2008. Adsorption and degradation of the cationic dyes over Co doped amorphous mesoporous titania–silica catalyst under UV and visible light irradiation. *Microporous and Mesoporous Materials*. 115, 416-425.
- Liqiang, J.; Yichin, Q.; Baiqi, W.; Shudan, L.; Baojiang, J.; Libin, Y.; Wei, F.; Honggang, F. and Jiazhong, S. 2006. Review of photoluminescence performance of nano-sized semiconductor materials and its relationships with photocatalytic activity. *Solar Energy Materials & Solar Cells*. 90, 1773-1787.
- Lu, S. X. and Liu, Y. C. 2007. Intense luminescence of amorphous Eu_2O_3 prepared by aqueous sol-gel method. *Journal of Non-Crystalline Solids*. 353, 1037-1040.
- Marci, G.; Palmisano, L.; Sclafani, A.; Venezia, A. M.; Campostrini, R.; Carturan, G.; Martin, C.; Rives V. and Solana, G. 1996. Influence of tungsten oxide on structural and surface properties of sol-gel prepared TiO_2 employed for 4-nitrophenol photodegradation. *Journal of the Chemical Society Faraday transactions*. 92, 819–821.
- Matsuo, S.; Sakaguchi, N.; Yamada, K.; Matsuo, T. and Wakita, H. 2004. Role in photocatalysis and coordination structure of metal ions adsorbed on titanium dioxide particles: a comparison between lanthanide and iron ions. *Applied Surface Science*. 228, 233-244.
- Mills, A. and Wang, J. 1999. Photobleaching of methylene blue sensitised by TiO_2 : an ambiguous system. *Journal of Photochemistry and Photobiology A: Chemistry*. 127, 123-134.
- Mizushima, K.; Tanaka, M. and Iida, S. 1972. Energy Levels of Iron Group Impurities in TiO_2 . *Journal of the Physical Society of Japan*. 32, 1519-1524.

- Mora, E. S.; Barojas, E. G.; Rojas, E. R. and González, R. S. 2007. Morphological, optical and photocatalytic properties of TiO₂-Fe₂O₃ multilayers. *Solar Energy Materials and Solar Cells*. 91, 1412-1415.
- Muruganandham, M.; Shobana, N. and Swaminathan, M. 2005. Optimization of solar photocatalytic degradation conditions of Reactive Yellow 14 azo dye in aqueous TiO₂. *Journal of Molecular Catalysis A: Chemical*. 246, 154-161.
- Nagaveni, K.; Sivalingam, G. and Heged, M.S. 2004. Solar photocatalytic degradation of dyes : high activity of combustion synthesized nano TiO₂. *Applied Catalysis B: Environmental*. 48, 83-93.
- Nakamoto, K. 1970. *Infrared Spectra of Inorganic and Coordination Compounds*. New York: Wiley.
- Ohtani, B.; Ogawa, Y. and Nishimoto, S. I. 1997. Photocatalytic activity of amorphous-anatase mixture of titanium(IV) oxide particles suspended in aqueous solutions. *The Journal of Physical Chemistry B*. 101, 3746-3752.
- Pal, B.; Hata, T.; Goto, K. and Nogami, G. 2001. Photocatalytic degradation of *o*-cresol sensitized by iron-titania binary photocatalysts. *Journal of Molecular Catalysis A: Chemical*. 169, 147-155.
- Qamar, M.; Saquib, M. and Muneer, M. 2005. Photocatalytic degradation of two selected derivative, chromotrope 2B and amino black 10B, in aqueous suspensions of titanium dioxide. *Dyes and Pigments*. 65, 1-9.
- Randorn, C.; Wongnawa, S. and Boonsin, P. 2004. Bleaching of methylene blue by hydrated titanium dioxide. *Science Asia*. 30, 149-156.

- Ranjit, K. T.; Willner, I.; Bossmann, S. H. and Braun, A. M. 2001. Lanthanide oxide doped titanium dioxide photocatalysts: Effective photocatalysts for the enhanced degradation of salicylic acid and *t*-cinamic acid. *Journal of Catalysis*. 204, 305-313.
- Rao, K. V. S.; Lavédrine, B. and Boule, P. 2003. Influence of metallic species on TiO₂ for the photocatalytic degradation of dyes and dye intermediates. *Journal of Photochemistry and Photobiology A: Chemistry*. 154, 189-193.
- Reddy, K. M.; Reddy, R. C. V. and Manorama, S. V. 2001. Preparation, characterization, and spectra studies on nanocrystalline anatase TiO₂. *Journal of Solid State Chemistry*. 158, 180-186.
- Reddy, K. M.; Manorama, S. V. and Reddy, A. R. 2002. Band gap studies on anatase titanium dioxide nanoparticles. *Materials Chemistry Physics*. 78, 239-245.
- Robinson, T.; McMullan, G.; Marchant, R. and Nigam, P. 2001. Remediation of dyes in textiles effluent: a critical review on current treatment technologies with a proposed alternative. *Bioresource Technology*. 77, 247-255.
- Ryu, Z.; Zheng, J.; Wang, M. and Zhang, B. 1999. Characterization of pore size distributions on carbonaceous adsorbents by DFT. *Carbon*. 37, 1257-1264.
- Sanchez, E.; Lopez, T.; Gomez, R.; Morales, A. and Novaro, O. 1996. Synthesis and characterization of sol-gel Pt/TiO₂ catalyst. *Journal of Solid State Chemistry*. 122, 309-314.
- Sauer, T.; Neto, G. C.; José, H. J. and Moreira R. F. P. M. 2002. Kinetics of photocatalytic degradation of reactive dyes in a TiO₂ slurry reactor. *Journal of Photochemistry and Photobiology A: Chemistry*. 149, 147-154.

- Senthilkumaar, S. and Porkodi, K. 2005. Heterogeneous photocatalytic decomposition of Crystal Violet in UV-illuminated sol-gel derived nanocrystalline TiO₂ suspensions. *Journal of Colloid and Interface Science*. 288, 184-189.
- Serpone, N.; Lawless, D. and Khairutdinov, R. 1995. Size effects on the photophysical properties of colloidal anatase TiO₂ particles: size quantization or direct transition in this indirect semiconductor. *The Journal of Physical Chemistry*. 99, 16646-16654.
- Silva, C. G.; Wang, W. and Faria, J. L. 2006. Photocatalytic and photochemical degradation of mono-, di- and tri-azo dyes in aqueous solution under UV irradiation. *Journal of Photochemistry and Photobiology A: Chemistry*. 181, 314-324.
- Skoog, D. A., and Leary, J. J. 1992. *Principle of Instrumental Analysis*. Philadelphia: Saunders Collage Publishing.
- Steven, N. 2008. The Ethics of Deception in Medicine. <http://www.sciencebasedmedicine.org/?p=29>. *Science Based Medicine*. (accessed 24/02/09).
- Stylidi, M.; Kondarides, D.I. and Verykios, X.E. 2003. Pathways of solar light-induced photocatalytic degradation of azo dyes in aqueous TiO₂ suspensions. *Applied Catalysis B: Environmental*. 40, 271-286.
- Sun, J.; Qiao, L.; Sun, S. and Wang, G. 2008. Photocatalytic degradation of Orange G on nitrogen-doped TiO₂ catalysts under visible light and sunlight irradiation. *Journal of Hazardous Materials*. 155, 312-319.
- Sung-Suh, H.M.; Choi, J.R.; Hah, H.J.; Koo, S.M. and Bac, Y.C. 2004. Comparison of Ag deposition effects on the photocatalytic activity of nanoparticulate TiO₂ under UV light irradiation. *Journal of Photochemistry and Photobiology A: Chemistry*. 163, 37-44.

- Suresh, C.; Biju, V.; Mukundan, P. and Warriar, K. G.K. 1998. Anatase to rutile transformation in sol-gel titania by modification of precursor. *Polyhedron*. 17, 3131-3135.
- Suriye, K.; Prasertdam, P. and Jongsomjit, B. 2007. Effect of surface sites of TiO₂ support on the formation of cobalt-support compound in Co/TiO₂ catalysts. *Catalysis Communications*. 8, 1772-1780.
- Suwanachawalit, C. 2005. The Metal-Doping on the Physical and Photocatalytic Properties of Nanosized TiO₂ powder. Master of Science Thesis, Prince of Songkla University, Songkhla, Thailand.
- Suwanchawalit, C. and Wongnawa, S. 2008. Influence of calcination on the microstructures and photocatalytic activity of potassium oxalate-doped TiO₂ powders. *Applied Catalysis A: General*. 338, 87-99.
- Tang, Z.; Zhang, J.; Cheng, Z. and Zhang, Z. 2002. Synthesis of nanosized rutile TiO₂ powder at low temperature. *Materials Chemistry and Physics*. 9319, 1-4.
- Tauter, S. J.; Fung, S. C. and Garten, R. L. 1978. Strong metal-support interactions. Group 8 noble metals supported on titanium dioxide. *Journal of the American Chemical Society*. 100, 170-175.
- Tong, T.; Zhang, J.; Tian, B.; Chen, F. and He, D. 2008. Preparation of Fe³⁺-doped TiO₂ catalysts by controlled hydrolysis of titanium alkoxide and study on their photocatalytic activity for methyl orange degradation. *Journal of Hazardous Materials*. 155, 572-579.
- Toor, A. P.; Verma, A.; Jotshi, C. K.; Bajpai, P. K. and Singh, V. 2006. Photocatalytic degradation of Direct Yellow 12 dye using UV/TiO₂ in shallow pond slurry reactor. *Dyes and Pigments*. 68, 53-60.

- Velasco, M. J.; Rubio, F.; Rubio, J. and Oteo, J. L. 1999. DSC and FT-IR analysis of the drying process of titanium alkoxide derived precipitates. *Thermochimica Acta*. 326, 91-97.
- Wang, Z. C.; Chen, J. F. and Hu, X. F. 2000. Preparation of nanocrystalline TiO₂ powders at near room temperature from peroxo-polytitanic acid gel. *Materials Letters*. 43, 87-90.
- Weckhuysen, B. M.; Heidler, R. and Schoonheydt, R. A. 2004. *Electron Spin Resonance Spectroscopy. Molecular Sieves - Science and Technology*. Heidelberg: Springer Berlin.
- Wu, J.C.S. and Chen, C.H. 2004. A visible-light response vanadium-doped titania nanocatalyst by sol-gel method. *Journal of Photochemistry and Photobiology A: Chemistry*. 163, 509-515.
- Xu, N.; Shi, Z.; Fan, Y.; Dong, J.; Shi, J. and Hu, M. Z. C. 1999. Effects of particle size of TiO₂ on photocatalytic degradation of methylene blue in aqueous suspension. *Industry and Engineering Chemistry Research*. 38, 373-379.
- Yamazaki, S.; Matsunaga, S. and Hori, K. 2001. Photocatalytic degradation of trichloroethylene in water using TiO₂ pellets. *Water Research*. 35, 1022-1028.
- Yang, S.; Liu, Y.; Guo, Y.; Zhao, J.; Xu, H. and Wang, Z. 2002. Preparation of rutile titania nanocrystals by liquid method at room temperature. *Materials Chemistry and Physics*. 9430, 1-6.
- Yang, Y.; Li, X.-J.; Chen, J.-T. and Wang, L.-Y. 2004. Effect of doping mode on the photocatalytic activities of Mo/TiO₂. *Journal of Photochemistry and Photobiology A: Chemistry*. 163, 517-522.

- Yanqing, Z.; Erwel, S.; Zhinzhan, C.; Wenjun, L. and Xingfang, H. 2001. Influence of solution concentration on the hydrothermal preparation of titania crystallines. *Journal of Material Chemistry*. 11, 1547-1551.
- Youn, H.-J.; Ha, P. S.; Jung, H. S.; Hong, K. S.; Park, Y. H. and Ko, K. H. 1999. Alcohol rinsing and crystallization behavior of precipitated titanium dioxide. *Journal of Colloid and Interface Science*. 211, 321-325.
- Yu, J.; Yu, J. C.; Leung, M. K. P.; Ho, W.; Cheng, B.; Zhao, X. and Xhao, J. 2003. Effects of acidic and basic hydrolysis catalysts on the photocatalytic activity and microstructures of bimodal mesoporous titania. *Journal of Catalysis*. 217, 69-78.
- Yuan, Z.; Zhang, J.; Li, B. and Li, J. 2007. Effect of metal ion dopants on photochemical properties of anatase TiO₂ films synthesized by a modified sol-gel method. *Thin Solid Films*. 515, 7091-7095.
- Zainal, Z.; Hui, L. H.; Hussein, M. Z. and Ramli, I. 2005. Removal of dyes using immobilized titanium dioxide illuminated by fluorescent lamps. *Journal of Hazardous Materials*. 125, 113-120.
- Zhang, Y. H. and Reller, A. 2001. Nanocrystalline iron-doped mesoporous titania and its phase transition. *Journal of Materials Chemistry*. 11, 2537-2541.
- Zhang, Z. and Maggard, P. A. 2007. Investigation of photocatalytically-active hydrated forms of amorphous titania, TiO₂•nH₂O. *Journal of Photochemistry and Photobiology A: Chemistry*. 186, 8-13.
- Zhao, X. K. and Fendler, J. H. 1991. Size quantization in semiconductor particulate films. *Journal of Physical Chemistry*. 95, 3716-3723.

Zhu, J.; Deng, Z.; Chen, F.; Zhang J.; Chen, H.; Anpo, M.; Huang, J. and Zhang, L. 2006. Hydrothermal doping method for preparation of Cr³⁺-TiO₂ photocatalysts with concentration gradient distribution of Cr³⁺. *Applied Catalysis B: Environmental*. 62, 329-335.